Karlsruhe Institute of Technology
INSTITUTE FOR NUCLEAR WASTE DISPOSAL (INE)

TC-MIGRATION IN ADVECTION/DIFFUSION CONTROLLED NATURAL SYSTEMS: INFLUENCE OF FERROUS IRON POOL

Zur Erlangung des akademischen Grades eines

DOKTORS DER NATURWISSENSCHAFTEN

(Dr. rer. nat.)

Fakultät für Chemie und Biowissenschaften

Karlsruher Institut für Technologie (KIT) - Universitätsbereich

genehmigte

DISSERTATION

von

DIPL.-CHEM. YURY TOTSKIY

aus

Tula, Russland

Dekan: Prof. Dr. Peter Roesky

Referent: Prof. Dr. Horst Geckeis

Korreferent: Prof. Dr. Thorsten Schäfer

Tag der mündlichen Prüfung: 23.10.2015

Erklärung / Declaration of Originality

Hiermit versichere ich, dass ich die vorliegende Arbeit selbstständig verfasst und keine anderen als die angegebenen Quellen und Hilfsmittel verwendet habe. Darüber hinaus versichere ich, dass alle Stellen der Arbeit, die wörtlich oder sinngemäß aus anderen Quellen übernommen wurden, als solche kenntlich gemacht sind und dass die Arbeit in gleicher oder ähnlicher Form noch keiner Prüfungsbehörde vorgelegt wurde.

_____ _____

Datum, Ort Unterschrift

CONTENTS

Abstract

The interaction of Tc(VII) with crystalline rock materials from the generic underground research laboratory in Sweden (Äspö Hard Rock Laboratory) and from a prospective site of nuclear waste disposal in Russia (Nizhnekansky massif) was investigated. The main focus of this work is laid on the effect of Fe(II) content in the mineral phase or rock, which is considered as the dominating redox partner for Tc(VII) reduction under far-field conditions in crystalline rock.

This work consists of three parts:

1. In the first part of the thesis the ferrous iron influence on the Tc(VII) immobilization using stoichiometric and partly oxidized (non-stoichiometric) synthetic magnetite ($FeO \cdot Fe_2O_3$) is investigated by means of batch experiments. Uptake parameters were derived from the experimental data, namely distribution coefficients (K_d), surface normalized distribution coefficients (K_a) and uptake rates (r). Tc uptake is quantitative ($K_a > 10^{-3}$ m) after three days contact time for the stoichiometric magnetite at pH 7 and 8 and $Eh_{(SHE)}$ of 68 mV to 110 mV with log $[Tc]_{tot}$ = -5, -8 and -9. Magnetite oxidation decreases the overall Tc uptake and samples with $Fe(II)/Fe_{tot}$ ratio $\leq$ 18.3% (ideal magnetite contains 33.3%) do not reduce Tc(VII) within the contact time of 56 days. Tc colloidal phase formation was not detected under the experimental conditions applied (I = 0.2 M). XPS and XANES analyses reveal only Tc(IV) on the magnetite surface. Based on the EXAFS measurements, Tc occupies octahedral sites in the stoichiometric magnetite, while in a partially oxidized sample (24.7% $Fe(II)/Fe_{tot}$) no Fe was found in the local environment suggesting the presence of $TcO_2 \cdot 1.6H_2O_{(s)}$ without structural incorporation into the iron oxide solid phase.

2. The second part of the thesis is devoted to Tc(VII) batch sorption studies with natural crystalline rock material, namely Äspö diorite (ÄD) and Nizhnekansky granite (NK). It was found that Tc(VII) immobilization on the crystalline rocks strongly depends on sample preservation conditions. That is, sorption values are ~ 2 times higher for un-oxidized material in comparison to oxidized samples. These results can be explained by Tc(VII) reduction to the insoluble Tc(IV) oxide by the Fe(II) pool available in the crystalline matrix estimated as 0.1 – 1 µg/g for oxidized NK, 1 – 3 µg/g for oxidized ÄD and 4 – 6 µg/g for un-oxidized ÄD. Limitation of Tc uptake by the Fe(II) pool becomes apparent by the lower uptake values for higher Tc concentrations. XPS and XANES analyses indicate Tc(IV) on the rock surface being associated with mafic minerals (biotite). K_a values determined for the crystalline rock

systems are lower than those for magnetite (from $(3.3 \pm 0.3)\times10^{-6}$ m for oxidized ÄD and 10^{-5} M Tc, up to $(5.3 \pm 4.9)\times10^{-3}$ m for un-oxidized ÄD and 10^{-9} M Tc) due to their lower Fe(II) content.

Again the formation of a colloidal Tc phase was not detected even under the low ionic strength groundwater conditions used in the NK system (pH 8, I = 0.005 M). Tc desorption from the rock samples is very low using un-spiked equilibrium ground water (< 6% with one month contact time), but after artificial oxidation under air technetium release is increased up to ~ 95%. These observations indicate rather low Tc mobility under natural far-field redox conditions but point to the possible Tc remobilization in case of contact with oxygenated groundwater, e.g. by the intrusion of oxygen containing melt water intrusion into a repository.

3. The third part of the work is devoted to Tc column migration studies using a single fractured drill core from the Äspö Hard Rock Laboratory drilled and preserved under anoxic conditions. Injections of HTO and ^{36}Cl showed long tailings due to the complex fracture geometry identified by µCT. No anion exclusion was observed for flow rates down to 0.2 ml/h (490 min residence time). Tc(VII) recovery is inversely dependent on residence time showing accelerated reduction as compared to batch sorption studies (0.61 ± 0.08 d^{-1} and 0.051 ± 0.008 d^{-1} for 10^{-9} M Tc in migration and batch studies, respectively) with $K_a > 5\times10^{-4}$ m for log $[Tc]_{tot} \leq -11$ and $K_a > 10^{-2}$ m for log $[Tc]_{tot} = -9$. Natural Äspö groundwater (ÄGWN) taken as an eluent instead of Äspö groundwater simulant (ÄGWS) also increases the uptake rate. However, Tc-ÄGWN interaction experiments revealed that the main Tc(VII) retention mechanism is heterogeneous reduction on the Fe(II)-containing mineral surface. Homogeneous reduction in the aqueous phase does not play a significant role under the experimental conditions studied (pH 8.1, I = 0.2 M, Eh ~ -100 – -200 mV, contact time up to one month). During the post-mortem analysis of the Äspö core Tc species were not detected on the fracture surface using XPS and SEM-EDX techniques, but Tc was recovered after air oxidation and leaching by ÄGWS under oxidizing conditions.

In summary, this manuscript presents a critical comparison of studies performed with natural un-oxidized crystalline rock with those accomplished using oxidized material with regard to the effect on Tc reduction and retention. The governing role of the Fe(II) pool in Tc immobilization is shown and proven with *state of the art* spectroscopic techniques including XANES/EXAFS and XPS. The data obtained within this work indicates rather low mobility of Tc under natural crystalline far-field conditions. However, this study also shows that under

oxidizing conditions Tc is prone to remobilization. These results are of a high importance for the predictive modelling of Tc behaviour under natural far-field conditions.

Zusammenfassung

Die Wechselwirkung von Tc(VII) mit kristallinen Gesteinsproben aus einem generischen Untertagelabor in Schweden (Äspö Hard Rock Laboratory) und aus einem prospektiven Standort der tiefengeologischen Endlagerung radioaktiver Abfälle in Russland (Nizhnekansky Massiv) wurde untersucht. Der Schwerpunkt dieser Arbeit liegt auf der Wirkung von Fe(II) in der Mineralphase Magnetit (Fe_3O_4) oder dem gesamten Wirtsgestein, wobei Fe(II) als dominierender Redox-Partner für die Tc(VII) Reduktion unter Fernfeldbedingungen in kristallinem Gestein angesehen wird.

Diese Arbeit besteht im Wesentlichen aus drei Teilen:

1. Im ersten Teil der Arbeit wird der Einfluss des zweiwertigen Eisens auf die Tc(VII) Immobilisierung unter Verwendung von stöchiometrischem und teilweise oxidiertem (nicht-stöchiometrischem) synthetisiertem Magnetit ($FeO \cdot Fe_2O_3$) mit Hilfe von Batch-Experimenten untersucht. Wechselwirkungsparameter wie Verteilungskoeffizienten (K_d), Oberflächen-normierte Verteilungskoeffizienten (K_a) und Sorptionskinetiken in Form von Aufnahmeraten (r) wurden bestimmt. Die Tc-Aufnahme ist quantitativ ($K_a > 10^{-3}$ m) nach drei Tagen Kontaktzeit für den stöchiometrischen Magnetit bei pH 7 und 8 und $Eh_{(SHE)}$ von 68 mV bis 110 mV bei $\log[Tc]_{tot}$ = -5, -8 und -9. Liegt der Magnetit teilweise oxidiert vor, verlangsamt sich die Rate der Tc- Aufnahme. Proben mit einem relativen Fe(II) Gehalt von $Fe(II)/Fe_{tot} \leq 18{,}3\%$ (idealer Magnetit enthält 33,3% Fe(II)) zeigen keine Tc(VII) Aufnahme innerhalb der Kontaktzeit von 56 Tagen. Die Bildung von Tc-Eigenkolloiden konnte unter den angewandten Versuchsbedingungen (I = 0,2 M) nicht nachgewiesen werden. Spektroskopische Untersuchungen mittels XPS und XANES konnten nur tetravalentes Tc auf der Magnetit-Oberfläche identifizieren. Basierend auf den EXAFS-Messungen, nimmt Tc(IV) Oktaederlücken im stöchiometrischen Magnetit ein, während spektroskopische Daten für eine teilweise oxidierte Probe (24,7% $Fe(II)/Fe_{tot}$) auf die Bildung einer oberflächenassoziierten $TcO_2 \cdot 1.6H_2O_{(s)}$ Phase ohne strukturellen Einbau hindeutet.

2. Der zweite Teil der Arbeit fokussiert auf Tc(VII) Sorptionsuntersuchungen an natürlichem kristallinem Gesteinsmaterial, nämlich Äspö Diorit (ÄD) und Nizhnekansky Granit (NK). Es zeigte sich, dass die Wechselwirkung des redox-sensitiven Tc(VII) mit diesen natürlichen Hartgesteinen stark von den Probenaufbewahrungsbedingungen abhängt. Sorptionswerte sind ungefähr zweimal höher für nicht oxidiertes Material im Vergleich zu oxidierten Proben. Die Ergebnisse können mit einer Tc(VII) Reduktion und der Bildung von unlöslichen Tc(IV)-

Phasen bedingt durch das vorhandene kationenaustauschbare Fe(II)-Reservoir in der kristallinen Matrix erklärt werden. Der Gehalt an kationenaustauschbarem Fe(II) wurde mit 0,1 – 1µg/g für die oxidierte NK Probe, mit 1 – 3µg/g für den oxidierten Äspö Diorit und mit 4 – 6 µg/g für den nicht oxidierten Äspö Diorit bestimmt. Das kationenaustauschbare Fe(II) Reservoir bestimmt auch die begrenzte Tc-Aufnahme bei höheren Tc-Konzentrationen. XPS und XANES-Analysen auf der Festgesteinsoberfläche zeigen eine Assoziation von Tc(IV) mit mafischen Mineralien (speziell Biotit). K_a-Werte für die kristallinen Gesteinssysteme sind auf Grund des niedrigeren Gesamt Fe(II)- Gehaltes niedriger als die für Magnetit gefundenen. Sie reichen von $(3,3 \pm 0,3)\times10^{-6}$ m für oxidierten Äspö Diorit bei 10^{-5} M Tc, bis zu $(5,3 \pm 4,9)\times10^{-3}$ m für nicht oxidierten Äspö Diorit bei 10^{-9} M Tc. Wiederum wurde die Bildung einer kolloidalen Tc-Phase nicht einmal bei den niedrigen Ionenstärken des NK Systems beobachtet (pH 8, I = 0,005 M). Diese Beobachtungen weisen auf eine eher geringe Tc Mobilität unter den natürlichen Redoxbedingungen des Fernfelds eines Endlagers im Kristallingestein hin. Die Analyse der Tc-Desorption vom Gestein durch Kontakt mit undotiertem Grundwasser gleicher Zusammensetzung (Kontaktzeit 1 Monat) sind mit < 6% sehr gering. Ein Kontakt von oberflächensorbiertem Tc mit Luftsauerstoff sollte den Einfluss von möglicherweise eindringendem sauerstoffhaltigem Gletscherschmelzwasser simulieren. Unter diesen Bedingungen konnte die Technetium-Desorption auf bis zu 95% erhöht werden.

3. Der dritte Teil der Arbeit widmet sich Tc - Migrationsstudien in Säulenexperimenten unter Verwendung eines unter anoxischen Bedingungen gebohrten und aufbewahrten Bohrkerns mit einer natürlichen Kluft aus dem Äspö Untertagelabor (HRL). Injektionen von HTO und ^{36}Cl zeigten lange Tailings in den Durchbruchskurven (BTC) aufgrund der komplexen Kluftgeometrie, die mittels µ Computer- Tomographie (CT) charakterisiert wurde. Es konnte kein Anionenausschluss unter den experimentellen Bedingungen bis zu einer unteren Fließrate von 0,2 mL/h (490 min Verweilzeit) beobachtet werden. Der Tc Wiedererhalt ist invers proportional zur Kluftverweilzeit und zeigt beschleunigte Tc(VII) Reduktionsraten im Vergleich zu den durchgeführten Batchexperimenten ($0,61 \pm 0,08$ d^{-1} in den Migrations- und $0,051 \pm 0,008$ d^{-1} in den Batch-Studien bei jeweils 10^{-9} M Tc). Die Sorptionskoeffizienten sind konzentrationsabhängig und liegen bei $K_a > 5\times10^{-4}$ m für log $[Tc]_{tot} \leq -11$ und bei $K_a > 10^{-2}$ m für log $[Tc]_{tot} = -9$. Experimente mit natürlichem Äspö Grundwasser (ÄGWN) als fluider Phase statt synthetischem Äspö Grundwasser (ÄGWS) führen zu einer deutlichen Beschleunigung der Rückhaltungsreaktion. Separate Tc(VII) – ÄGWN Wechselwirkungsexperimente zeigen jedoch, dass eine homogene Reduktion in der wässrigen Phase unter den Versuchsbedingungen nicht beobachtet wird (pH 8,1, I = 0,2 M, Eh ~ -100 – -

200 mV, Kontaktzeit bis zu einem Monat). Die Tc - ÄGWN Migrationsexperimente zeigen eindeutig auf, dass der Tc(VII)- Rückhaltemechanismus eine heterogene Reduktion an Fe(II) - haltigen Mineraloberflächen sein muss. In den spektromikroskopischen post-mortem Analysen mittels XPS und SEM-EDX war es wegen der geringen Tc-Belegung der Oberflächen nicht möglich, auf der Kluftoberfläche Tc zu detektieren. Allerdings konnte nach Oxidation der Kluftoberfläche an Luft und anschließender Kontaktierung mit ÄGWS eindeutig Tc in der Lösung nachgewiesen werden.

Zusammenfassend zeigt diese Arbeit deutlich den erheblichen Einfluss des Zustands von Gesteinsproben auf die Redox- Kapazität der untersuchten Proben und somit auf die Tc-Reduktion und Rückhaltung auf. Die Wechselwirkung von Tc(VII) mit natürlichen, nicht oxidierten kristallinen Gesteinsproben ist deutlich anders als die mit oxidiertem Material . Die dominierende Rolle des Fe(II) Reservoirs zur Tc Immobilisierung konnte mit modernsten spektroskopischen Techniken wie XANES/EXAFS und XPS gezeigt werden. Die im Rahmen dieser Arbeit gewonnenen Daten zeigen eher eine geringe Mobilität des Tc unter natürlichen kristallinen Fernfeldbedingungen. Allerdings zeigt diese Studie auch, dass unter oxidierenden Bedingungen und Anwesenheit von Sauerstoff Tc durchaus remobilisiert werden kann. Diese Ergebnisse sind für die prognostizierende Modellierung zum Tc Verhalten unter natürlichen Fernfeldbedingungen von hoher Bedeutung.

1. Introduction and Motivation

"All the waste in a year from a nuclear power plant can be stored under a desk."
Ronald Reagan

Radioactive waste is defined as material that contains, or is contaminated with, radionuclides at concentrations or activities greater than clearance levels as established by individual countries' regulatory authorities. The higher the concentration of radionuclides above established levels the greater the hazard the waste possesses. The hazard of radioactive waste depends on the nature of the radionuclides (i.e. half-life, type of radiation, physiological behaviour, biological half-life, etc.) and the concentration resulting in a radioisotope specific level of risk. This definition of radioactive waste is purely for regulatory purposes. A waste with activity concentrations equal to, or less than, clearance levels is considered non-radioactive. From a physical point of view, however, it is radioactive, although the associated radiological hazards are negligible. Radioactive waste may be accompanied by significant levels of radiation hence this waste requires not only immobilisation/isolation to prevent radionuclide migration into the biosphere, but also shielding and, in some cases, remote handling.

Classification of nuclear waste varies by country, but normally it is based on the type and level of radioactive material. According to the International Atomic Energy Agency (IAEA) classification [1] nuclear waste is divided into 6 categories presented in Table 1.

Table 1. *Classification of radioactive waste (based on the IAEA General Safety Guide [1])*

Waste class	Typical characteristics	Disposal options
Exempt waste (EW)	Waste that is at or below clearance levels.	Does not require provisions for radiation protection.
Very short-lived waste (VSLW)	VSLW contains only radionuclides with very short half-life (normally ≤ 100 days) often used for research and medical purposes with activity concentrations above the clearance levels.	Temporary storage until its activity has decayed below clearance levels.
Very low-level waste (VLLW)	Activity level is higher than for EW, but that does not need a high level of containment and isolation. Typically, it includes contaminated soil and rubble	Near surface landfill type facility with limited regulatory control.

Waste class	Typical characteristics	Disposal options
	with low levels of radioactivity.	
Low-level waste (LLW)	Waste that is above clearance levels, but with limited amounts of long-lived radionuclides.	Near surface facility or geological disposal facility.
Intermediate level waste (ILW)	It covers a very broad range of waste and may include short-lived radionuclides at higher levels of activity concentration and long-lived radionuclides, but only at relatively low levels of activity concentration.	Geological disposal facility with depth of tens of metres to a few hundred metres.
High-level waste (HLW)	Waste with levels of activity concentration high enough to generate significant quantities of heat by the radioactive decay process or waste with large amounts of long-lived radionuclides. Vitrified waste products from reprocessing belong to this category.	Geological disposal facility with depth of several hundred metres.

Some classifications [2] also include transuranic waste (TRU) which does not qualify as high-level waste but that contains more than 0.1 μCi (3.7 kBq) of long-lived ($t_{1/2}$ > 20 years) transuranic alpha-particle emitters per gram of material. The term "transuranic" refers to elements of atomic number greater than 92. These are formed in neutron-capture chains, starting with uranium.

The pathways of the waste disposal strongly depend on the level of hazard based on the country-specific regulations. VLLW, LLW and VSLW are commonly disposed in near-surface facilities at a depth of not more than 30 m. Some countries, including Australia, Belgium, Netherlands, Germany, Italy and Switzerland also place LLW in interim storage [3]. The underlying assumption is that deposited radioactive waste will decay to background levels before institutional control is lost (within about 300 years). Germany is also disposing LLW in mined geological repositories (Morsleben repository) [3].

The generally accepted concept of spent nuclear fuel and high-level waste long-term storage is its disposal in deep geological formations at a depth of 300 – 1000 meters. The repository is designed based on the multi-barrier concept where each barrier has an attributed safety function isolating or retarding the potential release of the disposed radionuclides into the biosphere. The overall set of the barriers is divided into engineered system (waste package, backfilling and sealing materials, configuration of the repository) and the natural system (natural environment around the repository) [2]. The "near-field" represents the engineered

barrier system and the host rock in contact and near the system. The “far-field” includes the geosphere (and biosphere) surrounding the repository [4]. Depending on the host rock type, the repository host rock plays different roles as a part of the multi-barrier system, namely isolation of the repository from the biosphere, stability (mechanical, hydraulic and chemical), containing waste and retardation the radionuclide migration [5]. Thus, the selection of the host rock formation with appropriate geochemical and hydro-geological properties is a key challenge in the task of nuclear waste disposal siting. The favoured host rock formations vary among countries, which is also a function of the available geology, but in general there are three types of host rocks being considered: crystalline, sedimentary formations and rock salt.

In 1993, by the request of Ministry of Atomic Energy (Minatom) the search for an appropriate site of underground facility for high-level radioactive waste disposal was initiated in the Russian Federation. In 2002, based on the research performed and taking into account criteria established by the International Atomic Energy Agency (IAEA) and the waste isolation concept chosen, a “Declaration of Intent” (DOI) was prepared and adopted by the State Atomic Energy Corporation, Rosatom. The DOI covers plans to construct an underground research laboratory in the Nizhnekansky granitoid massif, Krasnoyarsky Krai. In this massif, three potential locations for the laboratory have been considered (Yeniseisky, Itatsky and Kamenny, see Figure 1). In 2008, the revised DOI stated that the Yeniseisky site is the favourite candidate for further investigations, and the probable candidate for final disposal repository. The other sites should be considered as reserve options. Granitoid samples from Itatsky and Kamenny were taken for investigation within this work.

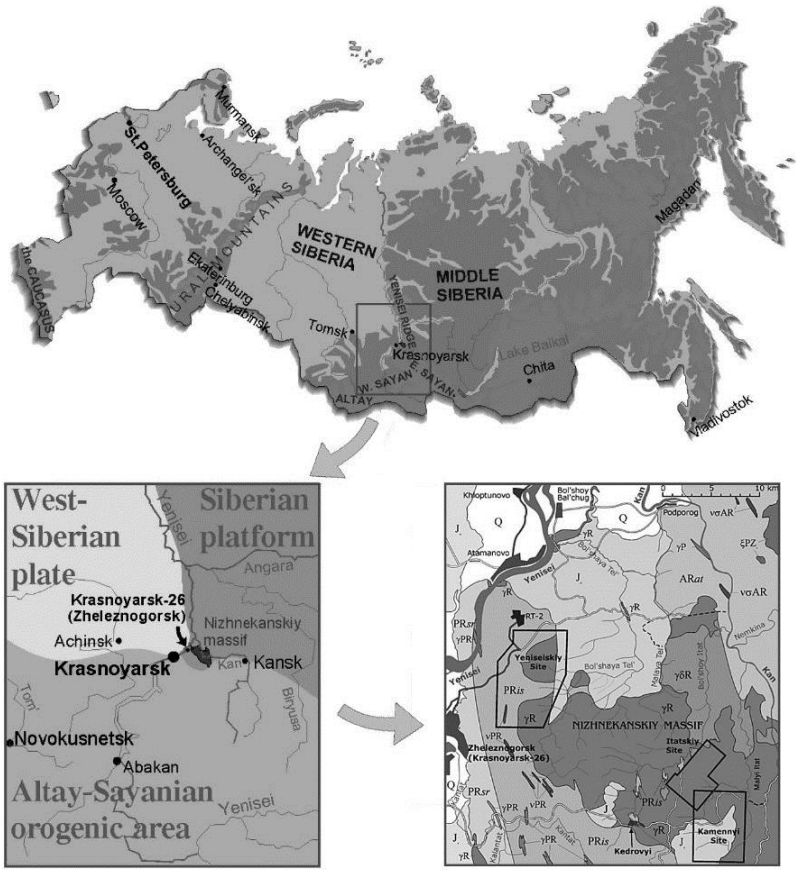

Figure 1. *Location of Nizhnekansky granitoid massif and three proposed sites for SNF final geological disposal (Yeniseisky, Itatsky and Kamenny sites). Based on Anderson et al. [6].*

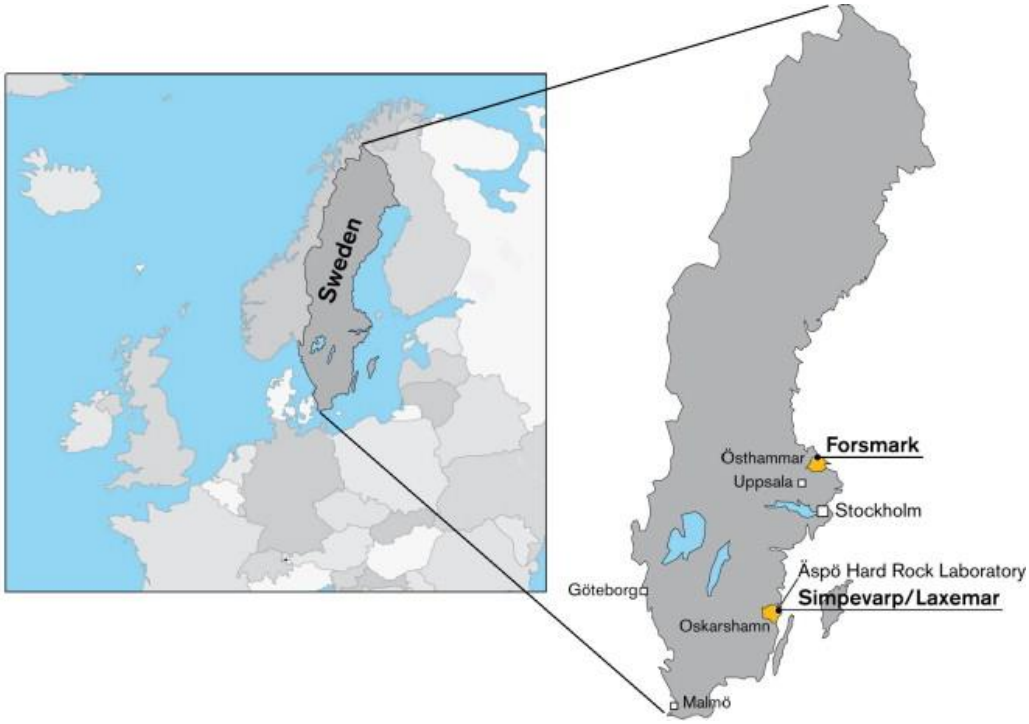

Figure 2. *Äspö Hard Rock Laboratory location. Based on Laaksoharju et al. [7].*

The Äspö Hard Rock Laboratory (HRL) is a generic URL in Sweden for *inter alia* in-situ studies of processes in crystalline formations concerning deep geological disposal of spent nuclear fuel. The facility began to be built in 1990 and was finished in 1995. According to the current concept of the nuclear waste disposal in Sweden, the Äspö HRL is not considered as a repository site. The Swedish deep geological disposal will be located at Forsmark, about 350 km to the northeast (see Figure 2). However, Äspö HRL provides a platform for gaining critical technical knowledge and confidence for facility siting and design, underlying engineering support, and evaluation of safety [8]. As a generic URL it has great facilities to work ~ 500 meters below surface under realistic environment and investigate processes to support the disposal of radioactive waste elsewhere in international collaboration [9].

^{99}Tc is one of the main long-lived U and Pu fission products in spent nuclear fuel (SNF) and it is as well generated by medical laboratories and research institutions. Because of relatively high fission yield (*ca.* 6%) and long half-life ($t_{1/2} = 2.1\times10^5$ years) technetium is considered as a radioactive component of HLW with significant toxic relevance [10]. Assuming that it requires 10 half-lives for technetium to decay to a safe level, the waste would have to be safely contained for over 2 million years without the intrusion into the biosphere. Furthermore, after ~ 10^5 years ^{99}Tc contributes significantly to the total activity of SNF (see Figure 3).

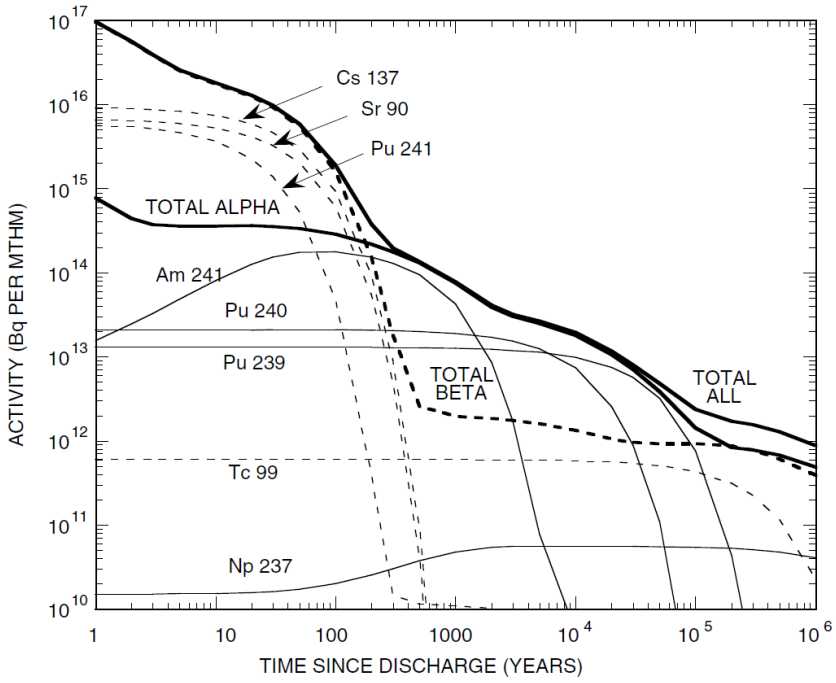

Figure 3. *Activity of the radionuclides most responsible for the activity in the waste for the period from 1 year to 1,000,000 years as a function of time (PWR reactor, ^{235}U enrichment of 3.75%, burnup of 40 GWd/t). Dotted lines correspond to beta-particle emitters and solid lines to alpha-particle emitters. Based on Bodansky [2].*

Technetium mobility in natural systems strongly depends on the redox state. The most stable Tc form under aerobic atmosphere is pertechnetate (TcO_4^-), which is very soluble under fully oxidizing conditions [11; 12]. Whereas Tc(VII) is frequently considered as a conservative tracer under oxidizing conditions (e.g. Hanford site), under anoxic conditions it is reduced to Tc(IV) and the solubility is limited by the oxyhydroxide solid phase $TcO_2 \cdot 1.6H_2O_{(s)}$ [13]. Therefore, distribution coefficients and apparent diffusion coefficients of technetium for natural minerals and rock matrices found in literature are very scattered. Moreover, they are rarely published together with the pe/pH conditions studied. Tc redox kinetics predominantly depend on the availability of reactive Fe(II) in host rock and the type of interaction with mineral surfaces (surface complexation, surface precipitation, ion exchange) [12; 14-18]. Geochemical parameters of host rock formations for deep geological disposal of radioactive waste and spent nuclear fuel (SNF) under discussion in Europe (Opalinus Clay, Callovo-Oxfordian argillite, crystalline host rocks in Sweden, Finland, Russia) are investigated [19-21] and transport models for radionuclide (RN) migration are developed. However, experimental mobility and migration studies in anoxic preserved natural host rock formations are scarce. Therefore, the main motivation of this work is to investigate technetium behaviour in crystalline rock materials from prospective sites of generic underground research laboratories (URL) of similar host rock formations favoured for SNF and HLW deep geological disposal.

Crystalline host rocks contain fractures, which are potential migration pathways in cases of radionuclide releases from a repository. Radionuclide transport depends strongly on the hydrogeological and geochemical conditions (pH, Eh, ionic strength) of ground- and porewater and different immobilization-remobilization processes may be active [22]. Furthermore, depending on the fracture formation history (ductile or brittle deformation, mylonite or fault gauge material, respectively, has been formed) fracture surfaces likely vary in mineralogical composition compared to the bulk rock matrix. Beside advective transport in water conduction features, matrix diffusion is expected to contribute significantly to radionuclide migration. Redox conditions have a tremendous impact on technetium mobility in natural systems. Both batch type sorption and column experiments with Hanford sediments [11; 12] have revealed that ^{99}Tc is highly mobile and shows virtually no retardation under fully oxidizing conditions.

Based on the literature survey, the main retardation factor of Tc in the host rock natural environment is the ferrous iron (Fe(II)) content of the system. Materials used can be comprehensively characterized before and after contact with radionuclides to reveal any

changes in tracer and mineral speciation using atomic scale spectro- microscopic techniques (XANES/EXAFS, XPS, SEM-EDX). The work presented here is divided into three main research foci:

1. The work was started with investigation on magnetite (Fe_3O_4) Tc interaction as Fe_3O_4 is a relevant Fe(II) containing mineral frequently found as accessory mineral in crystalline formations and most abundant stainless steel canister corrosion product. The most common approach to investigate radionuclide sorption on solids is to perform static batch-type sorption experiments. It provides experimental distribution coefficients (K_d) together with information about retention kinetics under certain well-defined conditions. To investigate the influence of structural ferrous iron on Tc immobilization stoichiometric magnetite, partially and fully oxidized (maghemite) magnetite was used in batch-type sorption studies.

2. A second focus of research was on the technetium behaviour in presence of crystalline rock materials from the Äspö HRL and the Nizhnekansky granitoid massif. Variation of groundwater composition allows testing different scenarios in the repository evolution. For instance, simulation of the natural groundwater composition represents the scenario of the water intrusion into the repository, while Grimsel groundwater simulates glacial melt water composition potentially coming in contact with the geotechnical barrier (compacted bentonite) within a future glaciation period [23]. Systematic batch sorption studies have been performed in the present work to provide a mechanistic understanding of Tc(VII)/Tc(IV) retention, its speciation including potential colloid formation and evaluation of sorption kinetics. Tc(VII) behaviour has been investigated on well-preserved un-oxidized crystalline rock material and a comparison with frequently used at least partially air-oxidized material has been conducted to better interpret the scatter of existing experimental data in the literature. The batch type technique is frequently under criticism for the crushed granite material as it determines the radionuclides interaction with artificially created fresh rock surfaces, which definitely differs from minerals in natural fracture surfaces.

3. Migration experiments using a well-characterized un-oxidized core containing a natural fracture were conducted by pumping a radionuclide spiked Äspö groundwater simulant (with the same composition as in batch sorption studies) to quantify the Tc retention under dynamic conditions. In this study the experiments were performed with a natural core, drilled within the EU CP CROCK project [24] in the Äspö URL

under anoxic conditions. Flow velocity (i.e. residence time) variation allows to compare retention rates with those observed in batch type sorption studies. The main aim of this part of the work is to obtain the relevant data for further modelling of Tc migration in the natural host rock environment. This information is important for the estimation of Tc mobility in the far field environment of a deep geological repository in crystalline rock for safety assessment purposes.

2. Theoretical background

2.1. Contaminants transport

The transport of chemical compounds in homogeneous porous media is well investigated and theoretical models have been developed. Unfortunately, geological media are much more complicated and the heterogeneity of natural material is hard to estimate and quantify. Neither deterministic nor stochastic models currently succeed in characterizing the transport of chemical compounds in natural groundwater systems. Presence of fractures or karstic media can greatly complicate the calculation. The key challenge is to adequately characterize geological structures with regard to fluid flow and transport [25].

Main processes of solute transport in groundwater include advection, diffusion and dispersion. The general scheme of transport modes in fractured media is shown in Figure 4.

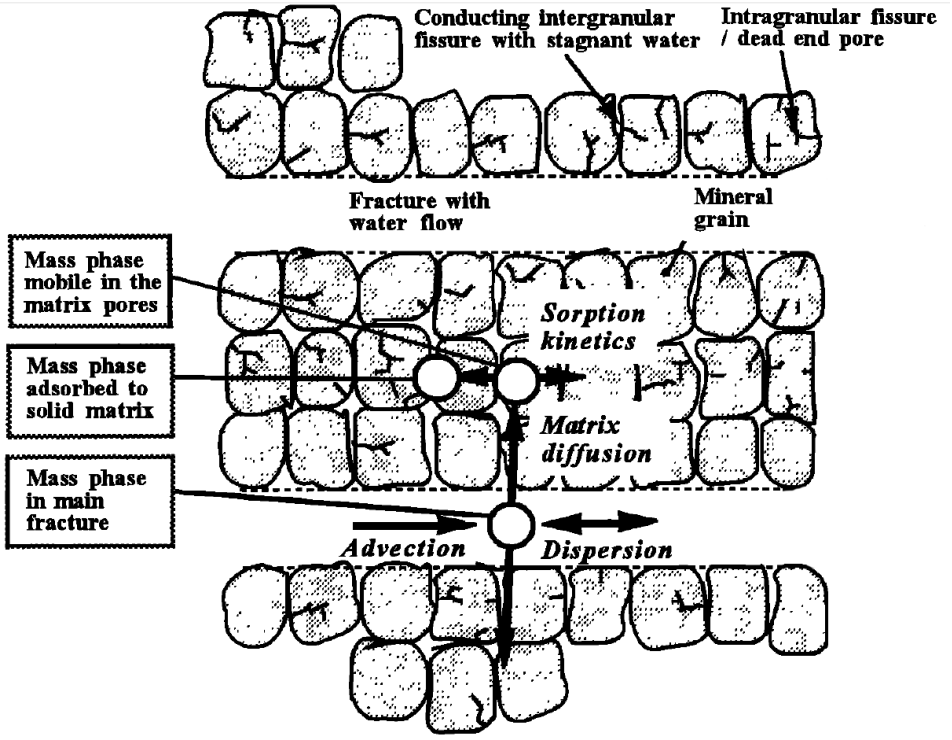

Figure 4. *Schematic illustration of radionuclide transport processes in mineral fractures. Based on Xu and Wörman (1999) [26].*

2.1.1. Hydraulic properties

Prediction of the contaminant transport through porous media requires knowledge of the groundwater retention and hydraulic permeability of the material. In general, the permeability

of a porous medium describes the ease with which fluid can move through pore spaces or fractures. For a given hydraulic head gradient, higher permeability results in higher flow velocities.

The hydraulic permeability is depending on two parameters of the material studied, namely anisotropy and heterogeneity. Anisotropic material has different permeability in different directions and variable permeability in a given direction is inherent to natural heterogeneous material. Natural soils and crystalline rocks normally possess both properties.

The hydraulic permeability of porous media is calculated using Darcy's law [27] according to the equation (1):

$$k = v\frac{\mu \Delta x}{\Delta p} \tag{1}$$

where k is the permeability of the medium (m^2), v is the average fluid velocity (m/s), μ is the dynamic viscosity of the liquid phase (Pa×s), Δp is the pressure drop (Pa) and Δx is the length over which the pressure drop is taking place (m).

Another hydraulic parameter related to the permeability is the hydraulic conductivity derived using the following equation:

$$K = k\frac{\rho g}{\mu} \tag{2}$$

where K is the hydraulic conductivity (m/s), ρ is the density of the fluid (kg/m^3) and g is the acceleration due to gravity (m/s^2).

2.1.2. Advection

Advection is a primary process by which solutes move together with groundwater due to a bulk flow driven by a pressure gradient. Direction and velocity coincides with that of groundwater. The one-dimensional flux of a solute through a porous medium can be expressed by the equation (equation (3)) [25]:

$$J = v_x C n_e \tag{3}$$

where J – solute mass flux per unit area per unit time ($mol/m^2/s$), v_x – average linear groundwater velocity in the direction of flow (m/s), C – concentration of solute (mol/m^3), n_e – effective porosity.

The assumption made for equation (3) is that the mass transport does not change the pattern of flow. This statement does not work in case of non-ideal solute-groundwater mixture, when

their flows may diverge. In addition, large particles (like colloids) can move faster than average water flow, because they are only able to travel through large pores where groundwater flow is faster. Charged particles may decrease their speed due to attraction to the mineral surface (in case of opposite charge) or remain in the centre of the pores due to repulsion (the same charge) in high-velocity zones of laminar flow profiles.

2.1.3. Diffusion

Molecular diffusion is the process of solute transfer along a concentration gradient due to random Brownian movement of molecules. Its direction and velocity does not depend on solution flux. One-dimensional diffusive motion under the steady state assumption is described by the empirical Fick's first law (equation (4)) [27]:

$$J = -D\frac{\partial C}{\partial x} \tag{4}$$

where J is the flux (mol/s/m^2), D – diffusion coefficient (m^2/s) C is the solute concentration (mol/m^3) and x is a spatial coordinate (m). Since the diffusion changes the concentration at point "x", the process should be time dependent. Applying a mass balance equation we obtain Fick's second law (equation (5)):

$$\frac{\partial C}{\partial t} = D\frac{\partial^2 C}{\partial x^2} \tag{5}$$

where t is the time (s).

2.1.4. Dispersion

Dispersion is a mechanical mixing phenomenon, which occurs only in presence of water flow. It is caused by combination of several factors:

1. Parabolic profile of flow velocity through the pores;
2. Simultaneous passing through several pores with different size;
3. Bending of the streamlines around the grains.

Together with diffusion, this process causes spreading of solute particles from the concentrated area by a mechanical mixing and dilution of the solute during the bulk movement of groundwater. Since the process is quite similar to the diffusion, it is mathematically described by equation (4) with a modified constant D.

All three transport processes can be summarized in one formula called advection–diffusion equation. In one dimension, it can be expressed as (equation (6)):

$$\frac{\partial C}{\partial t} = -v_x \frac{\partial C}{\partial x} + D \frac{\partial^2 C}{\partial x^2} \quad (6)$$

Here, the diffusion coefficient *D* includes dispersion processes. Taking the retention processes into account, the final equation is (equation (7)) [27]:

$$\frac{\partial C}{\partial t} = -v_x \frac{\partial C}{\partial x} + D \frac{\partial^2 C}{\partial x^2} + \frac{\partial q}{\partial t} \quad (7)$$

where q is the concentration of the immobilized species (mol/m^3).

2.1.5. Retention

2.1.5.1. Sorption

Sorption by surface adsorption and ion exchange are widely observed both in laboratory and field experiments, as well as in natural systems. According to IUPAC definition, adsorption is an increase in the concentration of a substance at the interface of a condensed and a liquid or gaseous phase due to the operation of surface forces [28]. This affinity may be predominantly caused by: (a) electrical attraction of the solute to the adsorbent (exchange adsorption); (b) van der Waals attraction (physical or ideal adsorption); or (c) chemical reaction (chemisorption or chemical adsorption). In real systems sorption is mostly a combination of several factors mentioned above.

Sorption is subdivided into three types:

1. Adsorption.

Adsorption can be defined as the accumulation of a substance at the interface (for instance solid-liquid). It does not include surface precipitation, which is the formation of a three-dimensional phase product on surface. For the metal ions, the most common mechanism of adsorption is surface complexation with the surface functional groups. The two types of surface complexation can be formed: outer-sphere and inner-sphere. If a water molecule is present between the ion or molecule and the surface functional group, the complex is called outer-sphere, otherwise the complex is termed inner-sphere [29].

2. Absorption.

Absorption is the incorporation of a substance in one state into another of a different state [30]. It is subdivided into physical and chemical absorption. In the case of geochemistry, physical absorption takes place when the mass of liquid moves into the mineral phase forming the solid solution. Chemical absorption implies chemical reaction between the absorbing and absorbed substances.

3. Ion exchange.

Ion exchange is a process of the replacement of a surface ion with an ion of the similar polarity from the solution. The ion exchange uptake of the metal ions is reversible under appropriate conditions [31].

A quantitative description of sorption can be expressed by the concept of the distribution coefficient (K_d), which shows the ratio between solute concentration on the sorbent and in the solution (in the case of a liquid-solid interface):

$$K_d = \frac{C_l}{C_s} \tag{8}$$

where C_l and C_s are the equilibrium concentrations of solute in aqueous and solid phases, respectively. The distribution coefficient for radionuclide sorption from the solution is calculated using equation (9).

$$K_d = \frac{A_0 - A_l}{A_l} \times \frac{V}{m_{solid}} \tag{9}$$

where A_0 and A_l are the initial and final aqueous activities of a radionuclide (Bq/mL), respectively, V is the volume of aqueous phase (mL) and m_{solid} – the solid mass (g). This equation is usually taken to estimate the extend of sorption [32; 33]. The K_d approach, however, is a very simplified method because it is not taking into account any changes in system parameters (pH, Eh, temperature, etc.), but it is relevant for certain specific and well-defined experimental conditions. Moreover, the K_d concept assumes fully reversible sorption reactions.

2.1.5.2. Precipitation and redox

Precipitation is the sedimentation of a solid material (a precipitate) from a liquid solution in which the material is present in amounts greater than its solubility in the liquid [28]. In natural systems radionuclides may precipitate because of its solubility limit exceeding of the initial

compound (for instance, due to change of ionic strength, pH, counter-ion concentration, etc.) or chemical transformation into another less soluble substance. For redox sensitive elements changes of redox conditions may change the oxidation state finally leading to precipitation reactions. Since a deep natural groundwater has reducing conditions in comparison with aerobic shallow groundwater, the most probable redox process in deep formations is a reduction. Stability fields of different oxidation states of an element can be represented by Eh/pH diagrams (Pourbaix diagrams). Pourbaix diagrams of Tc under experimental conditions applied are given in corresponding chapters of the Results and Discussions section (see Figure 24 and Figure 32).

2.1.5.3. Matrix diffusion

Since the contaminants diffusion into the rock matrix can enhance the retardation by orders of magnitude as compared to the retardation by the sorption/precipitation only, sometimes it is listed among other retention processes [34]. However, it might be also regarded as absorption (see paragraph 2.1.5.1). Characterization of the matrix diffusion in fractured rocks systems is an important and challenging problem for the performance assessment, discussed within several workshop and projects [35; 36].

2.2. Technetium chemistry

2.2.1. Technetium isotopes

Technetium (Tc), the element with the atomic number of 43, has no stable isotope. Tc was first synthesized and isolated by Perrier and Segre (1937) [37] as a product from the bombardment of molybdenum with accelerated deuterons or neutrons. So far, 45 isotopes of Tc, ranging from ^{85}Tc to ^{117}Tc, have been synthesized, and most of them are short-lived with half-lives of less than one hour. Table 2 lists the isotopes of Tc with half-lives more than one hour (based on the NuDat database [38]).

Table 2. *Technetium isotopes with a half-life of more than one hour.*

Isotope	Half-life ($t_{1/2}$)	Decay mode	Main γ-ray energy, KeV
^{93}Tc	2.8 h	EC, β^+	1363.0, 66% 1520.4, 24.4%
^{94}Tc	4.9 h	EC, β^+	702.6, 99.6% 849.7, 95.7% 871.1, 100%
^{95}Tc	20 h	EC, β^+	765.8, 93.8%; X-ray 17.5, 56.5%
^{95m}Tc	61 d	EC, β^+, IT	204.1, 63.3% 582.1, 30% 835.1, 26.6%
^{96}Tc	4.3 d	EC, β^+	778.2, 100% 812.6, 82% 849.9, 98%
^{97}Tc	2.6×10^6 y	EC	-
^{97m}Tc	90.1 d	EC, IT	X-ray 18.4, 27%
^{98}Tc	4.2×10^6 y	β^-	652.4, 100% 745.4, 102%
^{99}Tc	2.1×10^5 y	β^-	-
^{99m}Tc	6 h	β^-, IT	140.5, 89%

Since the Tc isotopes with highest half-life (^{97}Tc ($t_{1/2} = 2.6\times10^6$ y), ^{98}Tc ($t_{1/2} = 4.2\times10^6$ y) and ^{99}Tc ($t_{1/2} = 2.1\times10^5$ y)) are relatively short-lived compared to the age of the Earth (4.54×10^9 y) [39], technetium is generally considered as an «extinct» element. Both ^{97}Tc and ^{98}Tc are mainly formed by activation reactions with neutrons or charged particles, although very small amounts have been produced in anthropogenic nuclear processes, and negligible amounts of ^{97}Tc and ^{98}Tc occur in the environment.

^{99}Tc can be produced by thermal neutron induced fission of ^{235}U with a relatively high accumulated fission yield of 6.06%, making ^{99}Tc relatively high abundant among fission products [40]. Thus, the main source of ^{99}Tc is SNF produced on the nuclear power plants. Reprocessing of SNF (e.g. Sellafield reprocessing and decommissioning site, UK) and accidents at nuclear facilities (e.g. Chernobyl, USSR) are the potential pathways for ^{99}Tc to the environment [41]. Moreover, significant amounts of ^{99}Tc has been produced and released to the environment from nuclear weapon explosions. Relatively smalls amounts of ^{99}Tc are also produced by nuclear medicine departments via decay of ^{99m}Tc used for nuclear diagnostics. Hence, ^{99}Tc is the only environmentally significant Tc isotope.

Meanwhile ^{99}Tc can also be produced through neutron activation of ^{99}Mo. Figure 5 shows the formation and decay scheme of ^{99}Tc.

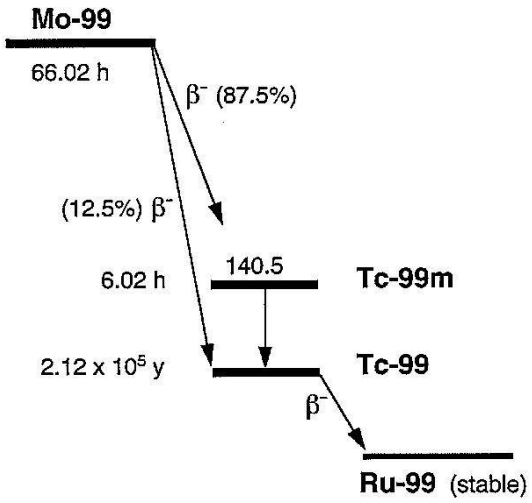

Figure 5. *Decay scheme of ^{99}Mo.*

2.2.2. Measurements techniques

^{99}Tc is the dominating Tc isotope and the most convenient for studying the environmental and biological behaviour of this element. It possesses high mobility under oxidizing conditions, high fission yield, and long half-life, which makes ^{99}Tc an important radionuclide in radioactive safety assessment in the environment, as well as in decommissioning of nuclear facilities and management of nuclear waste. The high water solubility of Tc (in the form of TcO_4^-) and the long half-life (and thus long residence time in the oceans) of ^{99}Tc discharged into the see by the reprocessing plants make it an ideal oceanographic tracer for investigation of movement, exchange and circulation of water masses. All these investigations and applications require an accurate determination of ^{99}Tc in various types of samples.

^{99}Tc is a pure β^- emitter with the maximum decay energy of 0.294 MeV. Therefore it can be measured by radiation counting [42]. The main technique for ^{99}Tc measurement is liquid scintillation counting (LSC). β-particle counting using gas flow proportional counter also can be used for this purpose. Due to the interference by matrix components (e.g. quenching during LSC analysis) and the spectrometric interference from other especially β emitting radionuclides, a thorough chemical separation of ^{99}Tc from the matrix and other radionuclides is required before measurement. Anion exchange chromatography and co-precipitation are widely used to pre-concentrate ^{99}Tc from samples [42; 43]. For further purification, solvent extraction is often applied to separate ^{99}Tc from other interfering radionuclides. In recent

years extraction chromatography using TEVA-SpecTM (TEVA) resin has been employed to purify ^{99}Tc from the interfering radionuclides [44]. The long half-life, and therefore low specific activity, of ^{99}Tc (0.64 Bq/ng) makes mass spectrometry a potentially sensitive method for measurement of ^{99}Tc. Accelerator mass spectrometry (AMS) [45], thermal ionization mass spectrometry (TIMS) [46] and inductively coupled plasma mass spectrometry (ICP-MS) [47; 48] have been applied for ^{99}Tc measurement as well. Among these techniques, ICP-MS is the most widely and frequently used mass spectrometric method for measurement of ^{99}Tc in many types of environmental samples due to its relatively low cost and accessibility as compared to other mass spectroscopy techniques. The main challenge in ^{99}Tc measurement by ICP-MS is the interferences of isobars and molecular ions. At the mass of 99 the stable isotope ^{99}Ru and the molecular ion $^{98}Mo^{1}H$ are the main interferences in the measurement of ^{99}Tc using ICP-MS. Highly efficient methods for purification of ^{99}Tc from these interferences before measurement are necessary. The chemical separation techniques used for radiometric methods can also be applied in the mass spectrometric determination of ^{99}Tc with main focuses on the removal of stable isotopic interferences with the mass of 99 atomic mass units [49].

2.2.3. Technetium redox chemistry

Technetium mobility in natural systems strongly depends on the redox state. Tc(VII) is frequently used under oxidizing conditions as conservative tracer, whereas Tc(IV) will form sparingly soluble oxyhydroxide solid phases. Numerous studies have been devoted to describing stability fields of the various technetium species in terms of Eh and pH. An early work by Bondietti and Francis [50] on a variety of natural samples showed considerable retention (by TcO_4^- reduction) in accordance with Eh/pH conditions. The potential of the TcO_4^-/TcO_2 couple was described with the equation (10):

$$E^0(TcO_4^-/TcO_2) = 0.738 - 0.0788 \times pH + 0.0197 \times \log\,[TcO_4^-] \qquad (10)$$

The fundamental stability quantification of reduced and oxidized technetium is achieved by measuring of the electromotive force of the TcO_4^-/TcO_2 couple [51]. Electromotive force of the TcO_4^-/TcO_2 couple was studied in several papers [52-54] and then reviewed by Rard et al. [55]. He found, that some results of these works were irrelevant due to the oxygen traces in the reaction cell, unachieved equilibrium, or lack of reversibility evidence. The pH-range in the experiments was between 1.05 and 3.99 with only a couple of measurements conducted at pH greater than 4. Main part of the data discussed by Rard et al. [55] was taken from the work of Meyer and Arnold [54]. In this investigation Meyer and Arnold [54] determined

experimentally the standard potential of the TcO_4^-/TcO_2 couple, which is represented by following reaction:

$$TcO_4^- + 4H^+ + 3e^- \rightarrow TcO_{2\,(s)} + 2H_2O \quad (11)$$

Anoxic atmosphere was established by conducting the experiments in an argon glove box. $TcO_2 \cdot nH_2O$ was prepared by electrodeposition on a platinum mesh. Steady state values were presented increasing confidence in the results. The plotted slopes of electrode potential vs. pH and activity of TcO_4^- were reported to be -0.0773 ± 0.0023 V/pH unit, which is in a good agreement with the theoretical slope of -0.0788 V/pH unit taking into account experimental uncertainty. Based on these results, the value of E° was reported to be 0.747 ± 0.004 V, and this value overlaps with E = 0.746 ± 0.012 V recommended by Rard et al. [55].

Technetium retention and mobility in the natural environment mainly depends on the redox conditions of the system. According to the published data [56], typical agricultural and horticultural soils have redox potential values between 100 and 600 mV with pH values from 4 to 8. In normal soil, nitrate reduction begins at Eh ~ 450 – 550 mV and Mn^{2+} formation is initiated between 450 to 350 mV. For wet soils, O_2 and NO_3^- are no longer detectable already at 230 and 320 mV, respectively. Formation of Fe(II) commences around 150 mV. For waterlogged soil, S^{2-} is starting to form at -50 mV and at -180 mV SO_4^{2-} is no longer detectable. Tc(VII) reduction at neutral pH values occurs between 200 and 100 mV [57], which is close to the conditions of Fe(II) formation and NO_3^- reduction [51].

Plant growth is optimal in soils with pH within 7.5 – 5.5 range and Eh values ~ 600 – 100 mV [56], which corresponds to TcO_4^- stability region, where technetium is the most mobile. However, in some cases technetium is present as Tc(IV), for instance, after uptake by plants [58-60]. These deviations from expected redox behaviour can be explained by the influence of biogeochemical processes or Tc(VII) reduction by organic compounds. Furthermore, even under the redox conditions of the system within the Tc(IV) stability field in some cases technetium still remains +7 oxidation state. These findings are most likely explained by the availability and steric distribution of electron donors, which are more critical than the measured redox potential. For instance, Cui and Eriksen [61] have shown that the reduction kinetics of Tc(VII) could be very slow even in the solutions containing high concentration of Fe^{2+} ions. Thus, even though the homogeneous reduction

$$Tc(VII)O_4^- + 3Fe^{2+} + (n+7)H_2O \rightarrow Tc(IV)O_2 \cdot nH_2O_{(s)} + 3Fe(OH)_{3\,(s)} + 5H^+ \quad (12)$$

is thermodynamically feasible (log K_{298} = -21.8) [62], the process is kinetically limited. The three electrons needed for the Tc(VII) reduction requires a high electron density for the reaction, which is limiting the overall kinetics. However, when Fe(II) is sorbed onto other minerals, surface-mediated heterogeneous Tc(VII) reduction takes place with much faster kinetics under pH > 6. This effect is even more pronounced for the iron-containing mineral phases [12; 15; 16]. According to this information, technetium behaviour strongly depends on the presence of iron species in the system. In the environment ferrous iron formed by microorganisms through the biochemical processes may play a significant role in Tc immobilization. Thus, even when pH/Eh conditions in the solution are not sufficient for Tc(VII) reduction, the process may take place on the Fe(II) containing solid mineral surface [51].

Under anoxic conditions Tc(IV) is not re-oxidized over an observation period of 220 days and an oxidation rate of 1.49-1.86×10^{-9} mol/(L×d) was determined under aerobic conditions in the medium of simulated granitic water [63].

2.2.4. Solubility and colloids formation

The solubility of Tc(VII) in pertechnetate-ion form is rather high but decreases in presence of bigger cations. $NaTcO_4$ has a solubility limit of 11.299 mol/kg at 25 ºC, NH_4TcO_4 0.594 mol/kg, $KTcO_4$ 0.104 mol/kg, $CsTcO_4$ 0.017 mol/kg, $TlTcO_4$ 0.0025 mol/kg [55].

Dissolution of $TcO_2 \cdot nH_2O$ described with equation (13)

$$TcO_2 \cdot nH_2O_{(s)} \rightarrow TcO(OH)_2 + (n-1)H_2O \quad (13)$$

has been investigated by several authors [13; 64] and the data was summarized by Rard et al. [55]. Some solubility measurements have been hampered by a number of factors. First, measurements must be made in a low-oxygen environment. Experiments that have been carefully performed to minimize the oxygen concentration report relatively low solubilities. Second, the effects of radiolysis must be taken into account. For example in Meyer et al. [13] it was found that radiolysis of the water near the surface of the $TcO_2 \cdot nH_2O$ crystals caused oxidation and dissolution of the solid to yield TcO_4^-. Analyses of the solution by liquid scintillation counting that ignored this quantity of TcO_4^- would yield spuriously higher solubility values. Meyer et al. [13] remedied this by separating TcO_4^- out of solution using tetraphenylarsonium chloride in chloroform. Third, the solubility depends on the crystallinity of the $TcO_2 \cdot nH_2O$. The solubility of amorphous technetium dioxide (TcO_2(am)) is about a factor of 10 times higher than that of crystalline $TcO_2 \cdot nH_2O$ [55]. Considering these caveats,

the accepted value of solubility of $TcO_2 \cdot nH_2O$ at 25°C in dilute solutions between pH 4 to pH 10 is $10^{-8.2}$ mol/L [64] to $10^{-8.44}$ mol/L [55], which reflects the uncertainty of experimental data. This translates into 621.6 Bq/L ^{99}Tc (as $TcO(OH)_2$ in neutral pH waters) in equilibrium with the hydrated crystalline TcO_2 phase, which is about 20 times higher than the drinking water standard (DWS) of 33.3 Bq/L established by the EPA. Accordingly, any remediation scheme that relies simply on reduction and precipitation of a TcO_2 solid will still result in concentrations of aqueous Tc above the drinking water limit [51].

The solubility of $TcO_2 \cdot nH_2O$ increases under acidic conditions. In the pH range from 4 to 0, the solubility of $TcO_2 \cdot nH_2O$ increases by nearly a factor of 104. Between pH 2.43 and 1.37 the dominant aqueous species is $TcO(OH)^+$ and below pH 1.37 the dominant aqueous species is TcO^{2+}. The solubility (K_s), hydrolysis (K_{h1} and K_{h2}), and dimerization (K_{dim}) constants are listed in equations (14) - (17):

$$TcO_2 \cdot nH_2O + (1-n)H_2O \rightarrow TcO^{2+} + 2OH^- \qquad K_s = 4.47\times10^{-33} \qquad (14)$$

$$TcO^{2+} + H_2O \rightarrow TcO(OH)^+ + H^+ \qquad K_{h1} = 4.3\times10^{-2} \qquad (15)$$

$$TcO(OH)^+ + H_2O \rightarrow TcO(OH)_2 + H^+ \qquad K_{h2} = 3.7\times10^{-3} \qquad (16)$$

$$2TcO(OH)_2 \rightarrow [TcO(OH)_2]_2 \qquad K_{dim} = 3.14\times10^{6} \qquad (17)$$

Based on the rom experimental data for both acidic and basic conditions, the average stoichiometry of n in equation (14), is 1.63 ± 0.28 [13].

$TcO_2 \cdot nH_2O$ solubility was also investigated under neutral to basic conditions by Eriksen et al. [64]. The values determined by these authors over the same pH conditions as in Meyer et al. [13] overlap within experimental uncertainty. Eriksen et al. [64] reported that at pH within the range from 10 to 12 the $TcO_2 \cdot nH_2O$ solubility increases by a factor of approximately 10 times. Based on these observations the authors described the dependency of the solubility on pH using following equation (18):

$$[Tc(IV)]_{tot} = K_{s1} + K_{s2}/[H^+] \qquad (18)$$

where $[Tc(IV)]_{tot}$ is the total amount of Tc(IV) species in the solution, $\log K_{s1}$ and $\log K_{s2}$ have the values of -8.16 ± 0.06 and -19.2 ± 0.3, respectively. Eriksen et al. also carried out experiments with addition of CO_2 in the system, which increased the solubility of $TcO_2 \cdot nH_2O$ approximately with a factor of 10 after increase of pCO_2 from 0 to 50 percent. The authors report the following equilibrium constants for $TcO_2 \cdot nH_2O$ complexes with CO_2:

$$TcO_2 \cdot nH_2O \rightarrow TcO(OH)_2 + (n-1)H_2O \qquad K_s = 6.76\times10^{-9} \qquad (19)$$

$$TcO_2 \cdot nH_2O + H_2O \rightarrow TcO(OH)_3^- + H^+ + (n-2)H_2O \qquad K_{s2} = 8.71\times10^{-20} \qquad (20)$$

$$TcO_2 \cdot nH_2O + CO_2 \rightarrow Tc(OH)_2CO_3 + (n-1)H_2O \qquad K_{s3} = 8.13\times10^{-8} \qquad (21)$$

$$TcO_2 \cdot nH_2O + CO_2 + H_2O \rightarrow Tc(OH)_2CO_3^- + H^+ + (n-2)H_2O \qquad K_{s4} = 4.47\times10^{-16} \qquad (22)$$

There are two points of view concerning solubility increasing due to presence of chloride-ions in solution. Meyer et al. [13] did not find evidence for an increase, whereas Hess et al. [65] concluded otherwise. These latter investigators reported that in chloride solutions of 1 mM to 5 M NaCl, the most stable complexes of Tc(IV) are negatively charged $TcCl_6^{2-}$ and neutral $TcCl_4$(aq). Lieser and Bauscher [57] reported the higher solubility limit for Tc(IV), however the conditions were more acidic. Generally, the data of the Hess and the Lieser groups are in a good agreement.

The aqueous Tc speciation under reducing conditions will be dominated by $TcO(OH)_2$(aq) in the pH range of interest. When increasing the redox potential of the system, technetium oxidizes and the aqueous speciation is dominated by the oxo-anion pertechnetate in a wide pH range [66].

Technetium concentration in groundwater is controlled by a solid phase of technetium dioxide ($TcO_2 \cdot 1.63H_2O_{(s)}$) even under very reducing conditions, as shown in Figure 6. Under oxidizing conditions, technetium is not solubility limited due to Tc(VII) formation.

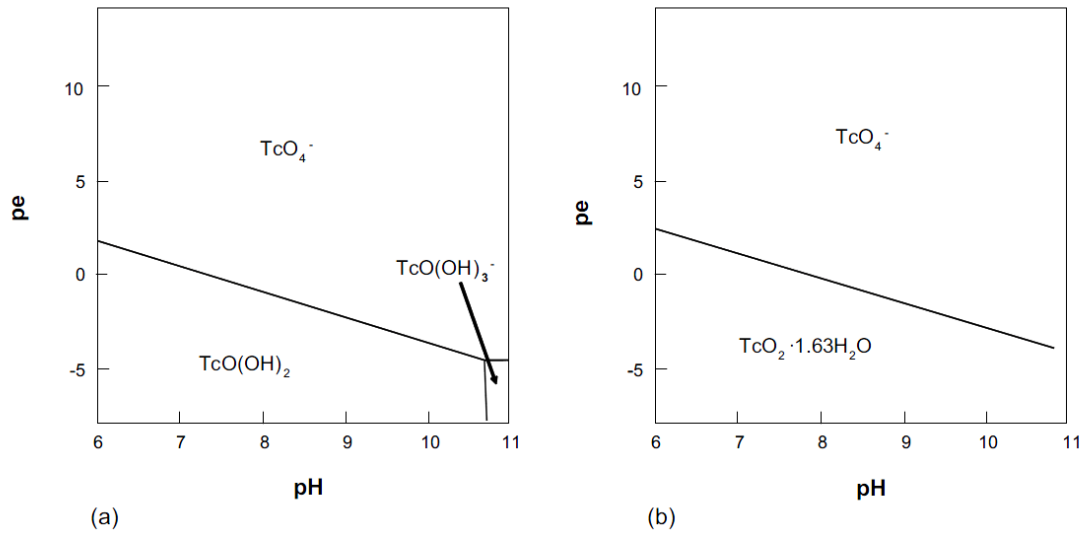

Figure 6. *pe/pH diagrams showing technetium species in liquid (a) and solid phases (b). [Tc] = 10^{-7} M. Based on Duro et al. [66].*

The higher stability of the aqueous species and the lack of pH influence on the solubility of technetium oxide is in agreement with the predominance of the $TcO(OH)_2$ species in the aqueous phase under near-neutral pH conditions (see Figure 7). The solubility increases in the alkaline range driven by the oxidation of the aqueous species to pertechnetate-ions. The small increase of the solubility observed in the neutral to acid range is due to the increase of the hydroxo-carbonate aqueous species in competition with $TcO(OH)_2$.

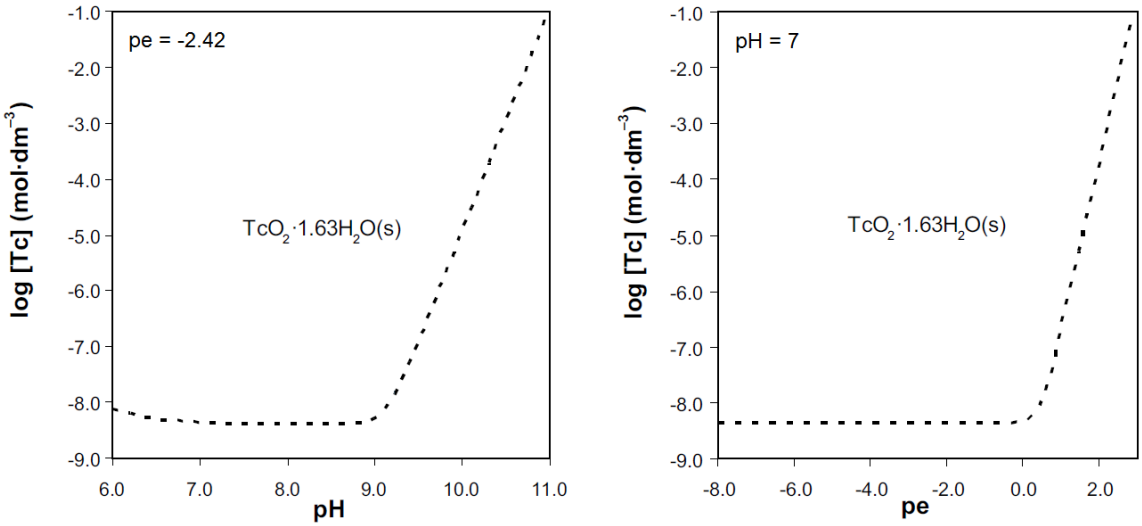

***Figure 7**. Solubility curve of $TcO_2{\cdot}1.63H_2O_{(s)}$ (a) as a function of pH (fixed pe = –2.42) (b) as a function of pe (fixed pH = 7), calculated by using the reference groundwater composition. Based on Duro et al. [66].*

The precipitation of metallic technetium is not generally considered due to the slow kinetics normally associated to the formation of metals from solution. Tc minerals are not found in nature. However, Tc oxides are easily formed in laboratory conditions while $Tc_{(cr)}$ is only obtained by prolonged reduction of previously formed oxides. Because of that, $Tc_{(cr)}$ is not presented as a possible solubility controlling phase. Under reducing conditions, the solubility limiting solid phase is the hydrous technetium dioxide.

Both batch-type sorption and column experiments (samples from the Nevada Test Site) [67] revealed that ^{99}Tc is highly mobile and shows virtually no retardation under fully oxidizing conditions in Hanford sediments [68] and consequently has been used to trace tank waste migration through the vadose zone. Under "mildly" reducing conditions distribution coefficient for ^{99}Tc changing from 1.22 to 378 L/kg. Solubility in carbonate-containing groundwater was found to be ~ 10^{-8}M $[Tc]_{tot}$.

Several investigators have reported formation of technetium colloidal phase at relatively acidic (pH ≤ 4) [57; 69] and under reducing conditions [70] for high initial technetium

concentrations (more than 10^{-5} M Tc). Sekine et al. [70] observed brown to brownish-black turbid solutions most probably due to the presence of colloidal particles. Technetium homologs, such as rhenium and ruthenium, may form domains or clusters of molecules at the same scale of colloids as well. However, generally for technetium this behaviour is not as usual as for ruthenium [71]. On the other hand, technetium is known to form dimers such as $[TcO(OH)_2]_2$ and even $[(H_2EDTA)_2Tc_2(\mu\text{-}O)_2]$, which can be synthesized in the presence of EDTA. In these dimers technetium in octahedral coordination is bonded with other octahedrons through double bridging between two ligands (i.e. edge-sharing polyhedra), rather than by direct metal-metal bonding. Sekine et al. [70] also showed that the technetium colloidal phase can be formed by the radiolysis of pertechnetate solutions under near-neutral or acidic conditions. In this case, radiolysis leads to Tc(VII) reduction and formation of Tc(IV) polymers and colloids, first as Tc(IV) aqueous species and then as $TcO_2 \cdot nH_2O$ phase for the higher pH values. Lukens et al. [72] found that exposure of pertechnetate solutions to the ionizing radiation can produce polymers with a structure similar to $(H_2EDTA)_2Tc_2(\mu\text{-}O)_2$, but under alkaline conditions. For this purpose the authors used Tc solutions containing citrate, dibutyl phosphate, and aminopolycarboxylates, similar to some of the organic matter in waste tanks at the Hanford site. X-ray absorption spectroscopy of the radiolysis products showed that the samples contained one-dimensional chains with bridging O atoms shared between two metal centres and water ligands in the *trans* position. Because of the tendency for colloids of technetium to form at concentrations above saturation, it is best to conduct solubility measurements from undersaturated conditions. Several investigators, such as Maes et al. [73], have studied the influence of colloidal phase on the geochemical behaviour of technetium. The authors established reducing conditions in the technetium containing groundwater solution and the resulting solution was equilibrated with natural sand from Gorleben (Germany). Based on the results, pertechnetate was rapidly reduced to Tc(IV) species, which were sorbed onto magnetite or pyrite grains. However, the concentration of technetium in the supernatant was much higher than expected and the authors attributed this to the presence of humic substances that increased the apparent solubility of technetium. A set of experiments in synthetic systems without the organic matter containing Gorleben sand was carried out with pure magnetite and pyrite mineral phases. In this case reduction kinetics were much slower, more than 200 days required before significant reduction was observed. According to the XANES analysis, after equilibration technetium was in the Tc(IV) oxidation state. As determined by EXAFS measurements, the technetium atoms were coordinated by

6.1 to 7.2 oxygen atoms at a distances of 2.01 to 2.03 Å, respectively. These results are in a good agreement with TcO_2-like structures proposed by Wharton et al. [74].

2.3. Tc sorption and migration

The term "sorption" implies here the quantity of chemical species immobilized at surfaces and by bulk solid material divided by the concentration of these species in the solution. Partitioning between solids and solution is generally assumed to take place under equilibrium conditions and is dependent on the solution composition (pH, Eh, temperature, concentration of competing ions, etc.) and solid phase characteristics (point-of-zero-charge, surface area, chemical nature of surface sites). Generally, this partitioning is quantified by the distribution coefficient (see paragraph 2.1.5.1) [51].

Although interaction of the dissolved ion with the solid phase is assumed to be surface sorption, there are a number of cases when precipitation occurs at the mineral surface, especially when the concentration of the aqueous species is relatively high. Accordingly, sorption should be regarded as an empirical value rather than a mechanistic description. Because technetium is also redox sensitive, its partitioning behaviour will depend on the Eh of the system and the presence of reducing agents, such as organic matter or inorganic compounds (Fe^{2+}, S^{2-}, etc.). As previously discussed, Lieser and Bauscher [57] have reported that reduction of Tc(VII) to Tc(IV) takes place between 200 and 100 mV at circumneutral pH values.

The behaviour of Tc(VII) and Tc(IV) concerning the accumulation at the solid surface is dramatically different due to low solubility of Tc(IV) and different charges of ions in solution. Pertechnetate sorbs poorly onto typical soil materials whereas Tc(IV) sorbs strongly onto a variety of materials. If Tc(VII) is reduced to Tc(IV), the sorption (almost irreversible) will increase by a factor of 103 [57]. Further, Tc(IV) is also prone to sorb onto FeS_2 [75], although it is not clear if the adsorbed technetium forms a Tc-S bond. Based on the work of Lukens et al. [76] and German et al. [77] reaction of Tc(VII) with S^{2-} yields polysulfides with a stoichiometry of Tc_3S_{10}.

Shallow aquifers are assumed to be in contact with the atmosphere, and because most arable soils display Eh values in the mildly oxidizing to oxidizing range [56], most sorption experiments are conducted under aerobic (oxidizing) conditions. Results of sorption experiments have demonstrated that pertechnetate uptake onto solid phases is low. For

example, Wildung et al. [78] have reported that 22 different soils equilibrated with pertechnetate for 24 hours yielded K_d values of 0.007 to 2.8 L/kg for ~ 10^{-7} M Tc. Subsequent studies under aerobic conditions yielded similar results. These results reflect the electrostatic repulsion between the negatively charged pertechnetate anion (TcO_4^-) and the negative surface charge carried by sedimentary materials (especially silicates at near-neutral pH values. Slightly positive to negative K_d values (-0.16 to +0.11 L/kg) for soils sampled from the Hanford Site, Washington State were reported by Kaplan and Serne [79]. Negative K_d values are possible because of the principle of excluded water. Water molecules will orient themselves with the positive end of their dipole towards the negatively charged mineral surface and, depending on the properties of the metal—oxygen surface species and ambient solution pH, a zone of structured water develops that repels negatively charged species, such as pertechnetate. Solution extracted from the experiment will typically not include the water sorbed at the surface of the mineral grains, so the pertechnetate is concentrated in the sampled "excluded" bulk solution. Thus, the concentration of pertechnetate in the final compared to the beginning solution may be higher, yielding negative K_d values (see equation (9)).

The observations in the natural reactor in Oklo indicate a very slow Tc migration due to precipitation or mineralization of Tc(IV) compounds [80]. Only a small fraction of ^{99}Tc have migrated from the uraninite layer during the time the natural reactor was running (which was 5×10^5 years) and afterwards during the ^{99}Tc decay [81]. Since ^{99}Tc has already decayed there, Tc retention was investigated by comparison of ^{99}Ru distribution to the distribution of other Ru isotopes.

2.3.1. Sorption on natural organic matter

A number of investigators [82-84] have reported a strong interaction between technetium species and organic materials (i.e., humic acids), with relatively high K_d values. It seems that pertechnetate is reduced to Tc(IV) oxidation state in the presence of organic matter, and treatment by hydrogen peroxide results in re-oxidation of technetium back to the Tc(VII) form. Thus, of technetium affinity to organic-rich soils may be much stronger than extraction using H_2O_2 would indicate due to high reducing capacity of the material. However, Geraedts [85] show that there is no direct interaction between pertechnetate and humic substances (HS), and for the complexing with HS Tc(VII) should be reduced first via a surface catalysed reaction. XANES investigation of the obtained products shows the presence of Tc(IV) [82].

Immobilization of Tc(VII) by organic matter under oxidizing conditions without reduction to Tc(IV) was shown by Kim t al. (2004) [86]. Using Re as a chemical analogue of Tc authors have shown a significant retention onto positively charged functional groups of organic polymers, namely amine $–NH_2$ group. Polymers with negatively charged groups (e.g. –COOH, $–SO_3H$) show no detectable interaction with ReO_4^-. The sorption mechanism of perrhenate onto cationic functional groups of the polymers was described as the ion pair formation in the diffuse double layer between positively charged surface groups and ReO_4^- anions in the solution. This process was found to be highly dependent on pH, ionic strength and the concentration of competing anions (the effect of NO_3^- concentration was investigated) [86].

2.3.2. Sorption on clays

Immobilization of Tc(VII) due to its reduction to the Tc(IV) state also was found in clay systems. Baston et al. [87] described the behaviour of technetium in an experimental setup which is simulating the reducing conditions expected for technetium disposal in Boom Clay. A pore water, presumably in equilibrium with the clay material, contains high amounts of organic matter as well. The pH of the system is near neutral (around 8) and the redox potential value was reported as -230 mV, which is in the Tc(IV) species stability field. Therefore, introduction of Tc(VII) to the system resulted in reduction and the authors proposed further Tc(IV) precipitation as the most probable mechanism for this immobilization of technetium. After filtration at 30,000 MWCO performed for removal of organic matter, Tc(VII) did not possess any sorption precipitation. Migration experiments yielded calculated K_d values from 0.8 to 1.8 L/kg, which are larger than the values typically reported in pertechnetate sorption studies. The same pattern of technetium distribution emerges from studies of marine sediments and suspended particulate matter. In near-surface waters, conditions are oxidizing and technetium is in the pertechnetate form. Distribution coefficients of less than 1 L/kg have been reported for pertechnetate distribution in seawater and suspended particles [88]. On the other hand, much higher K_d values were reported for sorption of technetium in reduced marine environments. Typical K_d values for technetium partitioning between marine sediments and seawater are between 10^2 and 10^3 L/kg. For example, McCubbin et al. [88] reported K_d values between approximately 3×10^2 L/kg and approximately 5×10^3 L/kg for the Irish Sea sediments sampled between 1995 and 2002. However, the presented K_d values were calculated based on technetium concentration in seawater, which can differ from the concentration in the pore water contacted with the mineral phase. McCubbin et al. emphasize

that the obtained distribution coefficients are about an order of magnitude larger than those obtained from experiments. The authors suppose that equilibrium between technetium species and the mineral phase in seawater was not achieved and K_d values in this system are kinetically governed.

Jansson and Eriksen [89] showed that in some spots in compacted clay (MX-80), the activity after equilibration was significantly higher than in general at the surface, which may be explained by selective reduction of some TcO_4^- by Fe(II)-containing minerals in the bentonite. However, in spite of strongly reducing groundwater conditions, technetium was found to diffuse mostly unreduced as TcO_4^-. The apparent anion diffusivity for the intra-lamellar diffusion was found to be 8.6×10^{-11} m^2/s for iodide with a capacity factor of 0.1, while the apparent diffusivity for the diffusion in external water was found to be 5×10^{-14} m^2/s with α = 2.26. The corresponding values for Tc were found to be $D_a = 6\times10^{-11}$ m^2/s, α = 0.1 and $D_a = 1\times10^{-13}$ m^2/s, α = 0.46, respectively. For pure bentonite Ramebäck et al. [90] have shown that the concentration profiles were very similar using different diffusion times. This is consistent with a partial reduction of Tc(VII) to Tc(IV) in the bentonite clay. From concentration profiles for technetium after 3 months of diffusion into the clay, an apparent diffusivity of 9.9×10^{-13} m^2/s was evaluated. However, after one year of diffusion, the apparent diffusivity was found to be by a factor of three lower. After six years of diffusion, an even lower value for D_a was found (6.1×10^{-14} m^2/s). The decrease in D_a after longer diffusion times differed by a factor almost corresponding to the ratio between the experiment times, again confirming the presence of kinetics prevailing.

2.3.3. Sorption on iron oxides

Zachara and co-authors [14-16; 68] have shown that the rate of Tc(VII) reduction at low Fe(II) concentrations in the solid phase (here ~ 250 µmol/g) decrease from pH 7.0 to 8.5. At high Fe(II) concentrations (~ 1750 µmol/g) the Tc(VII) reduction rate was pH independent. The authors argue that the non-structural Fe(II) (~ 350 µmol/g) was several times higher than the site density available for surface complexation, so the increasing Fe(II) in the precipitated (as $Fe(OH)_{2(s)}$) and ion exchange sites with increasing pH would not contribute significantly to the overall available Fe(II) content. In addition, the high Fe(II) concentrations may drive the Tc(VII) reduction so fast that pH-dependent differences may not be distinguishable.

According to the work of Peretyazhko et al. [15] at low pH (<6) Fe(II) speciation is dominated by surface complexed species and at high pH (>8) the precipitated and ion

exchange forms become more important. The heterogeneous reduction of Tc(VII) by Fe(II) adsorbed on the goethite and hematite was found to be orders of magnitude faster than the reduction by the Fe(II) adsorbed on the clays or by the reduced phyllosilicates.

Druteikienė et al. [91] compared Tc(VII) retention on hematite and magnetite at pH 8-9 and aerobic conditions. After 360 hours contact time with magnetite (40 g/L, ambient conditions) <1% of Tc(VII) remained in the solution, while hematite was not able to immobilize TcO_4^- within the same exposure time. Decreasing pH down to 2.7-4.5 increases the Tc(VII) retention on hematite, therefore the authors supposed that the process is pH dependent.

Haines et al. [92] showed by a Fourier transform infrared (FTIR) study that the reaction between TcO_4^- and magnetite occurs via surface-mediated reduction of TcO_4^- to Tc(IV) and by precipitation of Tc(IV) oxide on the Fe_3O_4 surface. The mechanism proposed is a positive electrostatic attraction by the magnetite surface for the TcO_4^-anions at pH values below the zero point of charge (zpc), which is around 6.5 [93].

Tc(VII) reduction to the insoluble Tc(IV) oxide is a three-electron process. Although stepwise one-electron transfer from the Fe(II) in solution is thermodynamically feasible, it is very improbable and kinetically hindered [94]. In the Fe(II)-bearing minerals the electron density is higher than in the solution, therefore the surface-mediated three-electron reduction is proposed by the authors as a dominating process.

In the work of McBeth et al. [95] several Fe(II)-containing biogenic minerals including bio-magnetite were investigated regarding there interaction with Tc(VII). Under the anoxic conditions applied (bicarbonate buffered pH ~ 7, 7 mM $[Fe(II)]_{tot}$, 1-5 µM $[Tc]_{tot}$) technetium was almost fully accumulated at the magnetite after two weeks contact time.

EXAFS investigations of Tc interaction with magnetite show that Tc(VII) after reduction to Tc(IV) can be incorporated into the magnetite structure [96; 97]. Tc(IV) and Fe(III) in octahedral site have similar ionic radii of 0.78 pm, so that Fe(III)-Tc(IV) substitution is feasible from the crystal chemistry point of view. The higher positive charge of the substitute is compensated by the increase of Fe(II)/Fe(III) ratio in the matrix, probably via coupled Fe(III)-Fe(II) substitution or creation of the vacancy sites in the crystalline structure [96].

Tc(VII) sorption onto magnetite under highly saline conditions performed by Yalcintas et al. [98] yielded R_d value of 10^3 L/kg (pH 8.7, 4.5 M $MgCl_2$, Eh = 10 mV). XANES investigations shown that Tc(VII) was reduced to Tc(IV).

2.3.4. Sorption on granitic rocks

The migration of ^{99}Tc in crystalline rock formations is a very important topic concerning the isolation of long-lived radionuclides in HLW deep geological disposals from the biosphere. ^{99}Tc was considered to be almost non-sorbing to host rock minerals, on the basis of experimental data obtained under aerobic conditions. However, there are as well experimental observations indicating that pertechnetate can be reduced to the less mobile Tc(IV) oxidation state in the presence of igneous rocks like basalt and granite [50].

In the early sorption studies performed in connection with the final nuclear waste disposal Tc was considering to exist solely as pertechnetate, because all experiments were performed under oxidizing conditions. The sorption of Tc was explained as ion exchange and supposed to be almost zero in rocks. Fried et al. [99] have reported K_d values of 0.52 L/kg for Tc sorption on the granite under aerobic conditions. But further investigation have shown that some deaerated systems containing biotite, chlorite, hornblende, pyrite and magnetite can sorb significant amounts of Tc [81].

Technetium reduction/sorption behaviour on the granitic bedrock has been studied by Allard et al. [100]. Batch studies were performed under aerobic conditions and a K_d value of < 1 L/kg was obtained, while the addition of 20 ppm Fe(II) to the groundwater simulant increased the distribution coefficient up to 50 L/kg. Fe(II)-containing minerals (e.g. magnetite) and S^{2-}-containing ones (e.g. galena) were reported to have a reducing effect on Tc(VII) in solution even after short contact time and after longer exposure even higher K_d values could be obtained. In the experimental system apparently the reduction from heptavalent TcO_4^- to tetravalent $TcO_{2(s)}$ is kinetically hindered. The authors also emphasized that most other investigations dealing with Tc sorption have been performed in aerated water systems where no reduction can occur, which is not representative for the actual repository conditions.

The batch experiments on granitic rock and fracture filling material (FFM) from Stripa Mine (Sweden) performed by Cui and Eriksen [61] shows a slow Tc reduction (0.0012 ± 0.0002 d^{-1} for granite and up to 0.0040 ± 0.0003 d^{-1} for FFM). Faster reduction in the case of FFM is explained by the higher Fe(II) content (f_{FeO} = 0.0082 for granite and 0.036 for FFM). The experiments were carried out under 1% H_2/Ar atmosphere with solid to liquid ratio of 95 g/L. Desorption of the reduced/sorbed Tc by argon-purged and even air-saturated groundwater was found to be a very slow process, and the Tc concentration during the leach solution corresponded to the solubility of $TcO_2 \cdot nH_2O$. Addition of H_2O_2 with a final concentration of 3 M increased the amount of recovered technetium.

^{99}Tc diffusion experiments through granite from Gansu Beishan (China) were performed by Liu et al. [101] under aerobic and anoxic conditions ($[TcO_4^-] = (2.5 - 9.8)\times10^{-8}$ M). According to the results obtained, the apparent diffusion coefficient of technetium under anoxic conditions is smaller than that under aerobic conditions and decreases with the increase of reductive component content in the crystalline rock material, i.e. Fe(II). K_d values were varying from 0.118 ± 0.014 L/kg for aerobic conditions to 0.315 ± 0.015 L/kg for anoxic ones.

Batch-type sorption experiments on freshly broken Äspö granite performed by Kienzler et al. [102] under natural groundwater conditions (no dissolved Fe found presumably because groundwater was re-oxidized during transport) with 7×10^{-7} mol/L Tc(VII) revealed low K_a values of 0.210±0.013 m for ^{99}Tc ($t_{contact}$ = 14 d), whereas altered material showed even lower values. It was stated, that Tc retention is not necessarily correlated to high Fe concentrations in the mineral phases. XPS analyses of granite sorbed Tc show a clear shift of Tc binding energy indicative to a reduced redox state compared to the initial Tc(VII) species. Significant Tc sorption was observed both onto iron containing areas and onto areas free of Fe. This is explained by the fact that Tc undergoes reduction in the solution and that the solid surface is not a requirement for the reduction of Tc(VII) to Tc(IV). On the other hand, Videnska and Havlova (2012) [103] have found a relationship between Tc sorption values and the mineral composition of the solid phase. Granitic rocks from the Bohemian Massive (Czech Republic) were used. Even under aerobic conditions Tc K_d values for crystalline rocks with a high concentration of mica minerals (approx. 13%) reached 8.6 L/kg, while on the samples with less mica minerals K_d was < 0.1 L/kg.

Äspö *in-situ* and laboratory migration studies (CHEMLAB-2) done prior to the CROCK project (http://www.crockproject.eu/) using Äspö derived natural groundwater revealed ~ 1% Tc recovery of the injected quantity after 254 days residence time of the Tc containing aqueous solution in a fractured granite core [102; 104].

According to the literature survey, the main factor in the Tc mobility behaviour is the reduction potential of the media. Tc(VII) reduction kinetics and sorption capacity is generally correlated with the Fe(II) content in the solid phase or/and in the groundwater. The existing published data on Tc apparent distribution coefficients and apparent diffusion coefficients in natural rocks and soils are scarce and vary by orders of magnitude, whereby relevant pH/Eh conditions often are not reported. The rock materials used in the literature are frequently

oxidized by air, which, however, is not relevant for the natural reducing far-field conditions of a repository.

Hence, a comprehensive research of Tc interaction with well-preserved crystalline rock material is needed for the reliable prediction of Tc migration in natural host rock formations.

3. Materials and Methods

3.1. Materials

3.1.1. Radionuclides

3.1.1.1. Tc isotopes

For batch sorption and migration studies with Tc concentration ≥ 10^{-9} M the stock solution of 13mM $Na^{99}TcO_4$ received from the Institute of Hot Chemistry, Nuclear Research Centre (now KIT) (Karlsruhe, Germany) was used.

For experiments with Tc concentrations lower than 10^{-9} M, the ^{95m}Tc isotope with a much shorter half-life (61 day) and a gamma emission line at 204.1 keV was applied. The isotope was produced by proton irradiation of a Mo foil (50 μm thickness) containing the natural isotopic composition at ZAG Zyklotron AG (Karlsruhe, Germany). After cooling the foil was transported to the Institute for Nuclear Waste Disposal (KIT-INE) and processed to separate technetium.

3.1.1.2. Other radionuclides

For core migration studies tritium (^{3}H, $t_{1/2}$ = 12.32 years) as tritiated water (HTO) was used as a conservative tracer. HTO was provided by the Tritium Laboratory Karlsruhe (TLK) of the Institute for Technical Physics, Karlsruhe Institute of Technology (KIT) (Karlsruhe, Germany).

The anion exclusion effect was investigated using ^{36}Cl ($t_{1/2}$ = 3.01×10^5 years) isotope in the form of a NaCl standard solution (Eckert&Ziegler Nuclitec GmbH, Braunschweig, Germany).

3.1.1. Iron oxides

3.1.1.1. Magnetite

Magnetite was synthesized in accordance with the procedure described in Schwertmann and Cornell (2000) [105] and produced at KIT-INE by oxidation of a Fe(II) solution under argon atmosphere in a glovebox. The amount of 80 g of $FeSO_4\times7H_2O$ was dissolved in 560 mL of MilliQ water (bubbled beforehand with Ar) in an 1 L glass beaker, and heated to 90º C (controlled by a thermocouple) in the water bath. Once the reaction temperature was reached, 250 mL of oxygen-free solution containing 44.9 g KOH and 6.46 g KNO_3 was added using a

drop-funnel during approx. 20 min. Then the reactor was heated for additional 30 min and cooled overnight. The product was purified by dialysis throughout 3 months with daily water change.

Synthesized magnetite was fully characterized with Raman spectrometry (Figure 8), XRD (Figure 9), XPS (29% Fe(II) were found; ideal value: 33% (Fe(II)), SEM (Figure 10) and BET (10.96 m^2/g specific surface area).

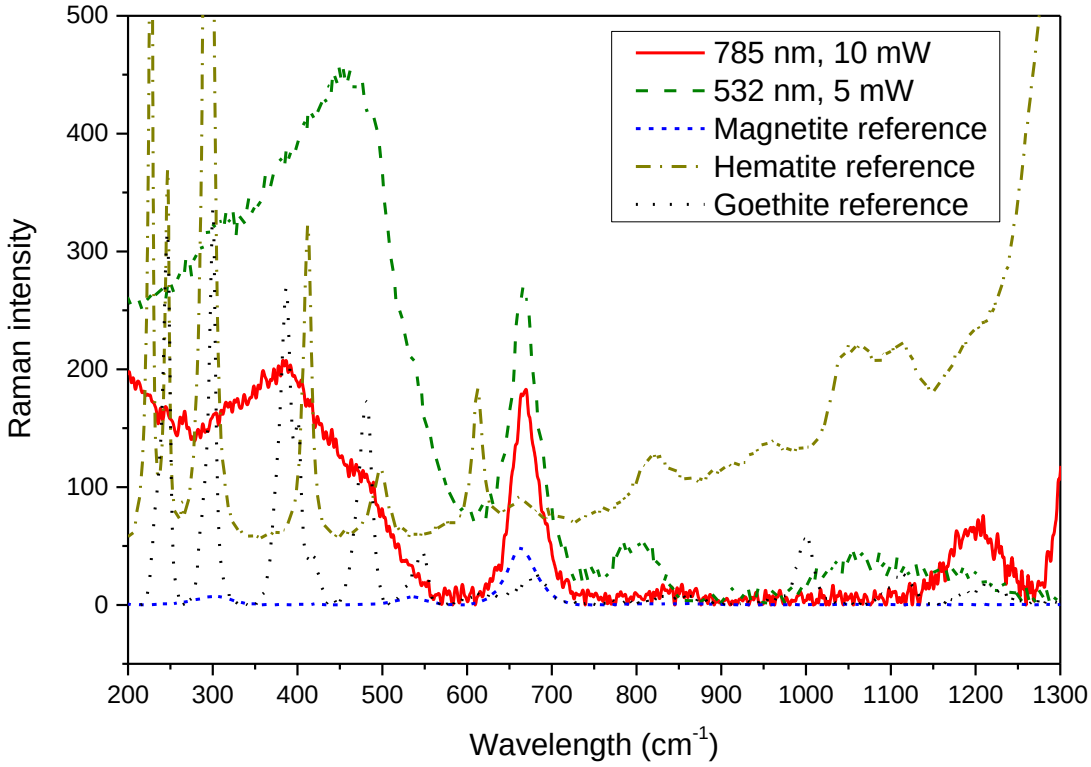

Figure 8. *Raman spectra of synthesized magnetite compared to the reference spectra of magnetite, hematite and goethite. All reference spectra were measured at 532 nm, 150 mW.*

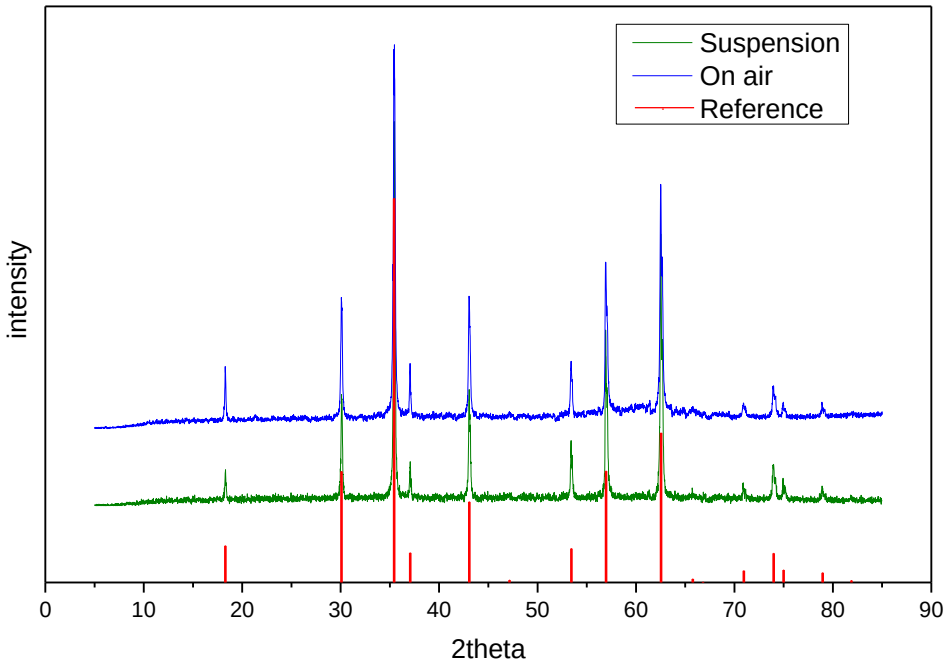

Figure 9. *XRD spectra of fresh magnetite (green), stored in air (blue) and reference magnetite lines (red).*

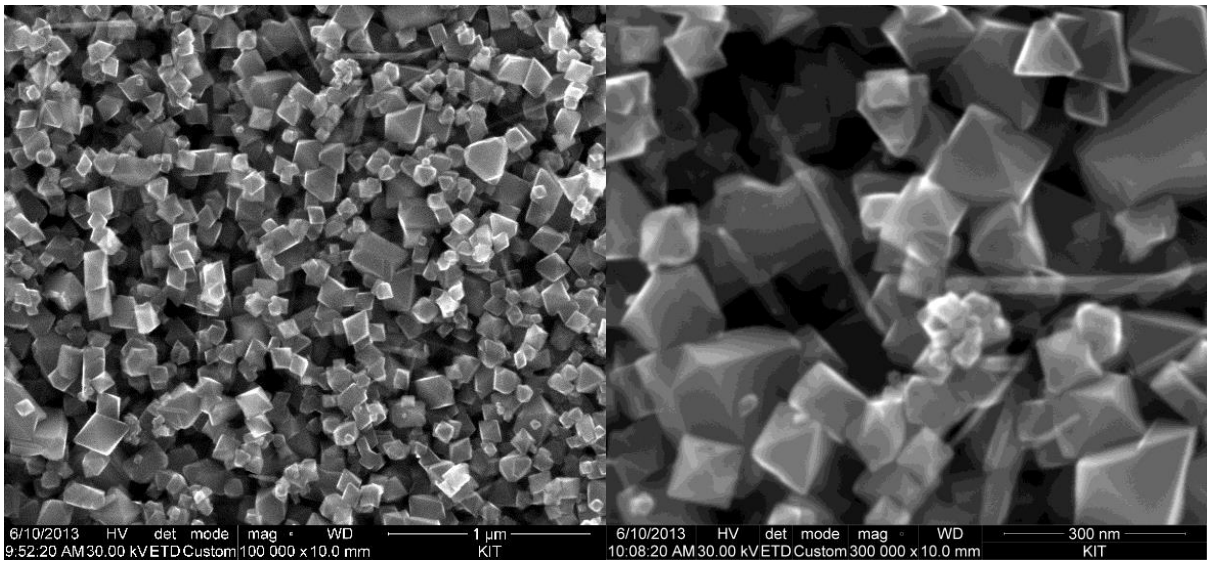

Figure 10. *SEM pictures of magnetite.*

The particle size measured with SEM is 100 – 200 nm. Some smaller needle-shaped crystals (see Figure 10, right) might be attributed to a minor goethite (α-FeO(OH)) fraction.

Raman spectra of the sample contain only the characteristic feature of the magnetite at ~ 664 cm^{-1} without any additional peaks from another Fe-O phases. XRD analysis verified that the pure magnetite without other iron oxides phases was synthesized.

Using the Scherrer equation (equation (23)) the mean crystallite size can be derived from the XRD spectrum [106].

$$\tau = \frac{K_{sch}\lambda}{\beta \cos\theta} \tag{23}$$

where τ is the mean size of the ordered (crystalline) domains (nm), K_{sch} is the Scherrer constant (a dimensionless shape factor), λ is the X-ray wavelength (nm), β is the full width at half maximum (FWHM) value of the XRD diffraction line (radians) and θ the Bragg angle (radians).

The typical value of the shape factor is 0.9 [107], the X-ray wavelength of the Cu K_α source is 0.154056 nm, β and θ are the experimental values taken from the spectrum. The mean crystallite size derived from the XRD spectra is similar for un-oxidized magnetite with 38±8 nm and for the material dried underair with 36±8 nm, respectively. The lower size in comparison to the one derived from the SEM measurements is explained by several factors. Firstly, the calculation with the Scherrer equation (23) does not take into account the instrumental broadening of the peaks. Secondly, the particles seen on the SEM picture can consist of several agglomerated crystallites. Also, the type of the shape factor K_{sch} may differ from the real values for various crystalline structures. In the present work the K_{sch} value of 0.9 was chosen.

The cell parameter *a* can be calculated by the Bragg's law (equations (24) and (25)):

$$\mathrm{d}_{hkl} = \frac{\lambda}{2\sin\theta} \tag{24}$$

$$\mathrm{d}_{hkl} = \frac{a}{\sqrt{h^2 + k^2 + l^2}} \tag{25}$$

The obtained values of the *a* parameter (8.392±0.002 Å and 8.393±0.002 Å for un-oxidized suspension and for the sample dried on air, respectively) are similar to the reference value (8.394 Å in JCPDS Card No. 79-0417)

Partially oxidized magnetite was prepared by adding hydrogen peroxide (H_2O_2) solution to the magnetite suspension. Fe(II) oxidation by H_2O_2 is described by equation (26).

$$2Fe^{2+} + H_2O_2 + 2H^+ = 2Fe^{3+} + 2H_2O \tag{26}$$

In accordance with this equation hydrogen peroxide amounts were added to oxidize from 1% to 10,000% (100 times excess) of total Fe(II) in the magnetite sample. Based on the technique described by Gorski et al. [108], the magnetite suspension was mixed with H_2O_2 solution and

allowed to react for one day on a shaker. Then the solid phase was separated by centrifugation (5,000 rpm, 15 min) and washed with MilliQ water 5 times to remove the unreacted hydrogen peroxide. In order to estimate Fe(II)/Fe_{tot} ratio in each sample partially oxidized magnetite was analysed with XPS as described in 3.2.7.1 section below.

3.1.1.2. Maghemite

Maghemite was produced from the magnetite applying the technique of Schwertmann and Cornell (2000) [105]. The magnetite suspension prepared as described above was frozen and dried under vacuum (freeze-drying technique). The powder obtained was heated in a ceramic crucible in a furnace at 250 °C for 2 hours and then milled in a mortar.

The structure of the synthesized maghemite was verified with XRD analysis (see Figure 11). The specific surface area was found to be slightly increased in comparison to original magnetite samples (N_2-BET, 12.65 m^2/g). The Fe(II) content and BET surface for magnetite and maghemite is shown in Table 3.

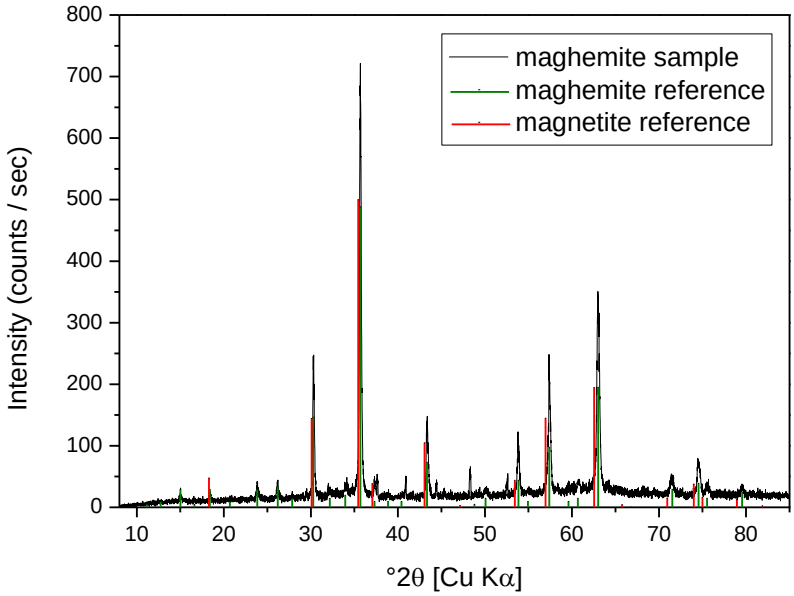

Figure 11. *XRD spectrum of synthetic maghemite.*

Table 3. *Characterization of synthetic magnetite and maghemite used in the present study.*

	S_{BET}, m^2/g	Fe(II)/Fe(tot)
Magnetite	10.96	29%
Maghemite	12.65	0%

The main differences between XRD spectra of magnetite and maghemite are in the additional peaks in the range of Bragg angles between 20º and 30º for maghemite. Furthermore, there is a small shift in the peak position to higher angles for maghemite due to the additional vacancies(□) through the oxidation of Fe(II) according to the equation (27) [105]:

$$\frac{8}{9}\mathrm{Fe}_3O_4 + \frac{2}{9}O_2 \rightarrow Fe_{8/3}\square_{1/3}O_4 \qquad (27)$$

The colour of the material changes from black to red-brown upon oxidation from magnetite to maghemite.

The particle size calculated from the XRD spectrum using the Scherrer equation (23) is 30±5 nm. The size estimation from the SEM analysis (see Figure 12) yielded the same values of 100 – 200 nm like for the original magnetite. However, the particles are more aggregated than in the magnetite sample.

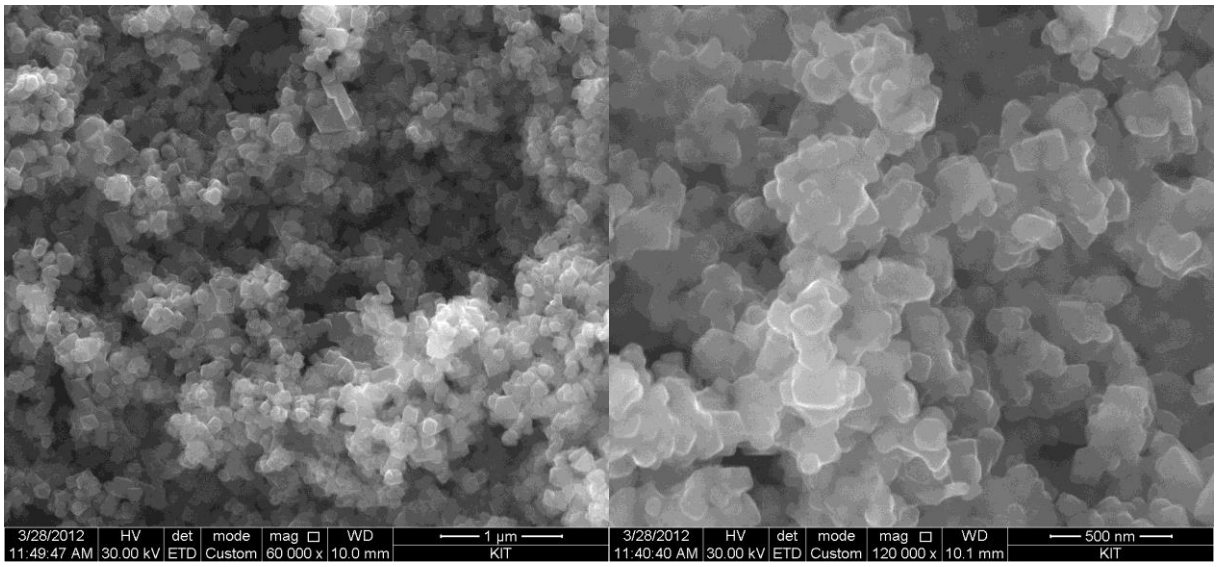

Figure 12. *SEM pictures of maghemite.*

3.1.2. Crystalline rock materials

Two different granitic rocks are used in the experimental program, namely Äspö diorite (Sweden) and Nizhnekansky granite. Mineralogical composition of both ÄD and NK materials was characterized with XRD and XRF.

3.1.2.1. Äspö diorite

Diorite is the dominating rock type in the Äspö area. The general mineralogical characterization of ÄD is presented in Table 4.

Table 4. *Petrographic characterization of Äspö diorite [109; 110] and Nizhnekansky granite [19].*

Material	Rock type	Mineralogical composition, %	Structural characteristic
Äspö diorite	Quartz monzodiorite/ granodiorite	Plagioclase, 30-50 Quartz, 10-25 K-feldspar, 10-30 Biotite, 10-25 Epidote, 3-15 Amphibole (mainly hornblende), < 10 Muscovite, titanite, apatite, fluorite, zircon, magnetite	Porphyritic, medium-grained
Nizhnekansky granite	Quartz diorite/monzo-diorite	Plagioclase, 45-50 Hornblende, 25 Quartz, 15 K-feldspar, 5-10 Opac minerals (magnetite, leucoxene, hematite), 2-3 Biotite, grothite, zircon	Hypidiomorpho-granular, monzonitic; evenly granular

Fresh Äspö diorite was obtained from a drilling campaign at the Äspö HRL (Sweden) in 2011 within the EU project CP CROCK. Details of the sampling procedure and material characterization were originally published within a CROCK S&T contribution [20]. During the core drilling, special care was taken to minimize the exposure of the solid material to air. Therefore, the drilling procedure was carried out with a double tube technique preserving to the best possible anoxic conditions. For this, natural Äspö groundwater permanently bubbled with N_2 was used as a drilling fluid. After a short visual inspection (max. 5 min) the cores were directly transferred into a wooden sampling box under tunnel atmosphere and placed into a transparent LD-PE bag, which was evacuated three times (~ -0.4 bar) and purged with nitrogen gas before welding. The same procedure was applied with an Al bag for the second confinement to prevent oxidation during transportation to the KIT-INE laboratories (see Figure 13, bottom).

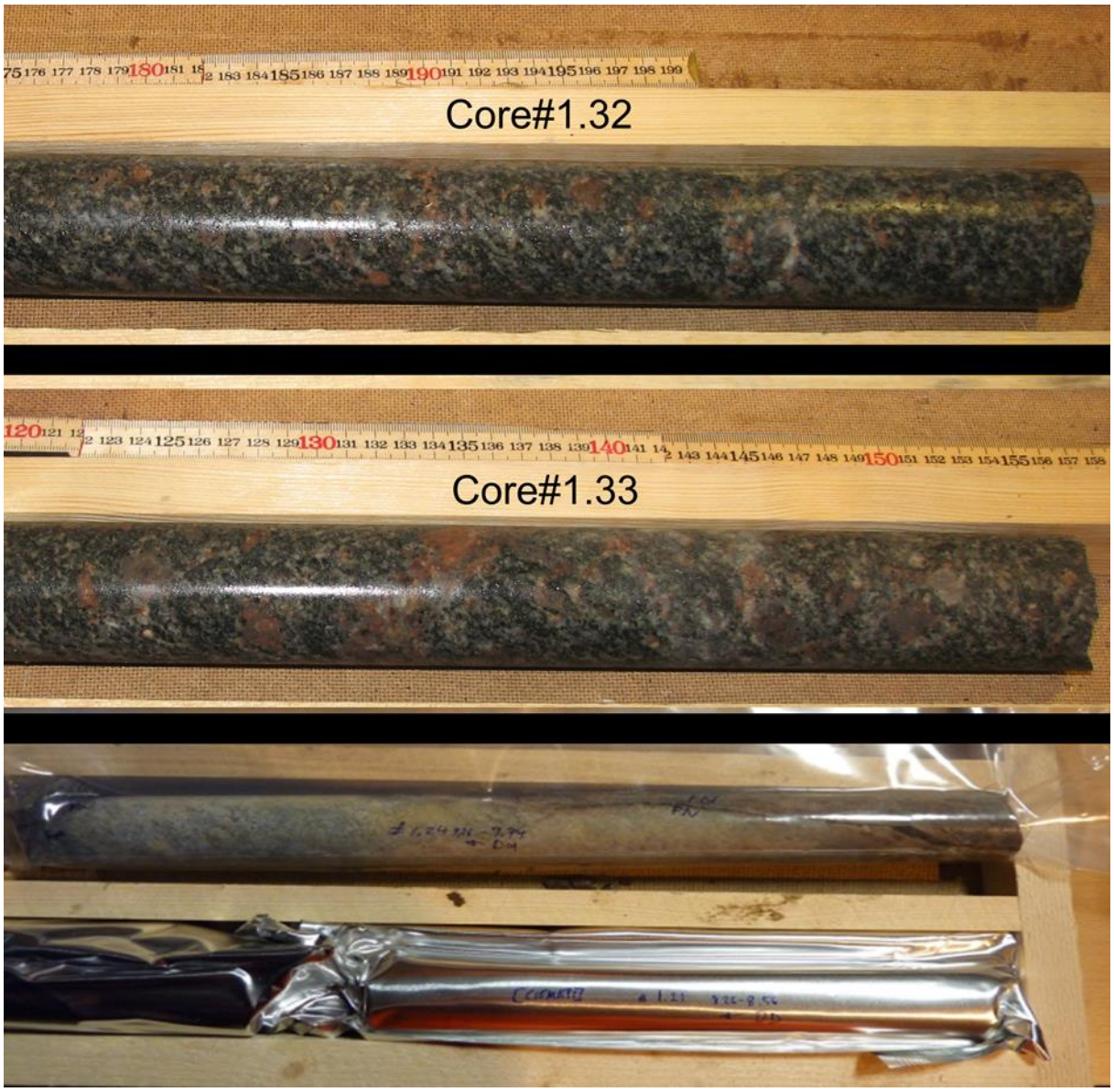

Figure 13. *(Top and middle) Cores used in the batch experiments directly after drilling. (Bottom) Two-layers packing of the cores, sealed into LD-PE and Al bags.*

At KIT-INE the cores were stored in a barrel under Ar atmosphere (~ 1 bar overpressure). The bore cores (borehole KA2368A-01, cores#1.32 and #1.33) of Äspö diorite (ÄD) were selected for the experiments. Both cores were chosen because of their (maximal) distance to the tunnel wall (13.04 – 13.52 m (core #1.32) and 13.52 – 14.00 m (core #1.33)) and their petrological characterization (fresh Äspö diorite) during the drilling campaign (Figure 13, top and middle). For preparation of the crushed material, the cores were transferred into an Ar glovebox equipped with a circular diamond saw and cut into small discs (0.5 – 1 cm in width). These discs were then manually crushed with a hammer and separated into several size fractions by sieving. For the sorption experiments the 1-2 mm size fraction was chosen. The N_2-BET surface area of 0.16 m^2/g was measured for this size fraction. This un-oxidized crushed

material was stored permanently in the glovebox under Ar atmosphere (≤ 1 ppm O_2). Part of this crushed diorite material was exposed to air for one week for artificial surface oxidation to investigate the influence of sample preservation and preparation on Tc uptake. The chemical composition of the rock material used was determined at the Institute for Geosciences, Johannes Gutenberg University (Mainz, Germany) by X-Ray fluorescence (XRF) spectrometry (spectrometer MagiXPRO, Philips) with a Rh anode operated at 3.2 kW).

In Table 5 the data for the material studied is compared to the oxidized Äspö diorite used in Huber et al. (2012 and 2010) [111; 112] and to the material from Byegård et al. (1998) [109]. Typical granodiorite composition [113] is also added in Table 5 for comparison.

Table 5. *XRF data on Äspö diorite (material used in this study, old oxidized ÄD samples used in (Huber et al., 2010 & 2012) [111; 112], oxidized ÄD from Byegård et al. (1998) [109]), Nizhnekansky granite and typical granodiorite [113] composition.*

Element (RMS_{rel})	Äspö diorite (this study), wt. %	Äspö diorite (old) [111; 112], wt. %	Äspö diorite [109], wt. %	Nizhnekansky granite (this study), wt. %	Typical granodiorite [113], wt. %
SiO_2 (0.4%)	62.71	66.06	60.1	60.17	66.88
Al_2O_3 (0.7%)	17.27	16.89	18.1	18.3	15.66
Fe_2O_3 (0.8%)	4.39	2.6	5.1	5.15	1.33
FeO (0.8%)	2.51	0.87	n.m.	n.m.	2.59
MnO (1.8%)	0.08	0.05	0.1	0.1	0.07
MgO (0.3%)	1.76	0.8	2.2	1.83	1.57
CaO (0.5%)	3.75	2.41	4.4	4.29	3.56
Na_2O (1.3%)	4.55	4.91	4.7	4.83	3.84
K_2O (0.8%)	3.05	4.38	3.2	2.65	3.07
TiO_2 (1.0%)	0.66	0.35	0.8	0.84	0.57
P_2O_5 (1.1%)	0.24	0.12	0.3	0.23	0.21
Loss on ignition (LOI)	0.67	1.37	1.0	1.16	0.65
Sum	*99.1*	*99.4*	*100*	*99.6*	*100*

Trace element (LLD)	Concentration, ppm	Concentration, ppm	Concentration, ppm	Concentration, ppm
Ba (10.5ppm)	1162	n.d.	1770	1387
Co (2.2ppm)	11	5	n.d.	8
Cr (5.3 ppm)	24	6	n.d.	13
Cu (1.6 ppm)	2	1	n.d.	4
Ga (1 ppm)	23	19	n.d.	n.d.
Nb (1.1 ppm)	15	9	n.d.	5
Ni (3.7 ppm)	18	6	n.d.	10
Pb (2.7 ppm)	17	16	89	19
Sc (2.7 ppm)	6	4	n.d.	n.d.
Sr (1.5 ppm)	1052	770	1300	954
Th (1.7 ppm)	9.5	5.7	5.2	n.d.
U (1.1 ppm)	4.4	1.8	2.1	n.d.
V (6.1 ppm)	62	36	n.d.	86
Y (1.3 ppm)	22	16	18.1	14
Zn (1.1ppm)	76	43	n.d.	78
Zr (0.9ppm)	168	139	256	258

n.d. – not detected, n.m. – not measured, RMS_{rel} – relative root square mean, LLD – lower limit of detection; RMS_{rel} and LLD are taken from the ÄD XRF analysis.

The general composition is typical for granitic rocks with high amount of SiO_2 and Al_2O_3 (quartz and feldspar) [113]. XRF data for the new material shows much higher amount of ferrous iron (~ 39% Fe^{2+}/Fe_{tot} vs. ~ 27% in old samples) as compared to the old oxidized ÄD. In the material from Byegård et al. [109] no information on Fe(II) compounds were reported.

The XRD spectrum obtained for the fine fraction (< 0.125 µm particle size) is shown in Figure S 1 in supplementary materials. The spectrum was fitted with DIFFRAC.Suite (Bruker AXS GmbH, Germany) and the mineral composition obtained is presented in Table 6.

Table 6. *Mineral composition of Äspö diorite and Nizhnekansky granite from the XRD analysis.*

Äspö diorite		Nizhnekansky massif granite	
Mineral	Content, %	Mineral	Content, %
Albite, calcian	38.7	Albite, intermediate	30.5
Quartz	18.9	Quartz	15.4
Anorthite, sodian	16.1	Anorthite, sodian	34.8
Microcline	12.8	Orthoclase	10.3
Biotite	7.6	Biotite	4.3
Epidote	4.7	Clinochlore	2.7
Magnetite	1.2	Hornblende	1.7
		Magnetite-Ti	0.2
		Apatite	0.1

3.1.2.2. Nizhnekansky massif granite

Granitic drill core material from Nizhnekansky (NK) massif was available from Kamenny (depth of drilling 100 – 700 m) and Itatsky (depth of drilling 90 – 500 m) sites. The cores were transferred to the Institute of Geology of Ore Deposits, Petrography, Mineralogy and Geochemistry RAS (IGEM RAS, Russia) under aerobic conditions, cut by a circular saw and subsequently transferred to KIT-INE. At KIT-INE the material was broken up by a jaw crusher into smaller fragments and sieved to obtain the 1 – 2 mm grain size fraction. Tc(VII) sorption kinetics were investigated using material only from a core from Itatsky site (core from an approx. depth of 92 m). A detailed description of the NK material used in this study can be found in Petrov et al. [19].

Petrographic characterization of the NK granite used in the present work was conducted at IGEM RAS. The results are given in Table 4. XRF measurements were performed at the Institute for Geosciences, JGU together with ÄD material (see Table 5).

XRD analysis was performed for the fine fraction (< 0.125 µm) obtained from sieving (see Figure S 2 in supplementary materials). Fitting of the spectrum (the same procedure like for Äspö diorite) is shown Table 6. The surface area of the material used was measured with N_2-BET analysis as 0.32 m^2/g.

3.1.2.3. Available iron content estimation

In order to estimate the cation exchangeable Fe(II) amount on the mineral surfaces of the Äspö diorite and the NK granite, a method proposed by Heron et al. [114] was applied using 10 mL 1 M $CaCl_2$ (pH = 7) in contact with 2 g of granite for 24 h. Afterwards, an aliquot was taken for Fe(II) quantification by the ferrozine technique. The application of ferrozine (3-(2-

pyridyl)-5,6-diphenyl-1,2,4-triazine-p,p'-disulfonic acid monosodium salt hydrate) for the determination of iron concentration in aqueous solutions was first suggested by Stookey (1970) [115] and later developed by Viollier et al. [116] for simultaneous measurement of Fe(II)/Fe(III) concentrations. Ferrozine reacts with divalent iron forming a magenta complex with maximum absorbance at 562 nm. In the first step, 1 mL sample aliquot was mixed with 100 µL 10^{-2} M ferrozine solution in 0.1 M ammonium acetate (CH_3COONH_4) in 1 cm plastic cuvette (Brand®). An absorption spectrum was recorded with UV-Vis-NIR spectrophotometer Cary 5E (Varian) to determine Fe(II) content. Then 800 µL of this solution was transferred into a second cuvette and mixed with 150 µL of a reducing agent (1.4 M hydroxylamine hydrochloride ($H_2NOH \cdot HCl$) in 2 M HCl), allowed to react for 10 minutes to complete Fe(III) reduction and after addition of 50 µL ammonium acetate buffer (approx. 10 M CH_3COONH_4 adjusted to pH 9.5 with 30% NH_4OH solution) the second absorption spectrum was recorded to determine the total iron content. Fe(II)/Fe(III) concentrations were calculated using a calibration curve.

Results of ion-exchangeable Fe(II) content measurements are given in Table 7. The rather high uncertainty in the measurements is attributed to the natural heterogeneity of the rock material (three samples were measured for each rock type).

Table 7*. Ion-exchangeable Fe(II) content in the crystalline rocks studied.*

	Un-oxidized ÄD	Oxidized ÄD	Oxidized NK
Ion-exchangeable Fe(II), µg/g	4 – 6	1 – 3	0.1 – 1

The content of ion-exchangeable Fe(II) is about three orders of magnitude lower than the Fe(II) amount in the bulk solid as obtained by XRF (see Table 5). However, the ratio of Fe(II) content in fresh to the amount in oxidized materials is around three and therefore similar in the bulk and at the surface.

3.1.3. Groundwater simulants

Different types of groundwater have been used in the experimental program. Besides the natural Äspö groundwater (ÄGWN) a synthetic groundwater simulant (ÄGWS) has been prepared to mimic the CROCK drilling site outflow groundwater composition (see Schäfer et al. [20]). All chemicals used for the preparation of the synthetic groundwater were of analytical grade. Solutions were prepared with deionized MilliQ water which was stripped

with Ar prior to use. ÄGWS has a comparable composition to natural Äspö groundwater sampled *in-situ* from borehole KA3600-F-2 sampled in an Ar pre-flushed 50 L Teflon-coated Al-barrel at the CP-CROCK site [117]. Chemical compositions of the ÄGWS used and natural groundwater samples from Äspö and Grimsel (taken as an analogue to glacial melt water with low ionic strength) are presented in Table 8. The relatively high Eh values of ÄGWS and GGW are explained by the low concentration of the redox couples in the solution, which cannot be measured accurately using a Pt-electrode.

Table 8. *Overview of the chemical compositions of the synthetic Äspö groundwater simulant (GWS), Äspö groundwater and Grimsel groundwater, respectively.*

	synth. Äspö GWS	Synth. Äspö GWS after 122h contact time	Äspö GW (KA-3600-F-2)	Grimsel GW (sampled from MI-shear zone)
pH	8.0	8.0	7.8	9.67
Eh	390	n.m.	-240	320
[Mg^{2+}]	103.64 ± 0.84 mg/L	104.6 mg/L	69.4 mg/L	12.6 µg/L
[Ca^{2+}]	1109.36 ± 94.46 mg/L	1134 mg/L	1135 mg/L	5.3 µg/L
[K^{+}]	19.346 ± 3.855 mg/L	21.56 mg/L	10.5 mg/L	
[Li^{+}]	2.526 ± 0.04 mg/L	2.50 mg/L	6.0 mg/L	
[$Fe^{2+,3+}$]	n.m.	n.m.	0.2 mg/L	< D.L.
[Mn^{-}]	2.32 ± 3.02µg/L	23.8 µg/L	0.338 mg/L	< D.L.
[Sr^{2+}]	19.678 ± 0.294 mg/L	20.14 mg/L	19.9 mg/L	182 µg/L
[Cs^{+}]	<D.L	< D.L		0.79 µg/L
[La^{3+}]	n.m.	n.m.		< D.L.
[U]	0.05 ± 0.01 µg/L	1.70 µg/L	0.105 µg/L	0.028 µg/L
[Th]	0.024 ± 0.005 µg/L	0.07 µg/L	0.001 µg/L	0.00136 µg/L
[Al^{3+}]	182.75 ± 56.29 µg/L	439.6 µg/L	13.3 µg/L	42.9 µg/L
[Na^{+}]	1929.25 ± 28.58 mg/L	1905 mg/L	1894 mg/L	14.7 mg/L
[Cl^{-}]	4749.408 ± 145.046 mg/L	4895.10 mg/L	4999 mg/L	6.7 mg/L
[Si]	n.m.	n.m.	4.7 mg/L	5.6 mg/L
[SO_4^{2-}]	408.682 ± 4.967 mg/L	411.88 mg/L	394.4 mg/L	5.8 mg/L
[F^{-}]	1.974 ± 0.093 mg/L	1.98 mg/L	1.41 mg/L	6.3 mg/L
[Br^{-}]	21.17 ± 0.37 mg/L	20.96 mg/L	23.2 mg/L	
[NO_3^{-}]	n.m.	n.m.	n.m.	< D.L.
[HCO_3^{-}]	n.m.	n.m.	n.m.	3.0 mg/L
[B]	306.54 ± 212.54 µg/L	146.1 µg/L	885 µg/L	

n.m. – not measured.

The groundwater simulant for experiments with NK material (NKGWS) was prepared in accordance with Petrov et al. [19] by dissolution of 62.5 mg/L $NaHCO_3$ and 187.5 mg/L $Ca(HCO_3)_2$ in MilliQ water flushed with Ar. The total amount of dissolved solids is 250 mg/L (ionic strength I = 0.005 M) and pH = 8 after equilibration with the rock material. By classical HCl titration of simulated groundwater samples it was shown that the short openings of the vials in Ar atmosphere did not change the carbonate concentration in the solution significantly.

3.2. Methods

3.2.1. Radionuclide concentration measurements

3.2.1.1. Liquid scintillation counting

Liquid scintillation counting (LSC) was applied in this work to measure the concentration of the beta-emitting radionuclides, namely ^{99}Tc, ^{3}H and ^{36}Cl.

The LSC technique is based on radiation-induced scintillation. Conjugated aromatic compounds act as scintillator molecules that emit photons of visible light by relaxation to the ground state after being excited by transfer of the kinetic energy of beta and alpha particles via solvent molecules. The number of photons emitted per decay event is proportional to the particle energy and the linear energy transfer of the emitted particle type. Different types of quenching processes can influence the photon emission rate, which is measured by two photomultipliers working in coincidence mode.

The samples for measurements were prepared in 20 mL screw-cap HDPE vials (Zinsser Analytic GmbH). The aliquots of 10 µL – 1 mL (depending on the activity) were mixed with 10 mL LSC cocktail (Ultima Gold™ XR, PerkinElmer, Inc.) and measured for 30 min – 1 hour with the low-background liquid scintillation counter LKB Wallac 1220 Quantulus (PerkinElmer, Inc.). The detection limit for ^{99}Tc measurement under the applied conditions was estimated to be ~ 10^{-10} M (see Figure 14). The solubility limit of Tc(IV) in a wide range of pH-Eh conditions representing most of the natural systems is about 4.4×10^{-9} M [66]. Thus, the detection limit of LSC lies roughly one order of magnitude below the Tc(IV) solubility limit.

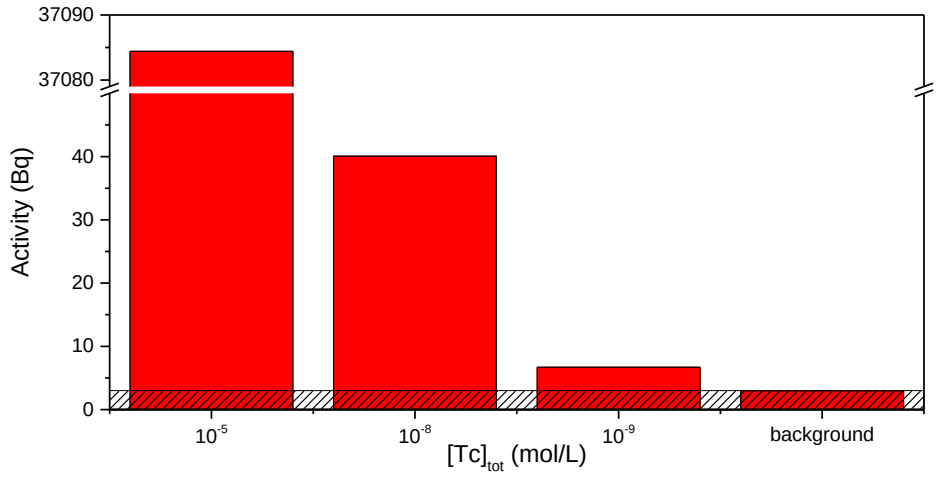

Figure 14. *Activities of the used Tc concentrations compared to LSC Quantulus background (10 mL of LSC cocktail + 1 mL of Tc solution).*

3.2.1.2. Gamma spectroscopy

The concentration of ^{95m}Tc was determined using γ-spectroscopy with a high-purity germanium (HPGe) semiconductor detector.

In this technique γ-radiation photons are detected by the measurement of the amount of charge carriers (electrons and holes) generated in a semiconductor detector crystal. The crystal is working as diode under the reverse (blocking) voltage. Passing through the detector the ionizing radiation is producing the electron-hole pairs. An electric field applied is moving electrons and holes to the charged electrodes producing an electric impulse. This signal is electronically amplified and used for analysis.

For the sample preparation the aliquots of 10 µL – 1 mL were diluted up to 10 mL in 10 mL vials (Kautex Textron GmbH & Co. KG) and measured for 10 minutes – 3 hours depending of the total activity using a coaxial HPGe detector (Canberra Industries). The data were collected and processed using the Genie 2000 software package (Canberra Industries).

The detection limit of gamma spectrometry under 10 mL geometry for ^{95m}Tc was estimated to be ~ 10^{-14} – 10^{-15} M (three hours measurement time).

3.2.2. ^{95m}Tc separation

^{95m}Tc was isolated from the irradiated Mo foil (see paragraph 3.1.1.1) according to the technique described in Boyd et al. [118]. The foil was dissolved in a mixture of concentrated H_2SO_4 and 30% H_2O_2 and the solution was slowly neutralized with saturated NaOH (up to alkaline pH). The obtained alkaline solution was passed through a column filled with the anion exchanger Dowex 1x8 (100-200 mesh particle size) with a total volume ca. 3 mL. The column was washed first with 20 mL 1 M $K_2C_2O_4$ to remove residues of molybdate and after rinsing with 20 mL of MilliQ water pertechnetate was eluted with 30 mL 1 M $HClO_4$. The last fraction was collected into 2 mL vials, which were measured with γ-spectrometry and samples contained in total ca. 90% of ^{95m}Tc were merged and neutralized with concentrated NaOH. The purification level was monitored with ICP-MS and γ-spectrometry.

The first foil processed was highly contaminated with rubidium isotopes ^{83}Rb and ^{84}Rb with the total activity comparable to the one of ^{95m}Tc. After the first separation step on Dowex resin rubidium was fully isolated (see Figure 15), but the Tc fraction contained substantial amount of Mo (350 ppm, natural ÄGW contains 10-25 ppm according to the ICP-MS analysis). Therefore, Tc-contained samples were merged, pH was adjusted to the alkaline

range and the separation was performed again. The final ^{95m}Tc fraction was mixed with ÄGWS with further pH and salts concentration adjustment.

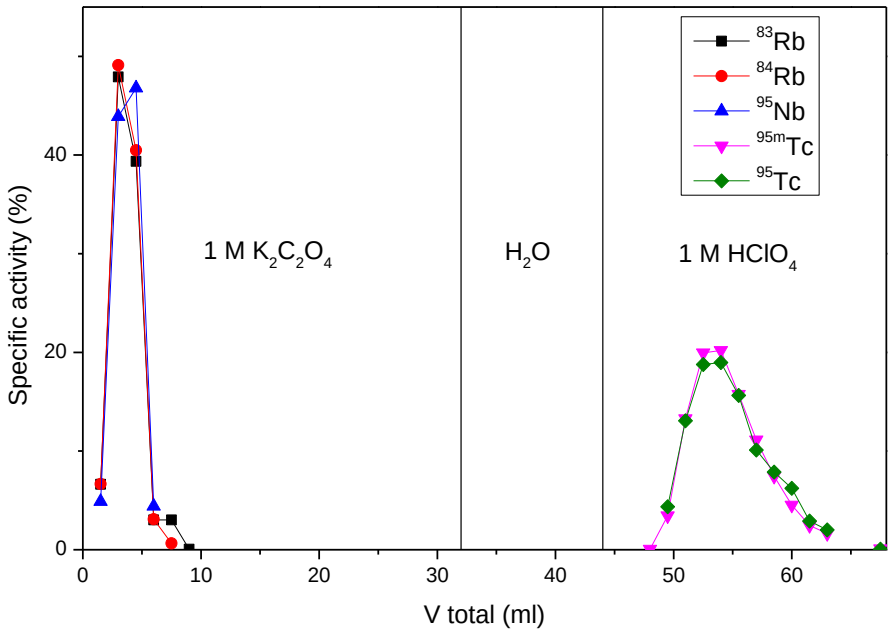

Figure 15. *Separation chromatogram of the irradiated Mo target using a Dowex 1×8 resin column (100-200 mesh, 3 mL column volume)*

The use of another column filled with Teva® Resin (Eichrom Technologies, LLC) prior to Dowex significantly increased chemical purity of Tc. Technetium separation on Teva Resin column was performed from ~ 1.5 M HNO_3 media and after washing the column with 2 M HNO_3 Tc was eluted with 8 M HNO_3 according to the technique reported in the literature [119]. A further separation step on the Dowex column results in the purification from NO_3^-, which may act as undesired oxidizing agent being absent in natural deep geological anoxic groundwaters. The nitrate concentration was initially controlled with nitrate test strips (Merck) and subsequent ion chromatography (IC) analysis. A Tc/NO_3^- separation chromatogram is shown in Figure 16.

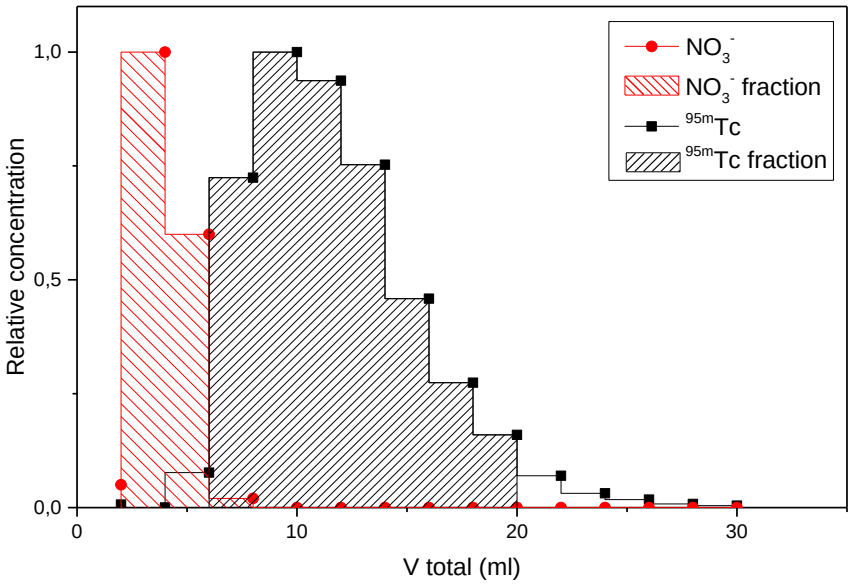

***Figure 16**. Separation of ^{95m}Tc from NO_3^- using a DOWEX 1×8 resin column (100-200 mesh, 3 mL column volume)*

3.2.3. Batch studies

All batch studies unless otherwise stated were conducted under anoxic conditions inside an Ar glovebox with O_2 concentrations ≤ 1 ppm at room temperature (20 ± 2° C).

3.2.3.1. Sorption studies

3.2.3.1.1. Tc sorption onto iron oxides phases

Batch type sorption studies with synthetic Fe oxides were carried out in 500 mL Kautex bottles. The solid phase content was 2 g/L, which corresponds to a similar surface area like in experiments with crystalline rocks. Tc(VII) solutions with concentrations of 10^{-5} M, 10^{-8} M and 10^{-9} M were prepared in 0.2 M NaCl as a background electrolyte. After mixing of the solutions with Fe oxide phases two pH values of 7 and 8 were adjusted for each Tc concentration. For each kinetics point 6 mL aliquot of suspension after homogenization was taken, solid state was separated with a magnet which was followed by ultracentrifugation of supernatant (Beckman Optima XL-90, 90,000 rpm, 694,000 × g, t = 1 h). pH was adjusted after each sampling. An aliquot of 1 mL of the supernatant was taken and measured with LSC.

3.2.3.1.2. Tc sorption onto crushed crystalline rocks

Before the start of the batch sorption experiments the crushed material was contacted with relevant groundwater simulant (GWS) during one day exchanging the water five times. This step was also conducted to remove any remaining fines/colloids from the sieving procedure. In case of un-oxidized ÄD the last step was performed with natural ÄGW to establish more realistic conditions.

The batch experiments were carried out in 20 mL HDPE LSC vials (Zinsser Analytic GmbH). The solid-liquid ratio chosen was 2 g of granitic rock and 8 mL of GW (250 g/L). Sample duplicates were prepared and kept closed during the sorption experiments to prevent oxidation of Fe(II) at the mineral surfaces. All sorption experiments were conducted at pH 8.1 ± 0.1. Tc(VII) concentrations of 10^{-5} M, 10^{-8} M and 10^{-9} M were used in the experiments. For measurement of the ^{99}Tc content in the sample supernatant after the desired contact time 1 mL aliquots were taken for analysis with LSC as described in section 3.2.1.1. To differentiate between potentially formed colloidal phases (e.g. Tc(IV) eigencolloids) and dissolved species a phase separation by ultracentrifugation (90,000 rpm) for 1 h was applied.

3.2.3.1.3. Calculation of sorption parameters

The temporal change in Tc concentration during the batch sorption experiment can be described with an exponential decay equation (28):

$$C_t = (C_0 - C_{eq})e^{-rt} + C_{eq} \quad (28)$$

where C_0 and C_{eq} are the initial and equilibrium Tc concentrations (M), respectively, and r is the sorption rate coefficient (time^{-1}). Hence, calculating the fraction of sorbed Tc S_t (29)

$$S_t = \left(1 - \frac{C_t}{C_0}\right) \times 100\% \quad (29)$$

the time dependent sorption data can be fitted to the rate equation (30):

$$S_t = S_{eq}(1 - e^{-rt}) \quad (30)$$

where S_t and S_{eq} are the fractions of sorbed Tc at the moment t and at equilibrium, respectively. A similar exponential fitting of time dependent sorption data is used in a number of works, for instance by Kohler et al. [120].

Distribution coefficients (K_d in L/kg) obtained for Tc sorption onto mineral phases were calculated using the following equation (31), based on the equation (9).

$$K_d = \frac{C_l}{C_s} = \frac{A_0 - A_l}{A_l} \times \frac{V}{m_{solid}} \quad (31)$$

where C_l and C_s are the equilibrium concentrations of solutes in aqueous and solid phases, respectively, A_0 and A_l are the initial and final aqueous radionuclide activities at equilibrium (Bq/mL), respectively, V is the volume of the aqueous phase (mL) and m_{solid} is the solid mass (g).

From a thermodynamic point of view the K_d approach deals with a fully reversible process, but in most papers it is used even when irreversible reduction/precipitation processes are involved [79; 100; 121]. In the report of The United States Environmental Protection Agency [122] authors describe "conditional" K_d values for interpretation of experimental data in cases when the rigorous application of the K_d approach is prohibited (non-equilibrium or irreversible systems). In the present work K_d values are considered as conditional distribution coefficients. Use of alternative approaches (R_d, R_f, etc.) are not considered in this study due to the lack of appropriate literature references for Tc behaviour on the mineral phases.

For a better comparison of the uptake behaviour on different materials, K_d can be normalized to the specific surface area of the solid material used in the experiments according to the equation (32):

$$K_a = \frac{K_d}{S_{BET}} (\times 10^{-6}) \quad (32)$$

where K_a is the surface area normalized distribution coefficient (m) and S_{BET} is the specific surface area of the solid (m^2/g).

3.2.3.2. Desorption studies

Subsequent to the sorption experiments, desorption studies have been conducted. The Tc containing supernatant of the sorption experiment samples (samples with three months contact time in the sorption kinetic experiments) was removed and 8 mL of fresh Tc-free groundwater added (natural AGW and Grimsel groundwater (glacial meltwater analogue) for ÄD samples, NKGWS in the case of NK material). For each contact time, the supernatant was completely removed, analysed by LSC and substituted with fresh Tc-free groundwater of the same volume. Part of the samples were oxidized under air for one month after the sorption experiments (initial Tc-containing liquid phase was removed) and the same desorption procedure was performed under aerobic atmosphere. For this experiment ÄGWS was used for

ÄD instead of natural ÄGW to keep oxidizing conditions. Desorption experiments cover a time range between few seconds and one month contact time.

3.2.4. Redox potential measurements

The redox potential of selected samples was measured using a Metrohm (Ag/AgCl, KCl (3 M)) electrode. The measurements were performed directly in the sample without phase separation. The Eh values were recorded every hour and then corrected for the standard hydrogen potential (against the standard hydrogen electrode (SHE)). The redox potentials after *ca.* one hour contact time were taken as the final values.

3.2.5. Tc liquid-liquid extraction

The technetium oxidation state in the solution was investigated with liquid-liquid extraction technique. Two different organic reagents were applied, namely (i) 1 mM tetraphenylphosphonium chloride (Ph_4PCl) in chloroform and (ii) 1 mM 1-phenyl-3-methyl-4-benzoylpyrazolone-5 (PMBP) in xylol. Ph_4PCl is extracting the pertechnetate ion [123], while PMBP is commonly used for extraction of tetravalent cations including Tc(IV) [124].

For liquid-liquid extraction 500 µL of Tc-containing aqueous phase was mixed with 500 µL of organic phase in a 1.5 mL glass vial and shaken for 15 minutes. After phase separation, aliquots from both organic and aqueous phases were taken and the Tc concentration was determined in both phases with LSC for ^{99}Tc and with γ-spectrometry for ^{95m}Tc solutions.

3.2.6. Core migration

3.2.6.1. Core preparation and characterization

An un-oxidized Äspö diorite drill core (core #2.2, 0.53-0.97 m, borehole KA2370A-01) was used in the migration experiments. The core contains a natural fracture at ~ 0.70 m that was opened during on-site handling at the Äspö HRL. The original drill core was sealed into a plastic bag (Figure 17) and transferred into an Ar glovebox. The core segment containing the natural fracture was cut with a saw and both fracture parts have been assembled together to obtain the original position and fixed with a sticky tape and a bar clamp without applying excessive pressure. Afterwards, the suture (outer rim) of the fracture was glued using high viscous Plexiglas glue. The gluing was done stepwise applying only small amounts of glue in each step to avoid potential intrusion of the glue into the fracture itself. Several layers of glue have been applied to guaranty that the fracture rim is fully sealed. The rim of the fracture was

facing downwards to avoid intrusion of the glue into the fracture. After finalization of the glue process the core was placed in a Plexiglas (poly(methyl methacrylate)) cylinder and the remaining void space between core and inner wall of the cylinder was filled up using the same glue as mentioned above. After solidification of the glue, the upper and lower bottom of the core was sawed again and carefully polished by hand. The last step in sealing of the core fragment (final length ~ 5.228 cm) was gluing of top and bottom caps with connectors to the fracture in- and outlet.

Figure 17. *Drill core #2.2 (0.53-0.97 m, borehole KA2370A-01) with a natural fracture.*

The core fragment was sealed in an Ar filled plastic bag as second confinement, transferred to the Federal Institute for Materials Research and Testing (BAM, Berlin) and characterized by 3D computer tomography (µCT) with resolution of 16 µm (Figure 18). The fracture volume after segmentation was estimated to be 0.415 mL and the total fracture surface area is 4.235×10^{-3} m^2.

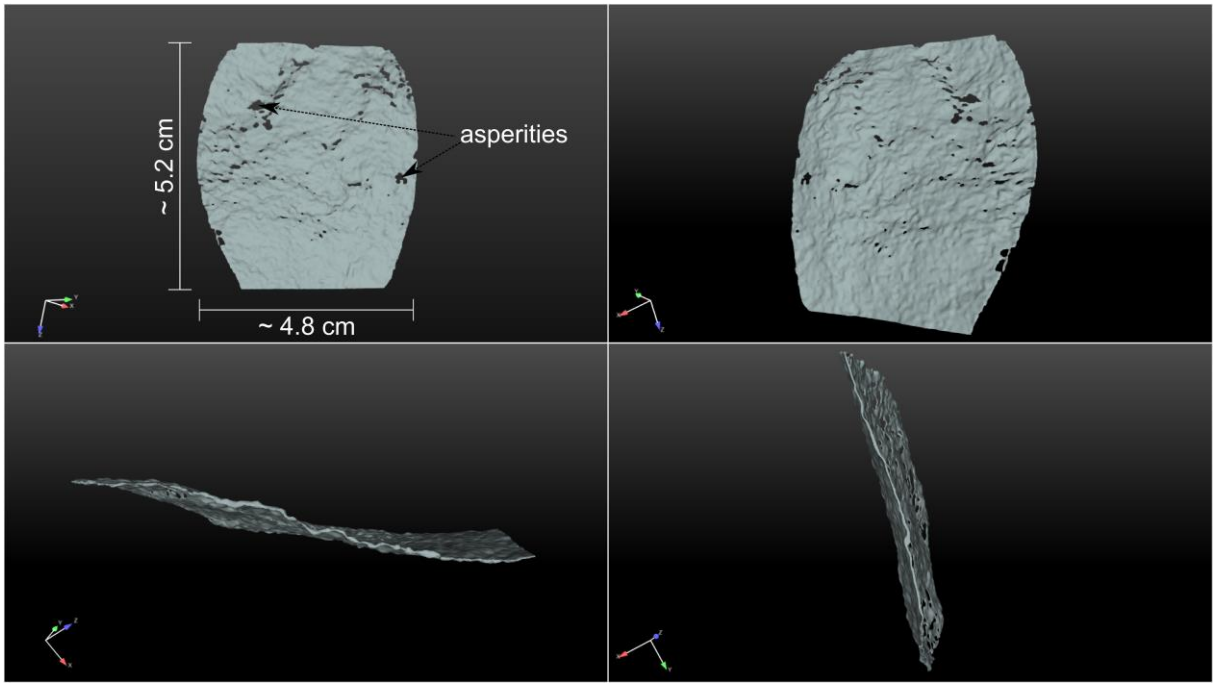

Figure 18. *Different views of the rendered fracture geometry obtained from the µCT dataset.*

3.2.6.2. Migration studies

The core was handled at KIT-INE solely inside the Ar glovebox with oxygen concentration < 1 ppm to avoid oxidation. For tracer migration experiments ÄGWS containing HTO and ^{36}Cl admixtures with a specific activity of ~ 3 kBq for each RN were applied. An injection loop was filled with 1 mL of solution, which was eluted through the core by ~ 50 mL of ÄGWS using a syringe pump under different flow rates (10 mL/h, 1.5 mL/h and 0.2 mL/h). The eluate was sampled with a fraction collector (Gilson FC 203b) and measured with LSC. The general set-up of the core migration experiment is presented in Figure 19. For Tc migration investigations the same procedure was performed by injecting ÄGWS with spiked Tc. Experiments at low Tc concentrations (~ 10^{-11} M) were possible due to the availability of ^{95m}Tc which can be measured with γ-spectrometry at very low mass concentration. For higher concentrations ^{99}Tc was added to the injection solution. In order to allow performing experiments where the Tc solution stay in contact with the fracture for a longer time period (1 – 17 days) the stop-flow experimental technique was applied. In this case the pump is paused for the certain time after a continuous injection of ~ 10 free fracture volumes with flow rate of 10 mL/h. The core is insulated by the valves around it and the experimental apparatus is washed with the groundwater to remove Tc from the tubing. After the required contact time is reached, the elution with groundwater through the core is continued. Tc uptake is calculated based on the Tc recovery from the fracture.

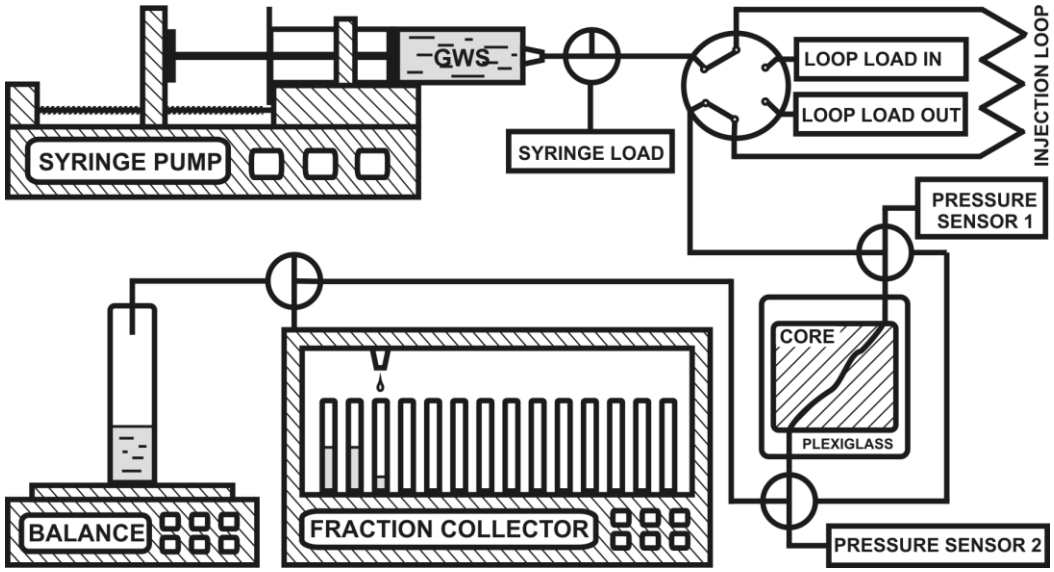

Figure 19. *Schematic illustration of core migration setup.*

For the comparison of the uptake data obtianed by batch and migration studies surface normalized distribution coefficients (K_a) (m) were calculated according to the equation (33):

$$K_a = \frac{c_{surf}}{c_{aq}} \tag{33}$$

where c_{surf} is a mass of solute on the mineral phase per specific surface area of the solid (g/m^2) and c_{aq} is a mass concentration of solute in the eluate (g/m^3). The same equation represents a classical way of the K_a calculation from the migration studies applied, for instance, by Park et al. [125].

For the post-mortem surface analyses of Tc speciation on the mineral surface inside the fracture the continuous injection of Tc-containing natural ÄGW (1 L, 5×10^{-7} M $[Tc]_{tot}$, flow rate ~ 1.5 mL/h) was performed. This experiment had the purpose to accumulate enough Tc on the mineral surface for the surface analyses (XPS, SEM). A high-performance liquid chromatography (HPLC) pump was applied for this experiment. The general scheme is shown in Figure 20. The Tc amount retained inside the core was calculated from the difference of Tc concentration in the in- and outflow solution.

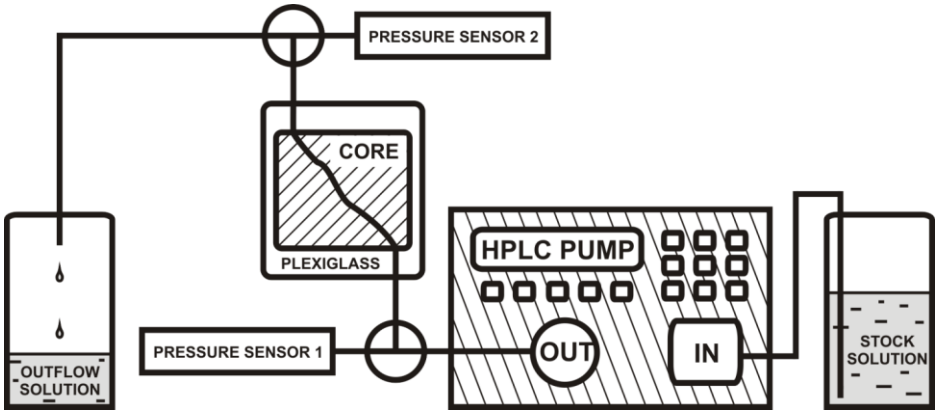

Figure 20. *Experimental setup of the continious Tc injection experiment.*

3.2.6.3. Post-mortem amalysis

After the migration studies the core was disassembled. The Plexiglass shell was sawn and the core was carefully taken out.

The radionuclide distribution on the mineral surface was investigated using autoradiography. The main purpose of this analysis was to localize Tc hotspots on the surface for further investigation. The fracture surfaces of the Äspö diorite core #2.2 after the migration studies were put on the autoradiography screen (MultiSensitive storage phosphor screen, PerkinElmer Inc., USA) covered with a thin plastic film to prevent screen contamination. Two 10 µL drops of 10^{-5} M and 10^{-7} M Tc solution were placed on the screen for activity calibration. The arrangement of the core fragments and the drops is shown in Figure 21.

Figure 21. *Äspö diorite core #2.2 fragments and the Tc reference drops (10 µL 10^{-5} M in the blue circle and 10 µL 10^{-7} M Tc in the red circle) on the autoradiography screen.*

Autoradiography exposition was carried out for 19 hours in a lightproof carton box inside the Ar glovebox. Afterwards the core fragments and the plastic film were removed from the screen, which was transferred from the glovebox to the Cyclone Plus Storage Phospor Scanner (PerkinElmer Inc., USA). Image processing was performed using OptiQuant (ver. 4.00, Packard Instrument Co.) software package.

The similar experiment was performed under vacuum in the antechamber of the Ar glovebox to decrease the electrons scattering. The exposure time was 24 hours.

Several hotspots found by autoradiography were cut using a chisel and hammer from one half of the core. Using XPS and SEM-EDX analyses the surface was investigated to locate Tc species and Fe(II)-containing minerals.

The second part of the core was oxidized under air, washed with ÄGWS (5 min and 1 day contact times) and analysed with autoradiography to distinguish natural radioactivity from immobilized Tc species. Alpha/beta discrimination was done by conducting an additional autoradiography analysis placing a paper sheet (HP Bright White Inkjet Paper) between the core and the phosphor screen to absorb α-particles.

3.2.7. X-ray spectroscopy

3.2.7.1. X-ray photoelectron spectroscopy (XPS)

To examine the Tc surface speciation X-ray photoelectron spectroscopy (XPS) has been applied. For XPS analysis small un-oxidized Äspö diorite fragments with unpolished faces after cutting by circular saw were contacted with 10^{-5} M Tc(VII) in GWS for two months and washed by MilliQ water for a few seconds to prevent salt precipitation directly before the XPS analysis. For magnetite samples a small drop (~ 5 µL) of magnetite suspension was placed onto the Al foil and dried. All preparation and measurement steps were performed under Ar atmosphere. Transport of the samples from the Ar glovebox to the XP spectrometer under anoxic atmosphere was achieved by using an O-ring sealed vacuum transfer vessel (PHI model 04-110). XPS measurements were carried out with the XPS system PHI 5000 VersaProbe II (ULVAC-PHI Inc.) equipped with a scanning microprobe X-ray source (monochromatic Al K_α (1486.6 eV) X-rays) in combination with an electron flood gun and a floating ion gun generating low energy electrons (1.1 eV) and low energy argon ions (8 eV) for charge compensation at isolating samples (dual beam technique), respectively. The angle between sample surface and analyser was set to 45°. Survey scans were recorded with an X-ray source power of 12 W and pass energy of 187.85 eV. Narrow scans of the elemental lines were recorded at 23.5 eV pass energy. All spectra were charge referenced to C 1s (hydrocarbon) at 284.8 eV. Data analysis was performed using ULVAC-PHI MultiPak program, version 9.5.

The XPS analysis allowed to estimate $Fe(II)/Fe_{tot}$ in the magnetite samples. For this purpose Fe 2p peaks were chosen, since they are more intense and more surface sensitive than Fe 3p peaks. Calculated multiplet peaks for Fe 2p3/2 spectrum was published by Grosvenor et al. [126], however the result of the linear combination fitting of the modelled Fe(II) and Fe(III) 2p peaks strongly depends on the background function applied [127]. The Fe(II) amount was estimated using the intensity of the shoulder (708.5 – 708.7 eV binding energy) on the Fe $2p_{3/2}$ peak on the lower energy side, which is representative for the Fe(II) content. The calculation of the $Fe(II)/Fe_{tot}$ ratio was conducted by the comparison of the shoulder intensity of the stoichiometric magnetite and hematite (α-Fe_2O_3) with the spectrum of the analysed sample. The relative error of this calculation was estimated to be ± 5%. It should be also mentioned, that this method is applicable only for the Fe-oxide systems with $Fe(II)/Fe_{tot}$ ratio between 0% and 33.3%.

3.2.7.2. X-ray absorption spectroscopy (XAS)

XAS experiments were performed at the INE-Beamline at the ANKA 2.5 GeV synchrotron radiation facility, Karlsruhe Institute of Technology (KIT) (Karlsruhe, Germany). The detailed description of the instrumental setup of the INE-beamline is presented in Rothe et al. [128]. Tc K-edge (21,044 eV) X-ray absorption near edge structure (XANES) and extended X-ray absorption fine structure (EXAFS) spectra were collected in fluorescence mode using one element VITUS Vacuum-Silicon Drift Detector (SDD) (Munich, Germany). The primary X-ray beam was monochromatized by a Ge(422) double crystal monochromator (DCM).

Uranium mineral meta-schoepite ($UO_3 \cdot nH_2O$) was measured simultaneously with all samples and the Tc(IV) and Tc(VII) references and the U L_2 (20,948 eV) edge XANES spectra were used for energy calibration. Pertechnetate solution with concentration of 10^{-2} M was taken as a Tc(VII) reference and $TcO_2 \times 1.6H_2O_{(s)}$ solid phase (Tc(IV) reference) was prepared by TcO_4^- reduction in the electrochemical cell.

The set of samples with Tc concentrations of ~ 10^{-3} M contacted with crystalline rock materials and magnetite was prepared and mounted in an inert gas cell under argon atmosphere (see Table 9 for description of all samples and references measured). During the measurement argon was pumped through the cell (Figure 22).

Table 9. *List of measured XANES samples.*

Sample	[Tc], M	Description	Number on scans
Tc(VII) reference	10^{-2}	TcO_4^- solution	4
Tc(IV) reference	-	Solid TcO_2 covered with supernatant	4
Tc on ÄD	10^{-3}	Centrifuged suspension	5
Tc on NK	10^{-3}	Centrifuged suspension	3
Tc on magnetite	10^{-5} & 2×10^{-3}	Centrifuged suspension	5

Table 10. *List of measured EXAFS samples.*

Sample	[Tc], M	Description	Number on scans
Tc_magn	10^{-5}	Tc on magnetite Centrifuged suspension	3
Tc_magn_ox	10^{-5}	Tc on partially oxidized magnetite, 24.7 % $Fe(II)/Fe_{tot}$ Centrifuged suspension,	4

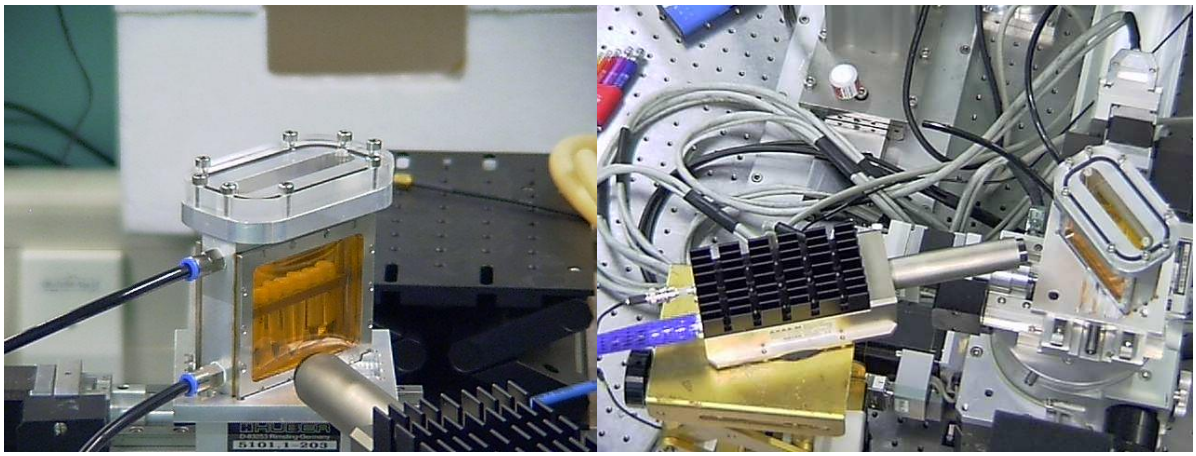

***Figure 22**. XANES measurement device and cell with Tc samples.*

Data reduction and normalization of the XANES spectra was performed with ATHENA program part of the IFEFFIT software package [129]. The number of the splined scans is given in Table 9. The oscillating χ(k) (EXAFS) parts of the X-ray absorption fine structure (XAFS) spectra of the samples measured (see Table 10) were extracted, Fourier transformed (FT) and modelled by using the ATHENA and ARTEMIS programs, which are both parts of the IFFEFIT program package [129]. The single scattering paths applied to model the experimental FT-EXAFS data were generated with the FEFF9.5 [130; 131] code by using the structural model of Fe_3O_4 (magnetite) reported in the American Mineralogist Crystal Structure Database (AMCSD) (database code 0002400). For the "Tc on magnetite" sample the χ(k) spectra within 3.7 – 8.2 $Å^{-1}$ range were weighted by k = 1, 2 or 3. Hanning windows with sills equal to 2 (Δk = 2) were used. The fit was performed in R space for 1 – 3.6 Å range. The amplitude reduction factor was fixed to 1 [96]. The obtained goodness of fit (r factor) reports 1% (r = 0.01) difference between data and model.

3.2.8. Thermodynamic modelling

Geochemical speciation calculations and simple sorption modelling were conducted with the geochemical speciation code PHREEQC (version 2) [132]. The SIT database provided with PHREEQC is used, in which the thermodynamic constants for Tc and Fe correspond to the ones selected by the NEA Thermochemical Database [133; 134]. Pourbaix diagrams were calculated and plotted with "Geochemist's Workbench" (version 8.0, Aqueous Solution LLC) code with the default database thermo.dat also modified for Tc species in accordance with NEA Thermochemical Database [133; 134].

Under the applied experimental conditions TcO_4^- and $TcO(OH)_2$ are the only relevant dissolved species for Tc(VII) and Tc(IV), respectively. The redox reaction is:

$$TcO_4^- + 4H^+ + 3e^- \rightleftharpoons TcO(OH)_2 + H_2O \quad (34)$$

$$K_{VII/IV} = \frac{[TcO(OH)_2]}{[TcO_4^-][H^+]^4[e^-]^3} \quad (35)$$

where $K_{VII/IV}$ is the conditional constant of the reaction (34). From here the redox potential pe (pe = 16.9×Eh at 25°C) is calculated according to the following equation:

$$pe = \left(\log K_{VII/IV} + log\left(\frac{[TcO_4^-]}{[TcO(OH)_2]}\right) - 4pH_c\right)/3 \quad (36)$$

where pH_c = - log $[H^+]$. The pe corresponding to an equimolar Tc(VII)/Tc(IV) ratio represents the redox borderline in a Pourbaix diagram pertaining only to the aqueous species (denoted pe_{aq} or Eh_{aq} for redox potential) is found as follows:

$$\mathrm{pe}_{aq} = (\log K_{VII/IV} - 4pH_c)/3 \quad (37)$$

Sorption of Tc(IV) onto mineral surfaces can also be taken into account. Because this study is restricted to pH ~ 8 and low ionic strength, no surface site protolysis or electrostatics are taken into account. We have considered the following simple reaction (38) to describe sorption onto the mineral surface:

$$\equiv S + TcO_4^- + 4H^+ + 3e^- \rightarrow \equiv STcO(OH)_2 + H_2O \quad (38)$$

where ≡S is a generic surface site and [≡S] can be calculated using equation (39) using the following parameters: site density: 1 site/nm^2; surface area: 0.16 m^2/g; S/V: 250 g/L.

$$[\equiv S] = site\ density \times surface\ area \times (S/V)/N_A = 6.64 \times 10^{-5}\mathrm{mol/L} \quad (39)$$

where N_A is the Avogadro constant. A similar surface complexation approach was proposed by Cui and Eriksen (1996) [61] for Tc uptake by Fe(II)-bearing minerals. According to the reaction (38), the equilibrium constant is calculated as:

$$K_{VII/IV,surf} = \frac{[\equiv STcO(OH)_2]}{[\equiv S][TcO_4^-][H^+]^4[e^-]^3} \quad (40)$$

Tc(IV) uptake on mineral surfaces is high [135], so that [≡STcO(OH)$_2$] is expected to be much larger than [TcO(OH)$_{2(aq)}$]. By contrast, Tc(VII) uptake on minerals can be neglected [136]. Using the surface complexation model, the Tc(VII)/Tc(IV) borderline in a Pourbaix diagram accounting for both processes in solution and at the mineral surfaces (denoted pe_{surf} or Eh_{surf}) is calculated as follows:

$$pe = \left(\log K_{VII/IV,surf} + log\left(\frac{[TcO_4^-]}{[\equiv STcO(OH)_2]} \right) - 4pH_c + \log[\equiv S] \right) /3 \quad (41)$$

$$pe_{surf} = \left(\log K_{VII/IV,surf} - 4pH_c + \log[\equiv S] \right) /3 \quad (42)$$

In other words, pe_{surf} is the pe value for 50% Tc uptake. Equation (42) applies only for sufficiently low $[Tc]_{tot}$ or high E_h, i.e. where the precipitation of $TcO_2 \cdot 1.6H_2O_{(s)}$ does not occur.

4. Results and Discussions

4.1. Batch studies

Here the term "sorption" implies the total Tc uptake by the solid mineral phase. The mechanism leading to the removal of Tc from solution may be attributed to (i) a sorption/surface complexation of a Tc(IV) species after reduction (Tc(VII) should show no or only very weak sorption) in solution by e.g. Fe(II) and/or (ii) a precipitation of insoluble $TcO_2 \cdot 1.6H_2O_{(s)}$ again due to Tc(VII) reduction by e.g. Fe(II) species. Especially in case of the highest Tc concentration reduction/precipitation process might occur, as the Tc(IV) solubility could be significantly exceeded. A third (iii) possible mechanism of Tc retention could be the Tc(VII) surface reduction by Fe(II) surface species. A general scheme of the processes potentially involved into Tc(VII) immobilization is shown in Figure 23.

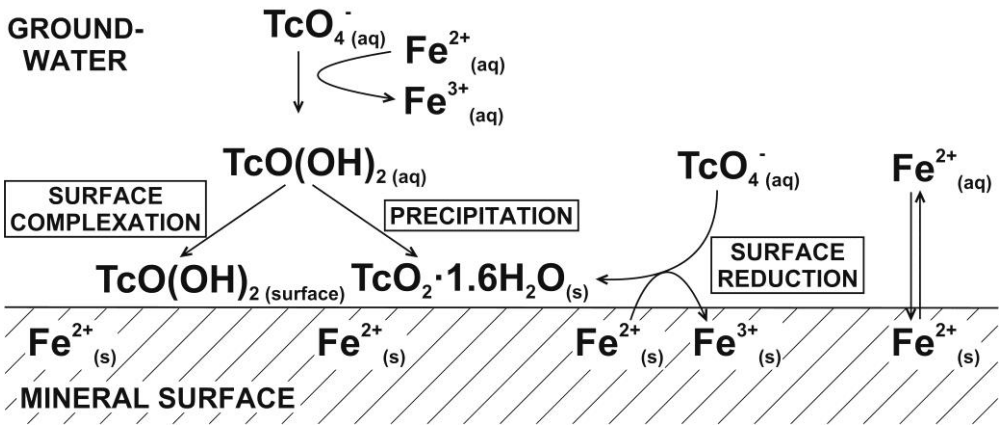

Figure 23. *General scheme of Tc(VII) sorption/reduction processes.*

Here, only Fe(II) is considered as a potential reducing agent for Tc(VII)/Tc(IV) transformation according to equation (43):

$$TcO_4^- + 3Fe^{2+} + 4H^+ \rightarrow TcO(OH)_2 + 3Fe^{3+} + H_2O \qquad (43)$$

From this equation the Fe:Tc ratio required for the complete Tc(VII) reduction is 3:1.

4.1.1. Tc sorption on iron oxides

To investigate the influence of Fe(II) content in the solid phase onto Tc(VII) immobilization, technetium batch sorption experiments on freshly synthesized magnetite as a reference material were carried out.

4.1.1.1. Redox potential measurements

The redox potential in all magnetite samples after one month contact time is shown in Figure 24 and in Table 11. An uncertainty of ~ ±50 mV should be considered for the data. The Eh values were recorded over a period of one day in an open vial in the Ar glovebox (< 1 ppm O_2). The measurements were performed under static conditions after sedimentation of the suspension with a magnet. Otherwise, the measurements of the continuously shaken suspension were not reproducible most probably due to deposition of the magnetite particles on the electrode surface. Nevertheless, under static conditions the equilibration of the electrode normally took several hours (up to one day).

Table 11. *Redox potential values for the Tc-magnetite system with different Tc concentrations after one month contact time.*

	Redox potential, mV		
	10^{-5} M Tc	10^{-8} M Tc	10^{-9} M Tc
pH 7	110	68	78
pH 8	91	99	93

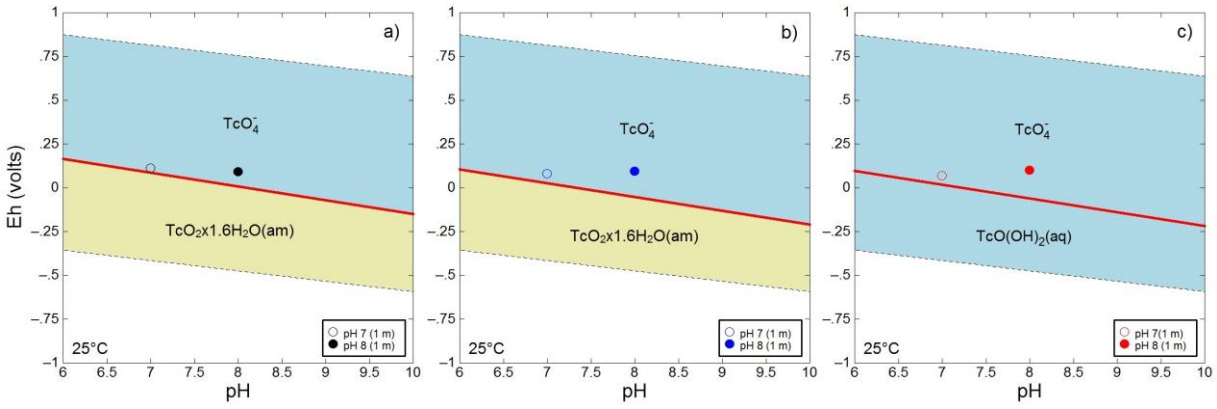

Figure 24. *Pourbaix diagrams of Tc with concentrations of 10^{-5} M (a), 10^{-8} M (b) and 10^{-9} M (c) in 0.2 NaCl.*

For the samples with pH 7 the redox potential values were directly on the Tc(IV)/Tc(VII) borderline representing the thermodynamic feasibility of the reduction in the aqueous phase. On the other hand, the samples with pH 8 exhibit values in the stability field of the Tc(VII) with a very low amount of Tc(IV) (can be calculated using equation (36)).

The iron speciation under the conditions applied (see Table 11) is illustrated in Figure 25. The hematite and goethite solid phases were supressed for the Pourbaix diagram calculation.

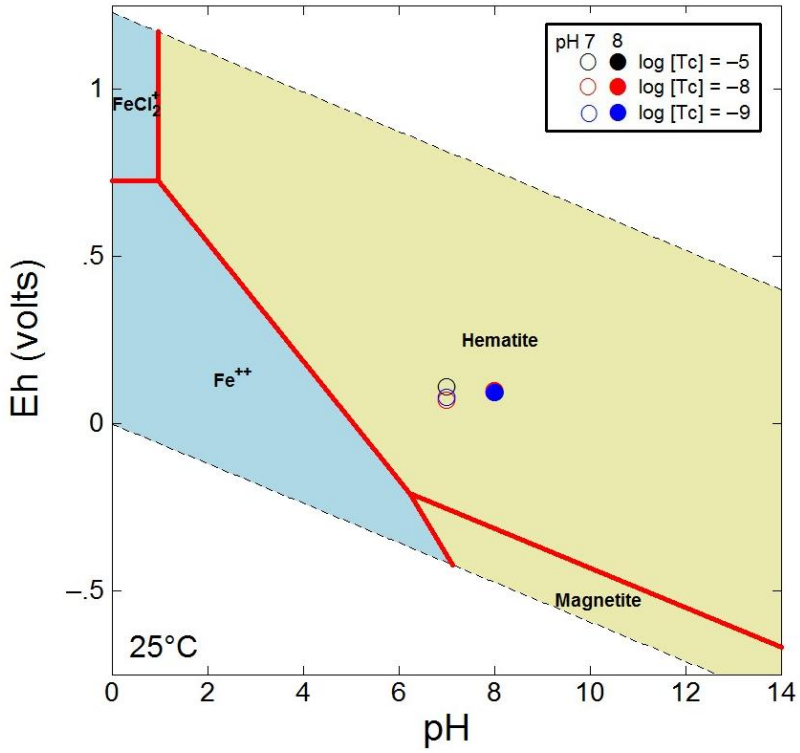

***Figure 25**. Pourbaix diagram of Fe together with the experimental Eh/pH conditions of Tc batch sorption studies. 2 g/L Fe_3O_4, I = 0.2 M.*

The redox potential values obtained for the Tc-magnetite system are higher compared to the investigations performed within the PhD work of Yalcintas [137], who measured ~ -100±50 mV under pH 8.68. The magnetite in the work of Yalcintas was synthesised using a different technique (direct precipitation from the Fe(II)/Fe(III) solution, described by Kirsch et al. [138]), which also might influence redox potential of the system.

Based on the presented predominance diagram the samples are located in the hematite stability field. However, according to the XPS studies (see paragraph 4.2.1.1) magnetite shows still stoichiometry under the conditions applied, which might be due to the slow kinetics of this transformation. The redox potential measurements could also be unrealistic because of the low Fe concentration in aqueous phase. The concentration of both components of Fe(II)/Fe(III) redox couple required for reproducible and thermodynamically defined redox potential measurements using a Pt-electrode is reported to be ≥ ~ 10^{-6} M [139].

4.1.1.2. Tc sorption on magnetite

The results of Tc batch sorption studies with magnetite are presented in Figure 26. The full set of sampling results is given in supplementary materials in Table S 1. Tc uptake reaches a plateau of ~ 100% after about one week contact time for all investigated cases in contrast to

the expectations by the Eh measurements, where significant fractions of non-sorbing TcO_4^- are expected (see Figure 24). Three different Tc concentrations (10^{-5} M, 10^{-8} M and 10^{-9} M) and two pH values (7 and 8) were studied.

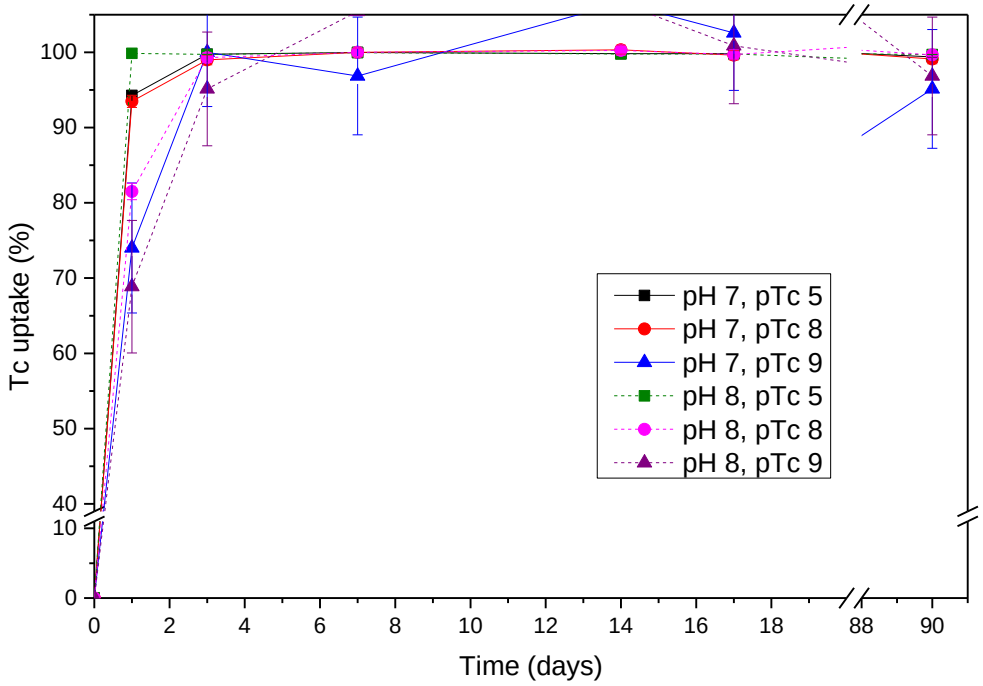

***Figure 26**. Sorption kinetics for different initial Tc concentrations onto magnetite at pH 7 and 8. Background electrolyte: 0.2 M NaCl.*

No suspended Tc colloidal phases were found by ultracentrifugation within experimental uncertainties for all samples (see Table S 1 in supplementary materials). We conclude that Tc does not form colloids under given conditions or the colloids formed are directly associated with the magnetite surface and cannot be differentiated by the rather simple separation technique.

For investigation of the influence of the magnetite stoichiometry (Fe(II)/Fe(III) ratio) a set of magnetite samples was oxidized by hydrogen peroxide solution. The XPS spectra with characteristic Fe(II) feature and $Fe(II)/Fe_{tot}$ ratios are presented in Figure 27. The ferrous iron content correlates with the resulting Fe(II) content. It is remarkable that even after treatment of the magnetite sample by the oxidant in 100-fold excess still contained 18.3% Fe(II). In the work of Gorski et al. [108], who applied a similar procedure to treat smaller magnetite crystals (~ 10 nm) the Fe(II) oxidation was also not complete. Most probably after the oxidation of the surface layers the further oxidation of the matrix is supressed or, at least, kinetically hindered.

For better interpretation of the results of XPS measurements it is important to know the penetration depth of the analysis. The attenuation length χ (nm) of the electron flux including elastic scattering can be calculated by equation (44) [140]:

$$\chi = 0.316a^{3/2}\left(\frac{E_k}{Z^{0.45}[ln(E_k/27)+3]}+4\right) \quad (44)$$

$$a = 10^7\left(\frac{m_a}{\rho N_A}\right) \quad (45)$$

where a is a lattice parameter corresponding to the mean atom size (nm), E_k is a kinetic electron energy (eV), Z is a mean nuclear charge of the material, m_a is a mean atomic weight (g/mol), ρ is a material density (g/cm^3) and $N_A = 6.022 \times 10^{23}$ is the Avogadro number.

The information depth providing 95% of signal is calculated as:

$$d_{inf} = 3\lambda \cos\varphi \quad (46)$$

where φ is the angle between photo-emitted electron beam and the surface normal.

For the stoichiometric magnetite the mean nuclear charge is 15.71, the density is 5.2 g/cm^3 and the mean atomic weight is 33.08 g/mol (http://www.mindat.org/min-2538.html). With these parameters λ of the Fe $2p_{3/2}$ (711 eV) [126] equals to 1.28 nm. Thus, applying equation (46) the information depth is 2.7 nm. Magnetite has a face-centred cubic spinel structure with a unit cell size a = 0.839 nm, Z = 8 (http://www.mindat.org/min-2538.html). Hence, XPS measurement covers ~ 3 unit cell layers with 8 Fe(II) atom in each unit cell.

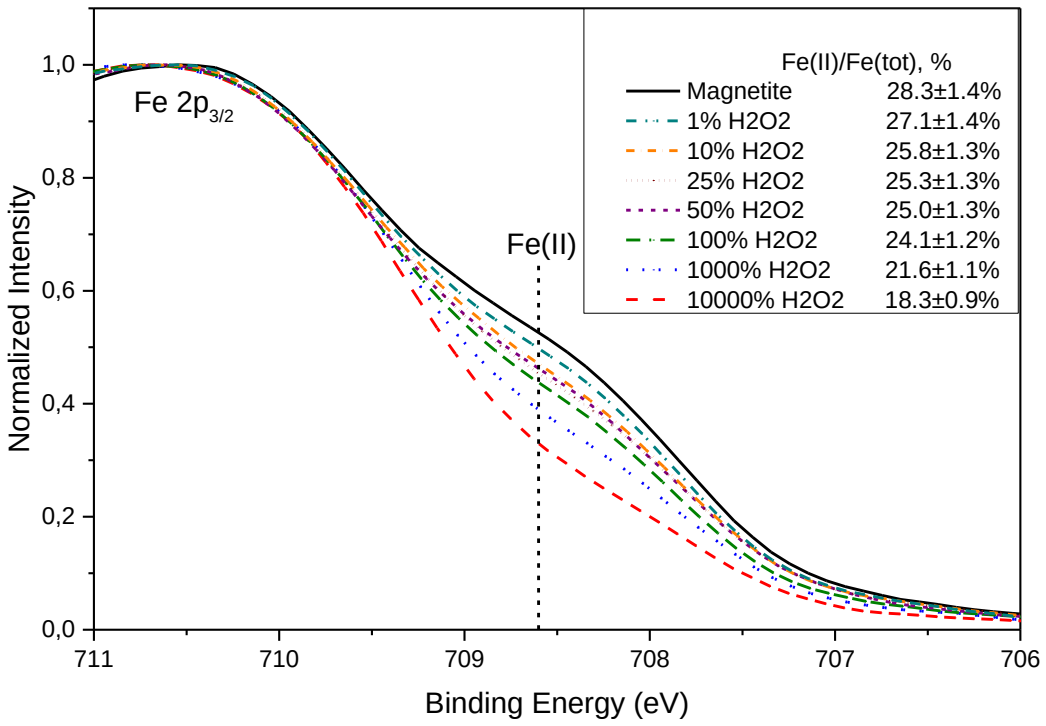

Figure 27. *XPS narrow scans of Fe $2p_{3/2}$ spectra of partially oxidized magnetite depending on H_2O_2 content.*

After determination of the Fe(II)/Fe_{tot} ratio several samples (with 18.3%, 22.6%, 24.7% and 27.1% Fe(II)) were chosen for technetium batch sorption studies. The time dependent Tc retention is shown in Figure 28 for both partially oxidized and non-oxidized samples. It was found, that even a minor decrease in the Fe(II) concentration at the magnetite surface retards the Tc reduction. When stoichiometric magnetite (here 29% Fe(II)/Fe_{tot}) reduces ~ 99.7% Tc after 3 days (log [Tc] = -5, 2 g/L solid to liquid ratio, pH 8), magnetite with 24.7% Fe(II)/Fe_{tot} reduces a comparable amount only after 3 weeks. However, after 204 days the Tc uptake by the samples with Fe(II)/Fe_{tot} > 18.3% is almost quantitative.

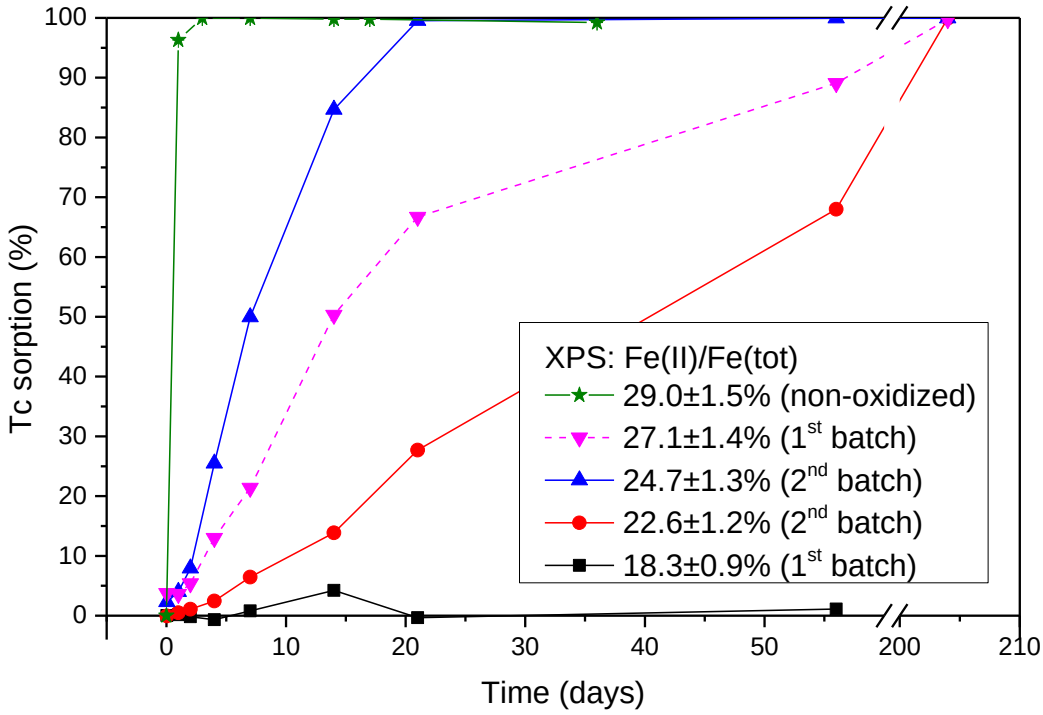

Figure 28. *Tc sorption kinetics on partially oxidized magnetite depending on the Fe(II)/Fe$_{tot}$ ratio.*

Slower reduction kinetics for 27.1% Fe(II)/Fe$_{tot}$ sample compared to 24.7% sample can be explained by its longer contact time with H_2O_2. The samples with 27.1% and 18.3% Fe(II) were prepared in the 1st test batch and analysed with XPS before other samples shown in Figure 28. Thus, the time before starting the experiment on interaction with Tc solution was ~ 2 weeks longer. Despite the fact that all magnetite samples were washed 5 times with MilliQ water after the contact with oxidizing peroxide solution, some H_2O_2 might be sorbed on the magnetite surface as was reported for TiO_2 [141]. Thus, the Fe(II) content in this particular sample might be lower than 27.1% or even 24.7% when the experiment with Tc was started. In addition, the analytical uncertainty of 5% for all Fe(II)/Fe$_{tot}$ estimations should be taken into account. For instance, the confidence intervals for 24.7% Fe(II) (23.5 – 26.0%) and 27.1% Fe(II) (25.8 – 28.5%) samples overlap.

The non-stoichiometric magnetite sample with 18.3% Fe(II)/Fe$_{tot}$ does not show any reduction activity towards Tc(VII) solution even after 56 days contact time. Based on the XPS penetration depth calculations mentioned above (see equation (46)) the surface layer could be fully oxidized. Since XPS analyses ~ 3 unit cells in depth and the original magnetite stock contained 29% Fe(II)/Fe$_{tot}$, after the complete oxidation of the outer layer of unit cells the measurement should show ~ 19% Fe(II)/Fe$_{tot}$, which is almost similar to the 18.3% obtained for the most oxidized sample. Thus, the complete oxidation of the surface layer might lead to

the magnetite passivation preventing the interaction between Fe(II) and Tc(VII). Furthermore, even with a stoichiometric magnetite core of the crystals the sample is still inert towards Tc(VII) in the observation period of 56 days.

Similar studies with U(VI) reduction by partially oxidized magnetite were performed by Latta et al. [142] and Huber et al. [143]. A comparison between this data with Tc(VII) reduction data obtained within the present work is shown in Figure 29. According to the diagram, there is a threshold in reactivity of partially oxidized magnetite between ~ 22% and ~ 27% Fe(II)/Fe_{tot}. Samples with lower Fe(II) content are almost inert towards Tc(VII) or U(VI) reduction, while slight oxidation of the material from 29% (for freshly prepared magnetite) down to ~ 27% Fe(II)/Fe_{tot} does not change its properties significantly. Since Tc(VII) and U(VI) interaction with partially oxidized magnetite has a similar trend, this threshold should represent a radical change in magnetite reduction properties.

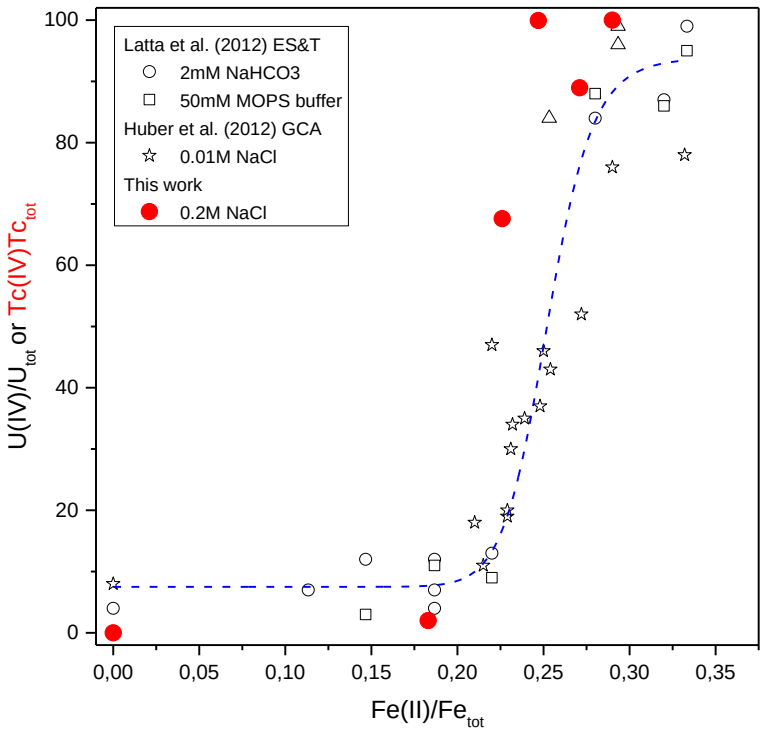

Figure 29. *Comparison between Tc uptake by partially oxidized magnetite with uranium data from Latta et al. [142] and Huber et al. [143]*

Gorski et al. [108] have reported the Eh values measured for different Fe(II)/Fe_{tot} of the partially oxidized magnetite under pH 7.2. The diagram showing the values obtained by Gorski et al. together with 50% Tc(VII)/Tc(IV) borderlines calculated using the equations (37) and (42) (see paragraph 3.2.8) is presented in Figure 30.

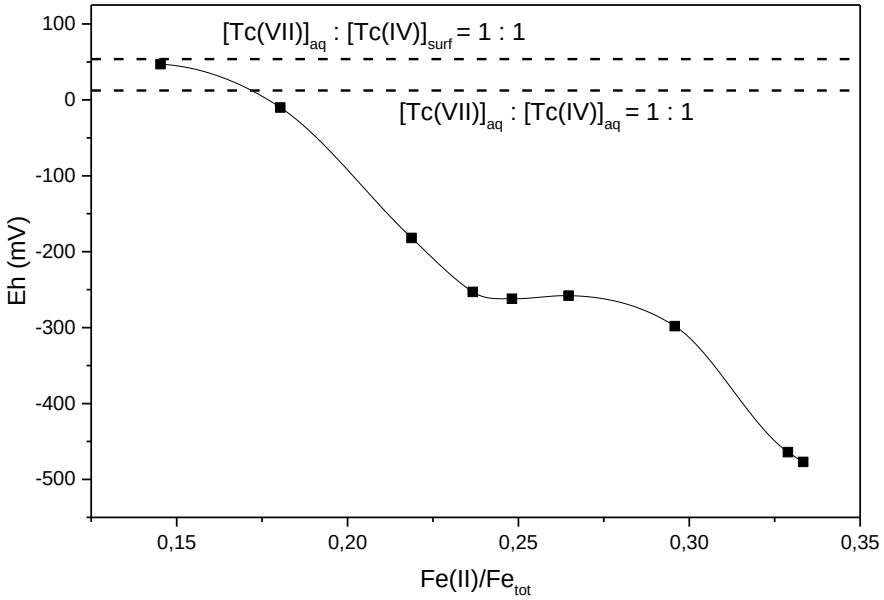

Figure 30. *Eh values of the partially oxidized magnetite against the stoichiometry (based on Gorski et al. [144]) plotted together with the Eh values of 50% Tc(VII)/Tc(IV) for pH 7.2.*

According to Figure 30 the non-stoichiometric magnetite with a Fe(II)/Fe_{tot} ratio ~ 15% should reduce Tc(VII) in presence of the solid phase. However, the experimental data of the present work shows no reduction for the magnetite sample containing 18.3% Fe(II)/$Fe_{tot.}$ One should also take into account that the Eh measurement technique in the paper by Gorski et al. is completely different from the common approach using a Pt electrode. A powder disk electrode made with the synthesized magnetite samples and a Ag/AgCl reference electrode (values converted to SHE) were used for to obtain open-circuit potential (E_{OCP}). Nevertheless, the general trend of an increasing Eh and decreasing Fe(II)/Fe_{tot} ratios might explain the observed tendency in reducing abilities of the magnetite samples shown in Figure 29.

4.1.1.3. Tc sorption on maghemite

Maghemite as an isostructural analogue of magnetite without ferrous iron was taken for batch sorption experiments to investigate pure Tc(VII) retention in the absence of its reduction by Fe(II). Sorption of technetium onto maghemite during batch type experiment was not detected within one month contact time. Technetium concentrations of 10^{-9} M, 10^{-8} M and 10^{-5} M were investigated under pH 7 and 8. Thereby, Fe(II) content is a driving force of Tc retention on magnetite. Furthermore, without reduction to Tc(IV) no Tc uptake was observed.

4.1.1.4. Tc sorption parameters

The main sorption parameters derived from the Tc batch sorption studies on the stoichiometric/non-stoichiometric magnetite are summarized in Table 12. The Tc uptake on the maghemite is included into the table as well.

Table 12. *Main parameters obtained for Tc (VII) sorption onto stoichiometric and partially oxidized magnetite.*

Fe(II)/ Fe_{tot}, %	pH	$[Tc]_{tot}$, M	Eh, mV	r, d^{-1}	K_d, L/kg	K_a, m	Tc sorbed, %
29±1.5	7	10^{-5}	110±50	2.83±0.02	$(5.2±4.8)×10^{7}$	4.8±4.3	100±0.01
		$(1.0±0.2)×10^{-8}$	78±50	2.02±0.03	$> 10^{6}$	> 0.1	100±0.4
		$(7.8±0.8)×10^{-10}$	68±50	0.75±0.04	$> 10^{4}$	$> 10^{-3}$	99±6
	8	10^{-5}	91±50	3.36±0.08	$(8±2)×10^{5}$	0.08±0.01	99.94±0.01
		$(1.0±0.2)×10^{-8}$	93±50	0.86±0.04	$> 10^{6}$	> 0.1	100±0.6
		$(7.8±0.8)×10^{-10}$	99±50	1.3±0.3	$> 10^{4}$	$> 10^{-3}$	100±6
27.1±1.4	8	10^{-5}	n.m.	0.046 ±0.003	$(4.2±0.3)×10^{4}$	$(3.8±0.2)×10^{-3}$	99.76±0.01
24.7±1.3				0.10±0.01	$(2.4±0.6)×10^{5}$	$(2.2±0.5)×10^{-2}$	99.96±0.01
22.6±1.2				0.017 ±0.002	$(1.9±0.4)×10^{5}$	$(1.7±0.3)×10^{-2}$	99.95±0.01
18.3±0.9				n.a.	1.12±0.01	10^{-7}	1.10±0.01
< DL	7&8	10^{-5}, 10^{-8}, 10^{-9}	~300±50	n.a.	n.a.	n.a.	< DL

n.m. – not measured; n.a. – not applicable.

The uptake rate coefficients (*r*) were calculated by fitting the sorption data (Figure 26 and Figure 28) to the equation (30). According to the experimental values, the uptake is faster for the higher initial Tc concentration. This trend can be generally explained by the collision theory.

Based on the Eh values measured, for pH 7 samples Tc(VII) reduction is thermodynamically feasible in the aqueous phase (see Figure 24). The solubility limit of $TcO_2 \cdot 1.6H_2O_{(s)}$ is reported to be ~ $4.4×10^{-9}$ M [66], bulk precipitation can be expected at log $[Tc]_{tot}$ = -5 and log $[Tc]_{tot}$ = -8 but not at log $[Tc]_{tot}$ = -9. Thus, for the various $[Tc]_{tot}$ the contribution of the bulk precipitation among the retention mechanisms mentioned in Figure 23 is different, which might additionally influence the uptake rate.

According to the Pourbaix diagram (see Figure 24), experimental Eh values for the samples under pH 8 are too high for Tc(VII) reduction in the solution. Nevertheless, taking into account the redox potential measurements uncertainty around ±50 mV [145] or ±25 mV [139] and the Pt-electrode detection limit for both parts of Fe(II)/Fe(III) redox couple ~ 10^{-6} M

[139], we assume that similar Tc(VII) reduction processes are also taking place under both pH 7 and 8.

Typical distribution coefficients (K_d) were calculated using the equation (31). For all investigated samples log K_d stays in the range between 4 and 7 except for the most oxidized magnetite sample with $Fe(II)/Fe_{tot}$ = 18.3%. Furthermore, for most of the samples the log K_d value is around 6 with small deviations, even for the partially oxidized magnetite. However, for the samples with log $[Tc]_{tot}$ = -8 and -9 only lower limits for K_d values could be determined, because the Tc concentration in the supernatant after the contact with magnetite was lower than the detection limit of LSC.

The surface normalized distribution coefficients (K_a) were derived using the equation (32). Similar to the K_d values, only a lower limit is available for K_a for those samples with total Tc concentrations lower than 10^{-5} M.

4.1.2. Tc sorption on crystalline rock materials

4.1.2.1. Redox potential measurements

Redox potential measurements of the samples were carried out after about two weeks and one month contact time in the sorption experiments. Every sample was measured over a period of one day in an open vial in the Ar glovebox (< 1 ppm O_2) to follow the Eh evolution with time. A typical time dependent Eh evolution is shown in Figure 31. The initial drop of the Eh is interpreted as the equilibration of the electrode with the sample, whereas the continuous increase in the later period is explained to be a result of oxidation due to traces of oxygen in the Ar glovebox (< 1 ppm O_2) that seems to be enough to compensate the redox capacity of the sample within 24 hours. Therefore, the lowest Eh value detected was used as most representative for the undisturbed rock/water system in the closed vial.

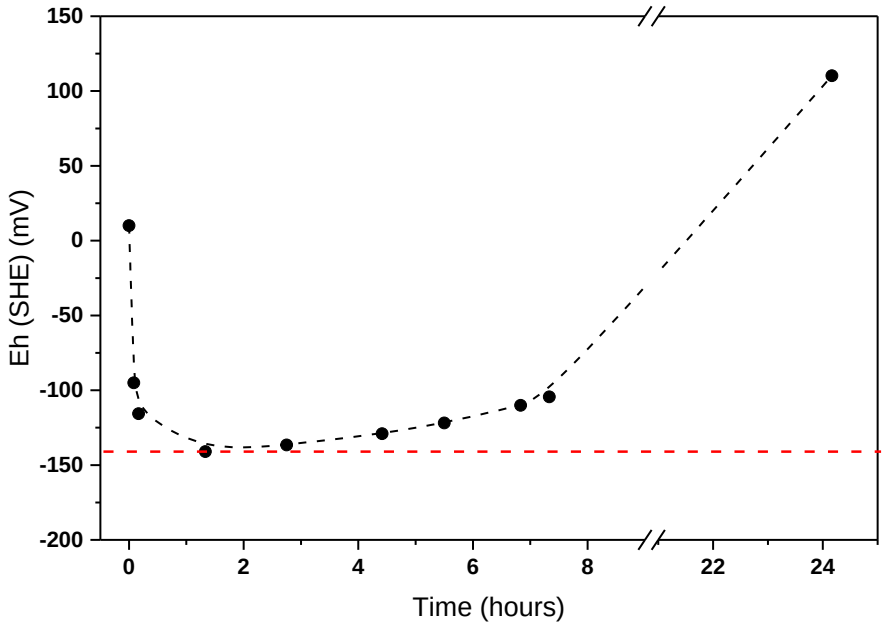

***Figure 31**: Typical evolution for measurement of Eh in synthetic Äspö groundwater simulant (ÄGWS) with un-oxidized diorite sample ([Tc] = 10^{-10} M).*

Redox potential measurements of Tc ÄGWS contacted with oxidized and un-oxidized ÄD for three different $[Tc]_{tot}$ after two weeks and one month are shown in Figure 32 together with Pourbaix diagrams calculated for the ÄGW composition. The Tc(IV)/Tc(VII) borderline in the diagram has the same position as for the magnetite system (see Figure 24) since the ionic strength is comparable (0.185 M for ÄGW and ÄGWS; 0.2 M NaCl for iron oxides aqueous phase in the sorption studies).

For oxidized ÄD material the redox potential (Eh_{SHE}) does not change significantly as a function of Tc concentration and is within the range of +230 to +280 mV. However, for un-oxidized ÄD material two trends were observed during the Eh measurements: (a) for low Tc concentration (up to 10^{-8} M) the Eh value decreases with time from 14 days to one month and (b) for the highest Tc concentration used (10^{-5} M) the Eh value was unchanged within the experimental uncertainty. Our explanation for the Eh trend observed is that log $[Tc]_{tot}$ = -5 is already sufficient to exceed the low redox capacity of the contacted diorite material with the solid to liquid ratio of 250 g/L used. In the cases of lower Tc concentrations the Fe(II) release from the crystalline rock is not fully countervailed by Tc(VII) reduction and the Eh value decreases. Tc speciation under these conditions is discussed in the modelling chapter of this work.

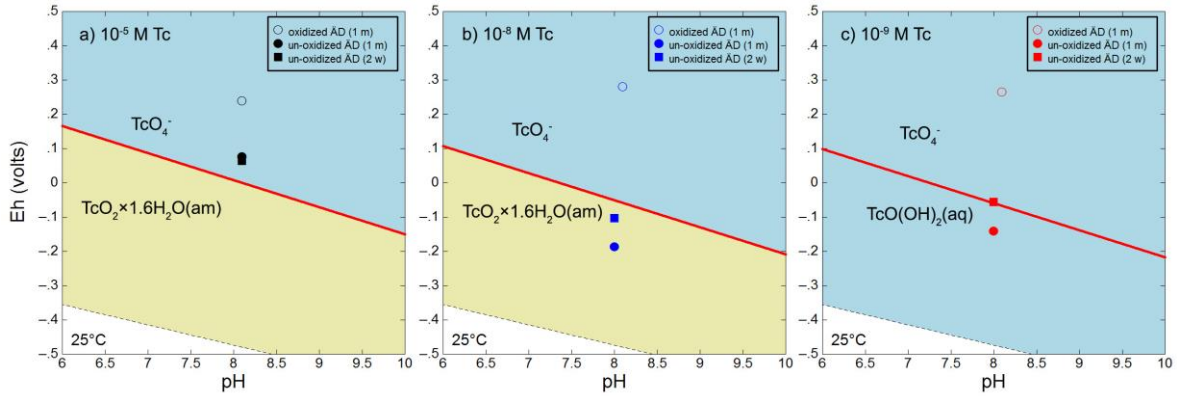

Figure 32. *Pourbaix diagrams for ÄGWS containing different Tc concentrations: (a) 10^{-5} M, (b) 10^{-8} M and (c) 10^{-9} M. Data points are given for oxidized (open symbols) and un-oxidized (filled symbols) ÄD for a contact time of two weeks (squares) and 1 month (circles).*

Redox potential values after one week of Tc sorption on NK material are similar (within error margins) to those found for experiments with oxidized ÄD (*ca.* +300 mV) and do not differ significantly for varying Tc concentrations. The same trend of decreasing Eh values was measured as already observed in the ÄD system. After one month of equilibration redox potentials were ~ +230 mV. According to the Pourbaix diagrams, Tc reduction in the supernatant is thermodynamically feasible only in the case of un-oxidized material with low Tc concentrations. For oxidized material Tc(VII)/Tc(IV) reduction may take place on the material surface or in pores, where Fe(II) concentration is possibly higher. This, however, would imply that a clear disequilibrium exists in the system. For further discussion it is referred to the "Thermodynamic calculations" section below.

4.1.2.2. Tc sorption on Äspö diorite

Kinetics of the sorption of Tc onto oxidized and un-oxidized ÄD at different Tc concentrations are given in Figure 33. Tc uptake values for the full set of samples studied are presented in supplementary materials in Table S 2.

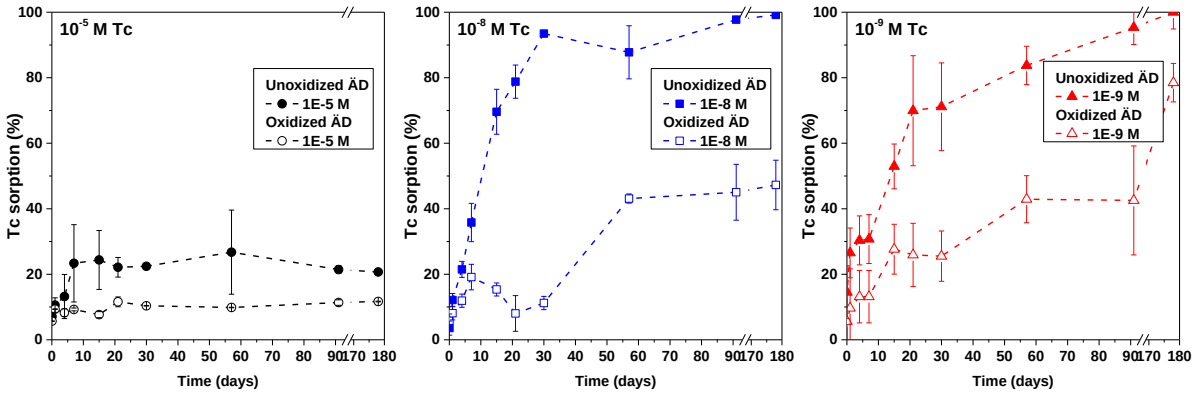

***Figure 33**: Tc sorption with time for different concentrations in presence of oxidized and un-oxidized ÄD (pH 8, I = 0.2 M).*

The formation of colloidal Tc phases (eigencolloids) by comparison of ultracentrifuged to non-ultracentrifuged samples was not detectable within the uncertainty limits (± 5-10%). Either these colloidal phases are not formed or are not stable under the Äspö GWS conditions chosen (ionic strength ~ 0.2 M, pH 8).

From the Tc sorption experiments, it is evident, that Tc uptake on un-oxidized material is much higher compared to that on the artificially oxidized granite. For the samples containing 10^{-8} M and 10^{-9} M $[Tc]_{tot}$ in contact with un-oxidized material plateau values of ~ 100% sorption are obtained (after 90 days contact time), whereas during the same observation period in experiments with oxidized ÄD only ~ 40% of total Tc are removed from solution. In samples with 10^{-5} M Tc much less uptake is observed showing a plateau level for sorbed Tc of around 20 – 25% for the un-oxidized samples and ~ 10% for the oxidized samples. The steady state is reached after approx. seven days which is much faster than for the lower $[Tc]_{tot}$. Based on the Eh/pH conditions established Tc(VII) reduction both on the surface of un-oxidized ÄD crushed material and in solution seems to be feasible from a thermodynamic point of view.

In order to estimate the amount of the ferrous iron buffer available in the oxidized and un-oxidized ÄD material we quantified the ion exchangeable Fe(II) fraction. Furthermore, XRF data for the new un-oxidized and old oxidized ÄD material are given in the Table 5, showing that the overall Fe(II) content is drastically reduced for the oxidized samples.

The assessment whether the available amount of Fe(II) is sufficient to reduce added Tc(VII) was conducted using the technique used by Heron et al. [114]. The ion-exchangeable Fe(II) content, estimated by 1 M $CaCl_2$ extraction, was taken as an approximation for the "available Fe(II)" and decreases from $(2.2\pm0.5)\times10^{-5}$ M in un-oxidized ÄD to $(9\pm5)\times10^{-6}$ M in oxidized ÄD and to the lowest values of $(2.5\pm2.0)\times10^{-6}$ M in the oxidized NK granite. Based on the

solid to liquid ratio chosen (250 g/L) these values give $(1.8\pm0.4)\times10^{-7}$ mol/vial Fe(II) for un-oxidized ÄD, $(7\pm4)\times10^{-8}$ mol/vial Fe(II) for oxidized ÄD and $(2.0\pm1.7)\times10^{-8}$ mol/vial Fe(II) for NK granite. These findings indicate that the investigated NK core was more oxidized than ÄD and/or the cores initially had a lower overall redox buffer capacity. The former explanation seems to be more likely given the fact that the material was extracted and transferred under normal ambient atmospheric conditions.

From the comparison of the Fe(II) content with the total amount of added Tc, 8×10^{-8} mol/vial (10^{-5} M Tc), 8×10^{-11} mol/vial (10^{-8} M Tc) and 8×10^{-12} mol/vial (10^{-9} M Tc), and taking into account that three electrons are required to reduce Tc(VII) to Tc(IV), i.e. 3 moles of Fe(II) are needed to reduce 1 mole of Tc(VII) (see equation (17)) Based on these rough estimations, oxidized ÄD still provides enough ion-exchangeable Fe(II) to reduce 30±20% of total Tc in the sample containing 10^{-5} M Tc, which is close to the experimental observation of 12±1% Tc being reduced. Furthermore, un-oxidized ÄD does not provide enough Fe(II) for the complete reduction of 10^{-5} M Tc. These estimations are supported by the finding that Eh values in the granite/water suspensions increase significantly when 10^{-5} M Tc(VII) are added. This amount apparently is sufficient to exceed the redox capacity of the diorite material at a solid to liquid ratio of 250 g/L. In all batch experiments the granite materials should provide enough Fe(II) for the Tc(VII) reduction at lower $[Tc]_{tot}$. Those considerations point to the fact that Fe(II) bound to the granite surface may act as a reductant for Tc(VII).

4.1.2.3. Tc sorption on Nizhnekansky granite

Batch sorption studies of Tc interaction with NK material were performed under conditions comparable to the ÄD experiments. The Tc sorption evolution for different initial Tc concentrations is shown in Figure 34. Table S 2 in supplementary materials contains the Tc uptake values for the full set of the samples investigated.

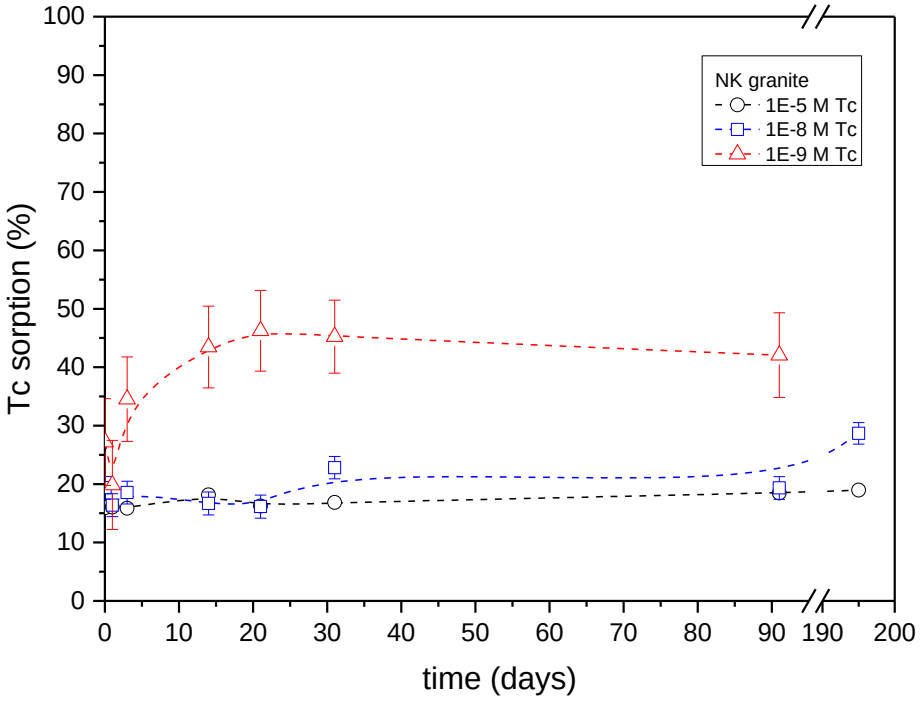

Figure 34. *Sorption kinetics for different Tc(VII) concentrations in contact with NK granitic rocks. pH 8, I = 0.005 M.*

After two weeks of contact time, plateau values of Tc removal were reached within the analytical uncertainty for all tested Tc concentrations applied, for log $[Tc]_{tot}$ = -5 it was reached almost immediately. In the case of the lowest Tc concentration (10^{-9} M) finally ~ 49% were sorbed, ~ 34% at 10^{-8} M Tc and for the highest initial concentration used (10^{-5} M) ~ 19%. These values are quite similar to the results found for Tc sorption onto oxidized ÄD, performed under similar conditions: ~ 40% for log $[Tc]_{tot}$ = -9 (after 3 months contact time), ~ 45% for log $[Tc]_{tot}$ = -8 and ~ 12% for log $[Tc]_{tot}$ = -5, respectively. Data on ion-exchangeable Fe(II) extraction (0.1 – 1 µg/g or $(2.5\pm2.0)\times10^{-6}$ M of Fe(II) for NK granite, and 1 – 3 µg/g or $(9\pm5)\times10^{-6}$ M for oxidized ÄD) indicate that the investigated NK cores were both stronger oxidized by air than ÄD and/or the cores had a lower overall redox buffer capacity. The former explanation seems more likely given the circumstance that the material was obtained and transferred under normal ambient atmospheric conditions and exposed to air atmosphere for several years. According to N_2-BET analyses the NK granite has a higher surface area of 0.32 m^2/g as compared to ÄD (0.16 m^2/g). However, since the mineral surfaces are not saturated with Tc, surface area does not limit Tc sorption and the Fe(II) content is considered to be the governing factor in the immobilization process.

Again, the formation of a Tc colloidal phase in the NK samples was not detected by comparison of ultracentrifuged with non-centrifuged samples. These findings are in-line with the results obtained for ÄD material. Furthermore, the ionic strength of the NKGWS is much lower (0.005 M) compared to the ÄGWS (0.2 M). This supports the hypothesis of either negligible formation of eigencolloids or its low stability under considered groundwater conditions.

4.1.2.4. Tc sorption isotherms

A separate set of un-oxidized and oxidized ÄD and NK samples was contacted with corresponding GWS containing different Tc concentrations in the range between 10^{-11} M and 10^{-5} M. The contact time was 5 months. The uptake values obtained from this experiment are given in supplementary materials in Table S 2 together with the data from batch studies. An illustration of the long-term sorption experiment results is given in Figure 35.

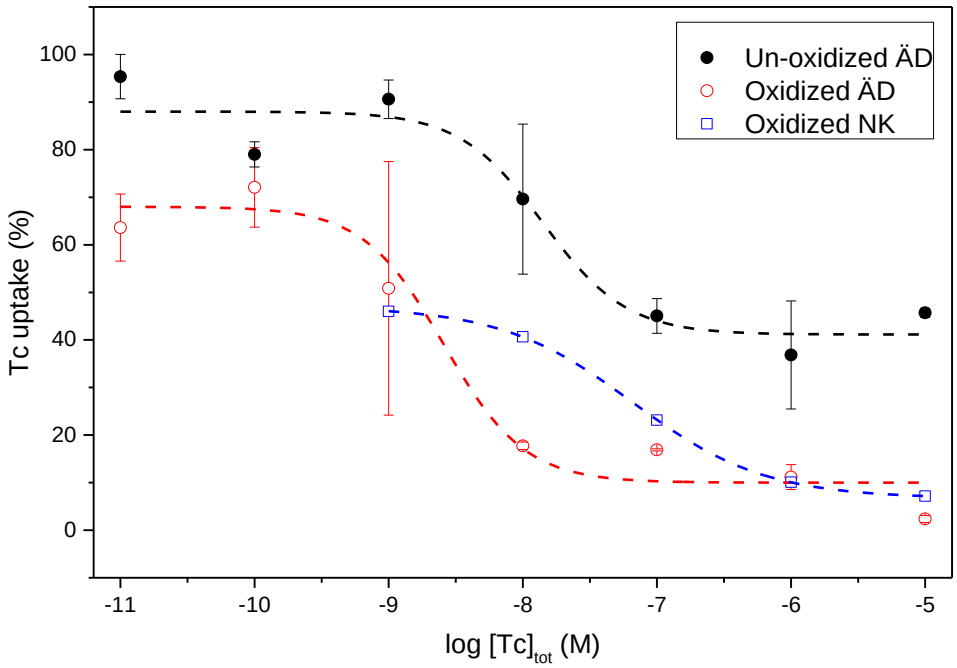

Figure 35. *Tc uptake after 5 months contact time with un-oxidized and oxidized ÄD and NK materials.*

According to the long-term interaction data of Tc-containing GWS with un-oxidized and oxidized ÄD and NK granite presented in Figure 35 both oxidized materials show lower relative uptake values than the un-oxidized rock. The data obtained can be plotted as a Freundlich isotherm in logarithmic scale (see Figure 36).

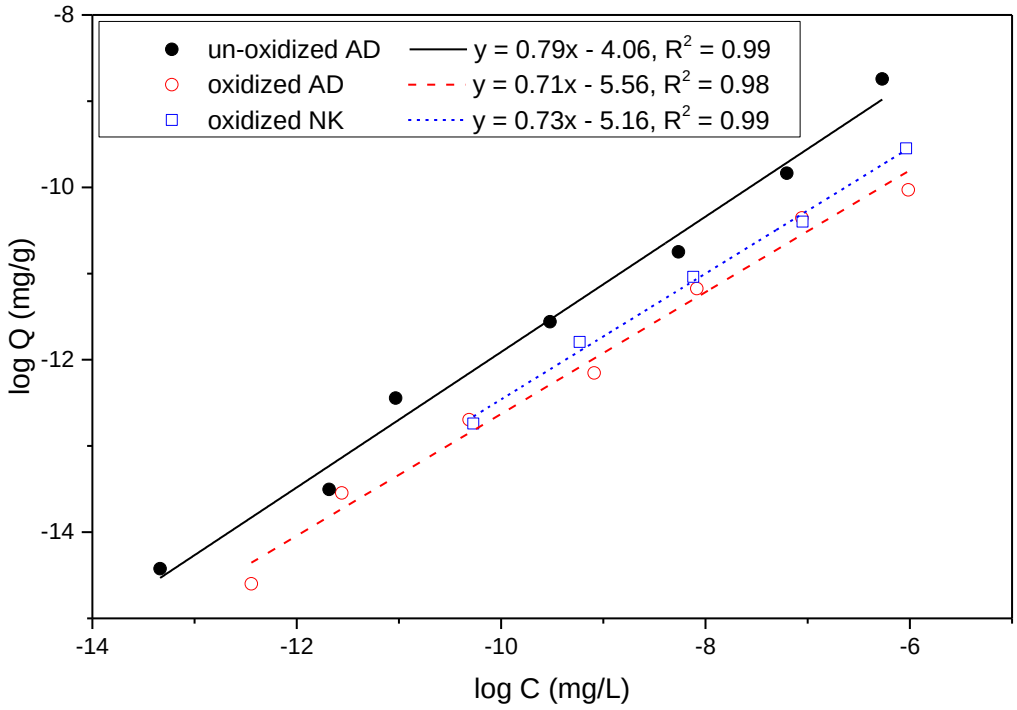

Figure 36. *Tc sorption isotherms for un-oxidized ÄD, oxidized ÄD and NK material.*

Linear fitting of the experimental data is providing the Freundlich isotherm [146] parameters based on the equation (47):

$$\log Q = \log K_f + \frac{1}{n} \log C \qquad (47)$$

where K_f is absorption value (in mg/g) at the adsorbate concentration of 1 mg/L, which is characteristic for the adsorbent and the adsorbate adsorbed; *n* is an empirical constant that shows the deviation from ideality (i.e. an ideal sorption behaviour corresponding to n = 1). The fitting parameters obtained are given in Figure 36. The values of n > 1 (~ 1.3 – 1.4 for the investigated systems) indicate the presence of different sorption sites or/and that the uptake is governed by more than one sorption mechanism [146]. This combination of processes involved may be attributed to surface complexation and precipitation, which are in addition dependent on prevalent redox conditions.

The empirical Freundlich adsorption parameters for the sorption of Tc(VII) to oxidized ÄD and NK materials are very similar (2.7×10^{-6} mg/g and 3.0×10^{-6} mg/g, respectively), while for the un-oxidized ÄD the K_f value is much higher (8.8×10^{-5} mg/g). This finding again shows the higher Tc uptake capacity of the well-preserved material compared to the oxidized one.

4.1.2.5. Thermodynamic modelling

The general modelling approach is described in the section 3.2.8. A similar concept was conducted in previous work for the modelling of Pu sorption on kaolinite [147] and Np sorption on illite [148] with respect to the differences in chemistry.

Figure 37 shows the Tc(IV) fraction in the aqueous phase modelled with PHREEQC for log $[Tc]_{tot} \leq -8$ as a function of the redox potential. For pH = 8.0 and I = 0.1 M, the $[Tc(VII)]_{aq}/[Tc(IV)]_{aq}$ borderline is at Eh = -53 mV (Eh_{aq}, calculated from equation (37)), as highlighted in Figure 37. To account for sorption processes (see equation (41)), log $K_{VII/IV,surf}$ is determined as follows. The site density is arbitrarily set equal to 1 site/nm^2, which is in the same order of magnitude as commonly observed for several minerals [149; 150]. The value for log $K_{VII/IV,surf}$ is strongly dependent on this arbitrarily chosen site density. At Eh values ≤ -90 mV almost all Tc is calculated to be Tc(IV) (see Figure 37). Such conditions prevail in the experiments with un-oxidized ÄD and log $[Tc]_{tot} \leq -8$. Taking these experimental data, log $K_{VII/IV,surf}$ is deduced by a fitting procedure and is found to be equal to 35.7 (see equation (40)). This value is kept constant for all the following calculations. The borderline redox potential where $[Tc(IV)]_{surf}$ and $[Tc(VII)]_{aq}$ exist in equimolar concentrations, Eh_{surf}, is found equal to -12 mV in accordance to the equation (42). In agreement with the findings of Marsac et al. [147; 148] for Np and Pu sorption to clays, the strong sorption behaviour of Tc(IV) shifts the borderline Eh to higher values as compared to that for the $[Tc(IV)]_{aq}/[Tc(VII)]_{aq}$ ratio, Eh_{aq}, in aqueous solution in the absence of mineral surfaces. For log $[Tc]_{tot}$ = -5 precipitation of $TcO_2 \cdot 1.6H_2O_{(s)}$ is predicted, which represents the 2nd retention mechanism, and extends the stability field of Tc(IV) further.

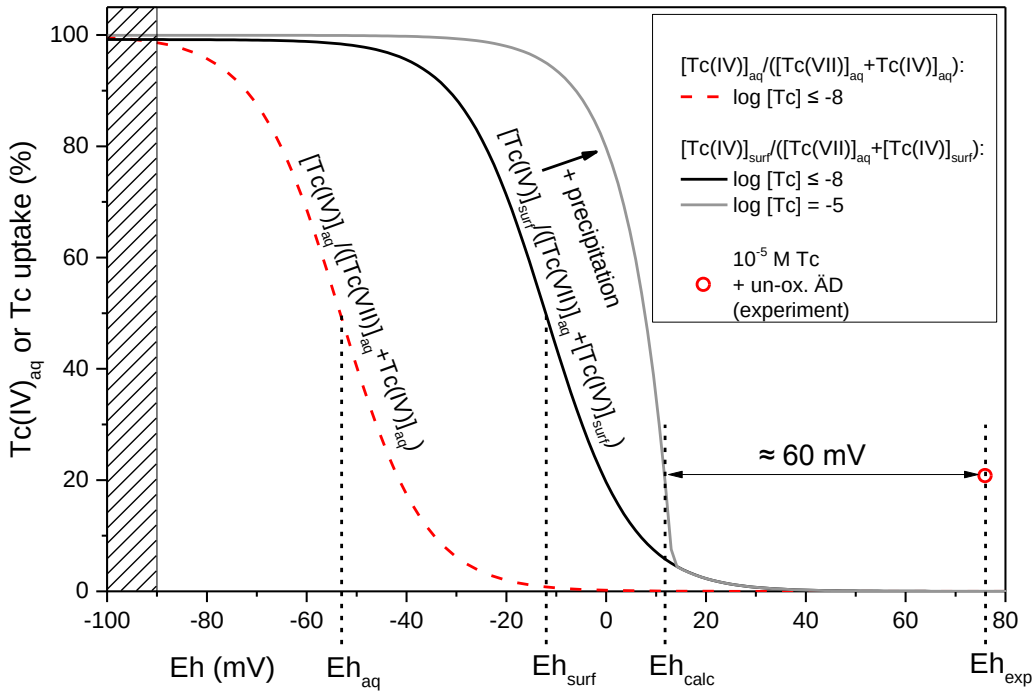

Figure 37. *Tc(IV) fractions depending on the redox potential (pH 8, I = 0.1 M) calculated according to the equations (36) and (41), respectively. Eh_{exp} corresponds to the measured redox potential; Eh_{calc} relates to the calculated redox potential where 21% of Tc is removed from solution in the experiment with log $[Tc]_{tot}$ = -5; $[Tc(VII)]_{aq}/[Tc(IV)]_{aq}$ and $[Tc(VII)]_{aq}/[Tc(IV)]_{surf}$ borderline redox potentials are as well marked by vertical dashed lines; the shaded area at the left side shows the Eh region where model calculations predict quantitative uptake.*

In the respective experiment the measured Eh value (Eh_{exp}) is 76 mV, where the model predicts insignificant uptake in disagreement with the experimentally observed ~ 21% uptake. Actually, the model is very sensitive to the redox potential. For instance, a change in Tc uptake from 2% to 80% is predicted by assuming a slight decrease in Eh_{calc} from +20 to 0 mV for log $[Tc]_{tot}$ = -5. Regarding the uncertainties of experimental Eh data in a range of ±50 mV [145] and the incertitude of model parameters, our simulation results are not so different from experimental data. The discrepancy of Tc uptake in simulation and experiment can easily be explained by uncertainties in redox potential measurements.

According to model calculations, the dominating uptake mechanism at log $[Tc]_{tot}$ = -5 is precipitation of $TcO_2 \cdot 1.6H_2O_{(s)}$. This is in agreement with XANES measurements performed with a 1 mM Tc-containing solution contacted with the crushed material material (see respective section 4.2.2.1 below). Tc(VII) found by XANES in the NK sample is most probably from the pore water, which was not completely removed during the washing procedure.

The model predicts almost 100% Tc uptake for Eh ≤ -90 mV in accordance with the experimental results for un-oxidized ÄD at log $[Tc]_{tot}$ ≤ -8 (see Table 13). However, relatively high Tc uptake (> 30%, see Table 13) of the oxidized materials at log $[Tc]_{tot}$ ≤ -8 and rather high Eh values (> 200 mV) cannot be explained by the thermodynamic model. No Tc reduction and no uptake is calculated above Eh ≥ ~ 30 mV (see Figure 37). Nevertheless, Tc uptake by the oxidized materials is significant but is lower as compared to that by the un-oxidized ÄD (see Figure 35). These findings may suggest that, although oxidized, a redox partner for the reduction of Tc(VII) to Tc(IV) is present in significant amounts for the reduction of Tc(VII) to Tc(IV), which, however, is not detected by the Eh measurements using a Pt-electrode. As was already mentioned, the amount of ion-exchangeable Fe(II) was estimated to be $(9\pm5)\times10^{-6}$ M for oxidized ÄD and $(2.2\pm0.5)\times10^{-5}$ M Fe(II) for un-oxidized ÄD. As was mentioned before, the concentration of both components of Fe(II)/Fe(III) redox couple for Eh measurements should be ≥ ~ 10^{-6} M [139]. Taking the above reported sensitivity of the redox potential measurements using a Pt-electrode and the ion-exchangeable ferrous iron concentration in the oxidized rock materials ($(9\pm5)\times10^{-6}$ M Fe(II) for oxidized ÄD and $(2.5\pm2)\times10^{-6}$ M Fe(II) for NK granite), we conclude that the Eh values measured for the oxidized systems might not be reliable.

4.1.2.1.Sorption parameters

The main sorption parameters calculated from the batch sorption studies are summarized in Table 13.

Table 13*. Main parameters obtained for Tc (VII) sorption onto ÄD and NK materials.*

Material	Fe(II) available, mg/g	Initial Tc concentration, mol/L	Eh, 1-2 months, mV	r, d^{-1}	K_d, L/kg	K_a, m	Tc sorbed after 6 months, %
ÄD un-oxidized	4 – 6	1.07×10^{-5}	76±50	0.36±0.14	1.1±0.2	$(6.8\pm0.8)\times10^{-6}$	21±2
		$(1.05\pm0.05)\times10^{-8}$	-187±50	0.078±0.008	500±200	$(2.9\pm1.3)\times10^{-3}$	99.2±0.6
		$(1.1\pm0.1)\times10^{-9}$	-142±50	0.051±0.008	900±800	$(5.3\pm4.9)\times10^{-3}$	99.5±6
ÄD oxi-dized	1 – 3	1.07×10^{-5}	238±50	0.15±0.04	0.53±0.05	$(3.3\pm0.3)\times10^{-6}$	12±1
		$(1.05\pm0.05)\times10^{-8}$	280±50	0.045±0.014	3.6±1.0	$(2.2\pm0.6)\times10^{-5}$	47±8
		$(1.1\pm0.1)\times10^{-9}$	264±50	0.015±0.006	22±8	$(1.4\pm0.5)\times10^{-4}$	84±6
NK	0.1 – 1	1.09×10^{-5}	235±50	n.a.	0.9±0.2	$(2.9\pm0.6)\times10^{-6}$	19±3

oxi-dized	$(1.07\pm0.03)\times10^{-8}$	205±50	n.a.	2±0.2	$(6.4\pm0.6)\times10^{-6}$	34±2
	$(1.1\pm0.1)\times10^{-9}$	230±50	0.19±0.13	3.4±0.9	$(1.1\pm0.3)\times10^{-5}$	46±7

n.a. – not applicable.

The sorption rate coefficients (*r*) were calculated from the sorption kinetics fitting according to the equation (30). The uptake rate increase for the higher Tc concentrations might be due to competition of several processes of Tc immobilization (see Figure 23), namely (i) bulk precipitation, (ii) surface Tc(VII) reduction and (iii) sorption of dissolved Tc(IV) species from the solution. Therefore, the uptake rate shows the same order of magnitude for log $[Tc]_{tot} \leq -8$ and a higher value for log $[Tc]_{tot} = -5$. As was shown in the "Thermodynamic modelling" chapter (see paragraph 4.1.2.5), $TcO_2 \cdot 1.6H_2O_{(s)}$ bulk precipitation is not expected for the samples with log $[Tc]_{tot} < -6$, while for log $[Tc]_{tot} = -5$ sample this is a dominating process. Since the higher the Tc concentration, the faster the uptake process, and the main difference in the mechanism for the higher Tc concentrations is increase the impact of precipitation, we conclude that with increase of the contribution of the bulk precipitation the overall uptake rate is also increasing. However, as was mentioned before (see paragraph 4.1.1.4), the collision theory predicts the higher reaction rate for the higher reagent concentration as well.

According to the results of Peretyazhko et al. [15] heterogeneous Tc(VII) reduction on the surface associated Fe(II) is by orders of magnitude faster than the homogeneous reduction by aqueous Fe^{2+} and may occur on the Fe(II)-containing mineral surfaces.

Exponential fitting of Tc sorption data from Bondietti and Francis [50] gives a rate value of around 1.1±0.4 d^{-1} for an initial Tc concentration of 1.1×10^{-7} M with Westerly granite as a solid material (167 g/L solid/liquid ratio). The pH/Eh values for this material were also comparable (pH 8, Eh -100 mV) to the conditions used in the present work, but neither Fe(II) content nor specific surface area of the material were specified in the paper, which could significantly contribute to the enhanced rates found in Bondietti and Francis [50].

Typical distribution coefficients (K_d) obtained within the present work were calculated using the equation (31) and summarized in Table 13 together with measured initial Tc concentrations, amount of ion-exchangeable Fe(II) and redox potentials.

Surface normalized distribution coefficients (K_a) values for the NK and ÄD material are calculated with equation (32) and shown in Table 13 as well. Since the surface area of oxidized and un-oxidized ÄD remains the same, this normalization does not affect their relative magnitude. Oxidized NK and ÄD materials show the same K_a values for log $[Tc]_{tot}$ =

-5, but for log $[Tc]_{tot} \leq$ -8 NK granite possesses lower K_a values most probably due to lower available Fe(II) content.

The K_d values obtained for the oxidized material (see Table 13, 10^{-5} M Tc) in this study are in a good agreement with recently published data of Videnska and Havlova [103] who reported a K_d value of 0.3 L/kg under oxidizing conditions for 1.6×10^{-4}M ^{99}Tc on granitic rocks from Melechov Massive, Centre Bohemian Massive, Czech Republic (> 0.8 mm size fraction), taking into account the higher Tc concentration used. Since the surface area was not mentioned in the publication, K_a values cannot be calculated for these results.

Since no batch studies for Tc uptake on well-preserved un-oxidized crushed granitic rocks has been presented in the literature, the data obtained is compared to the experiments performed under artificial reducing conditions. Ito and Kanno [151] compared the Tc distribution coefficient on granitic rocks (0.49 – 0.83 mm size fraction, 10^{-12} M [^{95m}Tc]) together with a number of other minerals depending on oxidizing/reducing conditions. Under oxidizing conditions (in 0.16 M $NaNO_3$) K_d values of 0.1 L/kg ($K_a = 4.8\times10^{-7}$ m) were obtained, while under reducing conditions (0.1 M $NaBH_4$ and 0.16 M $NaNO_3$) values of 45.6 L/kg ($K_a = 2.2\times10^{-4}$ m) increasing up to 68 L/kg ($K_a = 3.2\times10^{-4}$ m) with decreasing of NO_3^- concentration down to 0.016 M could be determined. The paper by McKinley and Scholtis [152] summarizes the data for Tc K_d values on different materials including granitic rocks used for safety assessment of waste disposal at that time. Here the values range from 0 to 250 L/kg depending on the experimental conditions and the origin of the rocks. The authors emphasize that Tc sorption under oxidizing conditions is normally very low or zero, and for reducing conditions K_d values increase by 1 – 2 orders of magnitude.

4.1.2.2. Desorption studies

4.1.2.2.1. Desorption experiments without artificial oxidation

Tc desorption was experimentally monitored over one month using samples where Tc had been previously equilibrated with rock material for three months. Very low Tc desorption was observed in all cases studied for both ÄD and NK materials irrespective of the nature of the material (oxidized or un-oxidized) used for sorption. For the case of ÄD samples two types of natural groundwaters – Äspö and Grimsel GWs (representing glacial melt water composition with low ionic strength, see Table 8) were used. Tc was detected in the liquid phase only for samples after contact with 10^{-5} M Tc ÄGWS. After one day contact time desorption achieved values of up to 7% of the Tc amount sorbed after the batch studies. This level remained

relatively stable up to 30 days of contact time. For lower Tc concentrations (10^{-8} M and 10^{-9} M initial concentration for sorption experiments) no desorption was detected with the detection limit of the analytical method of ~ 10^{-10} M. Taking into account the amount of sorbed Tc we conclude that less than ~ 10% are desorbed under the experimental conditions in the case of 10^{-9} M $[Tc]_{tot}$ and less than ~ 2% in the case of 10^{-8} M.

It is important to notice, that Tc was detected in the liquid phase after desorption of log $[Tc]_{tot}$ = -5 sample only during the first washing step (one day contact time) without further desorption within one month. The current interpretation of these results is that surface associated Tc(IV) was not re-mobilized and the measured Tc emerged from the porewater residual Tc(VII) from the liquid phase of the sorption studies, which was not completely removed.

4.1.2.2.2. Desorption experiments after artificial oxidation

Pre-oxidation of the ÄD samples under air for one month before addition of ÄGWS changed the Tc desorption behaviour drastically (Figure 38, left). Both sorption experiments with originally oxidized and un-oxidized materials revealed the same desorption behaviour possibly indicating a comparable Tc surface species. Desorption is fast with the main part of technetium being released after a few seconds contact time and after one day a concentration plateau value was reached. Desorption kinetics for both ÄD and NK materials with different $[Tc]_{initial}$ after sample pre-oxidation is given in Figure 38.

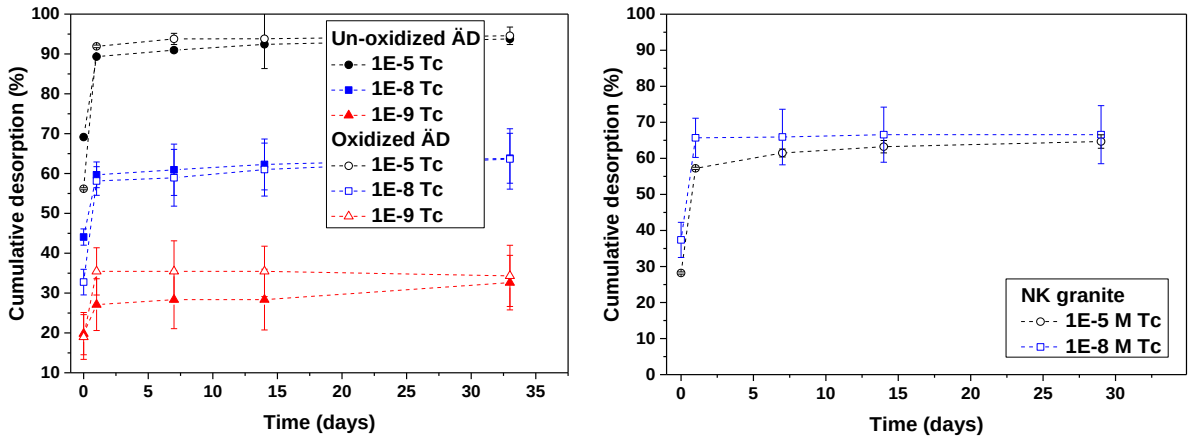

Figure 38. *Desorption kinetics of Tc sorption experiments performed with oxidized and un-oxidized ÄD material by ÄGWS (left) and oxidized NK granite by NKGWS (right) after one month pre-oxidation under atmospheric conditions.*

The general trend of the fast desorption up to the plateau value might be explained by the initial oxidation of surface associated Tc(IV) to the +7 oxidation state. Tc(VII) is remobilized

in the form of the pertechnetate anion, whereas Tc(IV) does not have any significant contribution to the desorption processs. The same observations were obtained by numerious investigators [153-155], where Tc(IV) oxidation was found to be a driving force for the Tc desorption process.

According to the thermodynamic modelling, two different mechanisms (predominantly surface complexation for log $[Tc]_{tot} < -7$ and $TcO_2 \cdot 1.6H_2O_{(s)}$ precipitation for log $[Tc]_{tot} > -7$) govern the Tc sorption process. Consequently, for the same initial Tc concentration, a similar Tc desorption behaviour can be assumed for oxidized and un-oxidized systems, which is in a good agreement with the experimental data observed for the ÄD. Higher desorption values observed for the samples with increased $[Tc]_{initial}$ can be explained by the relatively easier oxidation of the surface associated $TcO_2 \cdot 1.6H_2O_{(s)}$ phase in comparison to the surface complexed Tc(IV) species (see Table 14) which are probably more recalcitrant to remobilization during oxidation. Similar presumptions were expressed in several investigations [153-155], but the mechanistical nature of this resistance is still a matter of research (e.g. matrix diffusion).

Table 14. *Comparison of the sorption/desorption values for the un-oxidized and oxidized ÄD and NK materials.*

Material	-log $[Tc]_{initial}$	Tc sorption, %	Tc desorption, %
ÄD (un-oxidized)	5	21±2	93.7±0.6
	8	99.2±0.6	64±7
	9	99.5±6	33±7
ÄD (oxidized)	5	12±1	94±3
	8	47±8	64±8
	9	84±6	35±8
NK	5	19±3	65±2
	8	34±2	67±8
	9	46±7	< 50% (based on D.L.)

n.d. – not detected.

Comparison of the data obtained for oxidized ÄD and NK rock materials shows the same desorption values only for experiments performed at log $[Tc]_{tot} = -8$. In those experiments

performed at lower Tc concentrations and NK samples we could not obtain desorption data most probably because Tc concentrations were below the detection limit (~ 10^{-10} M).

4.2. Surface analyses

4.2.1. X-ray photoelectron spectroscopy (XPS)

4.2.1.1. Magnetite

Technetium oxidation state on the magnetite surface was determined by XPS (Figure 39, left). For this analysis magnetite contacted with 10^{-5} M Tc solution in 0.2 M NaCl background electrolyte was taken. It was proven, that Tc is reduced by Fe(II) and occurs only as Tc(IV) (Figure 39, right). No detectable traces of Tc(VII) were found on the magnetite surfaces. The Fe(II)/Fe(III) ratio in magnetite remained constant during the experiment due to excess of Fe(II), which was verified by XPS. The total Fe(II) amount was about $7.5 \cdot 10^{-3}$ mol/L versus the highest Tc concentration of 10^{-5} mol/L.

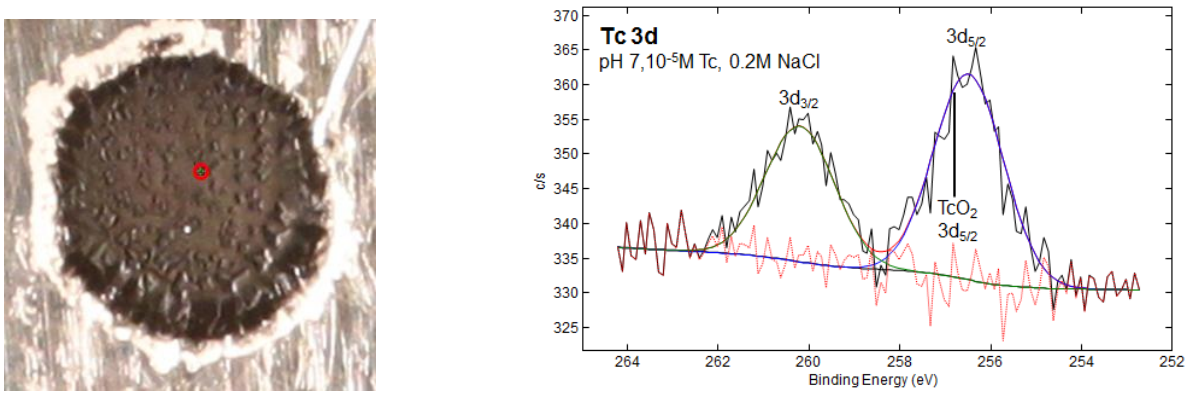

Figure 39. *Magnetite sample for XPS (left) after contacting with Tc(VII)-containing solution. Red circle indicats the region where the XPS narrow scan (right) of Tc 3d spectrum was measured.*

4.2.1.2. Crystalline rock

XPS analysis of an un-oxidized ÄD disc fragment after contacting with 10^{-5} M Tc(VII) in GWS for two months under Ar atmosphere in the glovebox revealed that Tc is associated to mafic (dark) minerals only (see Figure 40, left), whereas on felsic (light) minerals no Tc was measurable. Figure 40 (right) shows the measured Tc 3d XPS spectra with the characteristic $3d_{3/2}$ and $3d_{5/2}$ peak positions. Due to the rather low Tc concentration used in the sorption experiment on the ÄD disc surface the spectra is rather noisy. Both Tc(VII) and Tc(IV) have two 3d peaks ($3d_{5/2}$ and $3d_{3/2}$). Since there are only two peaks in the area of interest, the

conclusion is that there is only one Tc oxidation state present at the mineral surface, and the position of Tc(IV) $3d_{5/2}$ (TcO_2) at 256.8 eV reference line is closer to the experimental data (255.9 eV) than the Tc(VII) $3d_{5/2}$ ($NaTcO_4$) 259.7 eV reference line. Binding energy reference lines for TcO_2 and $NaTcO_4$ were taken from [156].

As mentioned above, the Tc signal was detected only on dark mica-type mineral surfaces (most likely biotite), which contains Fe(II). It is well known that Tc is concentrated at Fe(II)-containing minerals [18; 95; 157] as "hotspots" due to surface (heterogeneous) reduction into an insoluble Tc(IV) oxide phase or/and due to homogeneous reduction in the solution into soluble Tc(IV) species which subsequently sorb on the mineral surface. As reported by Peretyazhko et al. [15] heterogeneous Tc(VII) reduction by Fe(II) on the mineral surface including biotite is much faster than the homogeneous reduction by aqueous ferrous iron.

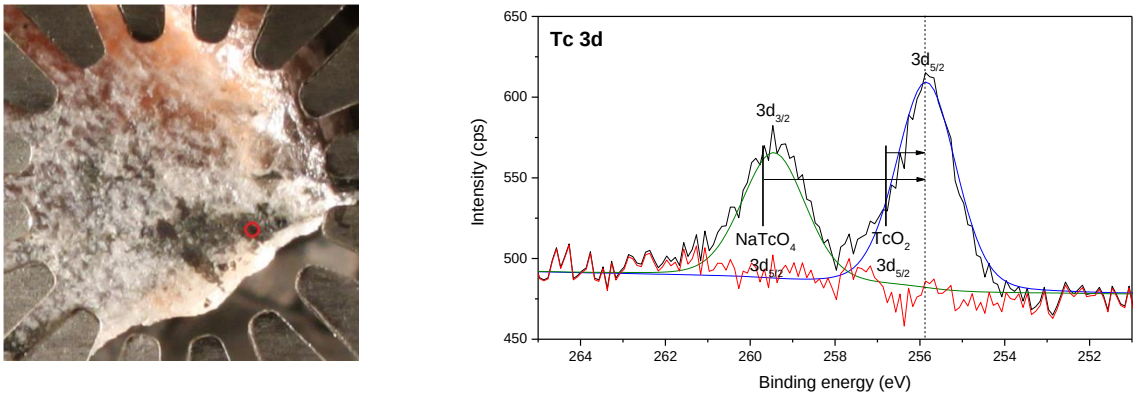

Figure 40. ÄD sample for XPS (left) after contacting with Tc(VII)-containing ÄGWS. Red circle indicates the region where Tc(IV) was found and the XPS narrow scan (right) of Tc 3d spectrum was measured.

4.2.2. X-ray absorption spectroscopy (XAS)

4.2.2.1. X-ray absorption near edge structure (XANES)

XANES analysis provides bulk information on Tc oxidation state after interaction with minerals.

The Tc K-edge XANES spectra of the TcO_2 and TcO_4^- reference materials have characteristic spectral features, which facilitate Tc oxidation state characterization. For example, the spectrum of the Tc(VII) reference, where Tc is surrounded by four oxygen atoms in tetrahedral conformation, exhibits a pre-edge absorption resonance at about 21,050 eV generated by the 1s → 5p/4d transition [158]. The Tc K-edge XANES spectra of the Tc-

magnetite samples were calculated by using two structural models, i.e. Tc substitutes Fe in tetrahedral (Figure S 4a) or octahedral (Figure S 4b) sites.

The spectrum in the Figure S 4b resembles closely the experimental XANES spectra of the "Tc on magnetite" and "Tc on partially oxidized magnetite" samples (see Figure 41), whereas the pre-edge peak from the spectrum of Tc in tetrahedral sites (Figure S 4a) is not present in the experimental XANES spectra. The Tc K-edge XANES spectrum of the "Tc on partially oxidized magnetite" sample appears very similar to the spectrum of "Tc on magnetite", which strongly suggests that Tc has also local octahedral geometry in this sample.

Based on the XANES results, Tc(IV) dominates in both Tc-magnetite samples studied. The energy positions of the rising absorption edges appear at slightly higher energy position for "Tc on magnetite" and "Tc on partially oxidized magnetite" samples compared to TcO_2 reference. This is most probably due to larger broadening of the most intense absorption resonance white line of the spectra of the Tc-magnetite samples compared to spectrum of the TcO_2 reference.

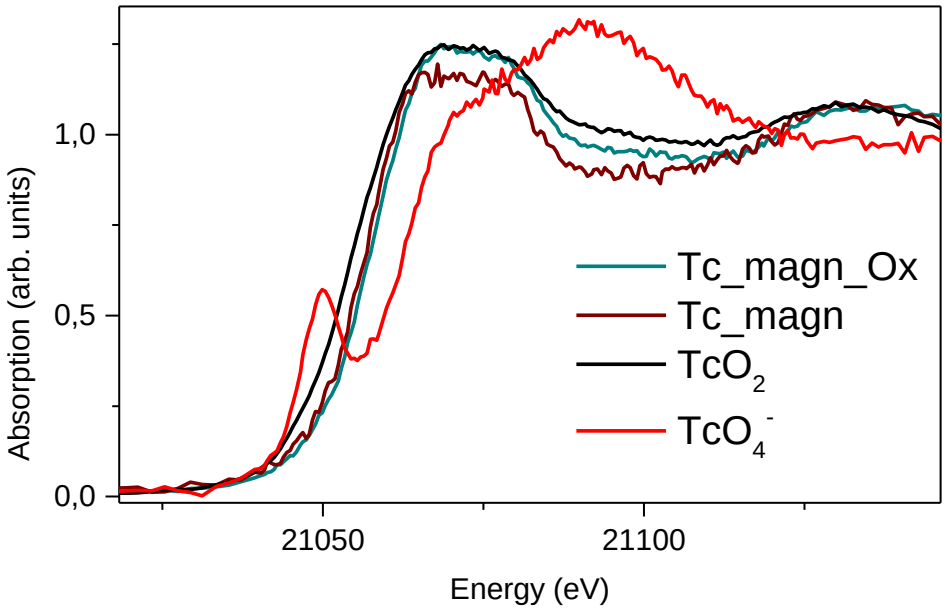

Figure 41. *Tc K edge XANES spectra of "Tc_magn" and "Tc_magn_ox" samples together with TcO_2 and TcO_4^- references.*

Normalized Tc K-edge XANES spectra are presented in Figure 42 for Tc on ÄD, NK and magnetite samples together with Tc(IV) and Tc(VII) references.

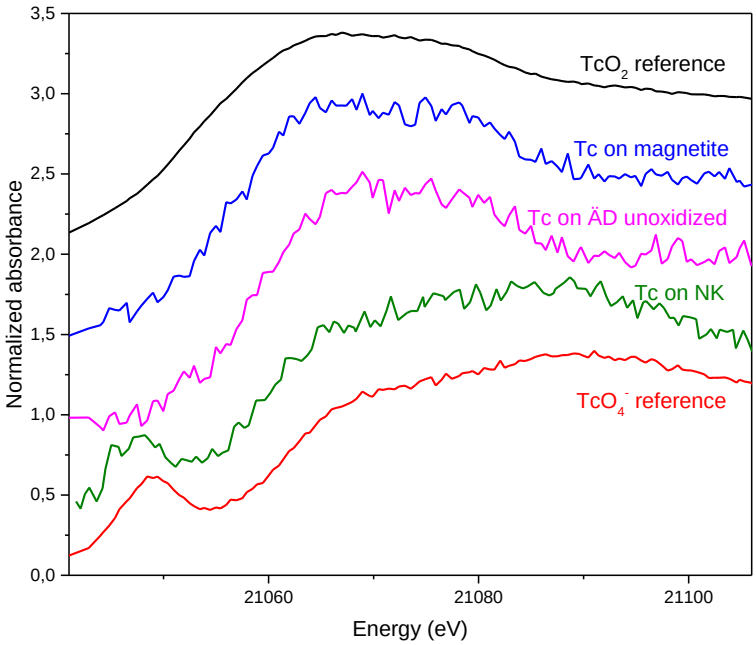

Figure 42. *Normalized Tc K-edge XANES spectra of samples after sorption of Tc onto ÄD and NK rock materials and magnetite.*

The overall shape and energy position of the rising absorption edge of the Tc K-edge XANES spectrum of Tc on Äspö diorite is similar the TcO_2 reference without the pre-edge feature of Tc(VII). In contrast, the Tc K-edge XANES spectrum of Tc on NK resembles closely the spectrum of the TcO_4^- reference. This fingerprint approach allows to identify Tc(IV) and Tc(VII) as dominating species on Äspö diorite and on NK samples, respectively. Based on the batch sorption studies, Tc(IV) oxide concentration on the mineral surface is low for both ÄD and NK materials for the XAS measurements. Tc(VII) present in the rock pores is likely to dominate the spectrum of the Tc on NK sample. However, the characteristic for Tc(VII) pre-edge feature in the "Tc on NK" spectrum has lower intensity and is shifted about 1.5 ± 0.25 eV to lower energy compared to the TcO_4^- reference spectrum. This result suggests that the NK sample contains a minor amount of Tc(IV) [159; 160]. The signal to noise ratio of the "Tc on NK" spectrum is too low to allow reliable quantitative analysis.

4.2.2.2. Extended X-ray absorption fine structure (EXAFS)

Extended X-ray absorption fine structure (XAFS) analysis allows determining the local atomic structure of the selected atomic species. It provides information on atomic distances, coordination numbers and species of the atoms surrounding the chosen element [161].

The best fit to the EXAFS data of the "Tc_magn" sample is presented in Figure 43. The fitting obtained reports 4.6 ± 0.3 O atoms at 1.97 ± 0.01 Å and 7.2 ± 2.4 Fe atoms at 3.49 ± 0.01 Å in the first and second coordination shell of Tc, respectively. The spectrum in the k range is comparable to the Tc K-edge EXAFS spectra of similar systems reported in the literature [96; 97]. However the low signal to noise ratio restricts the usable k range and prevents resolving two Tc-Fe distances described in previous works [96; 97]. The obtained interatomic distances and coordination numbers strongly suggest that Tc is incorporated preferentially in octahedral magnetite sites. The Fe^{2+}/Fe^{3+} in magnetite octahedral sites are coordinated by 6 O atoms at 2.056 Å and 6 Fe^{2+}/Fe^{3+} (octahedral sites) at 2.97 Å, 6 Fe^{3+} (tetrahedral sites) at 3.48 Å. The EXAFS result is confirmed by quantum chemical calculations of the Tc K-edge XANES spectrum with the multiple scattering FEFF9.5 code (see Figure S 4 in supplementary materials).

The EXAFS spectrum of the "Tc_magn_ox" is significantly different from the spectrum of the "Tc_magn" sample indicating some variations in the Tc short range structure. These two samples have different $Fe(II)/Fe_{tot}$ ratio, namely "Tc_magn" has 29% Fe(II) and "Tc_magn_ox" sample has 24.7%. The best fit of the "Tc_magn_ox" spectrum reports 4.6 ± 0.3 O at 1.97 Å and 0.8 ± 0.2 Tc at 2.58 ± 0.01 Å suggesting geometric structure comparable to the Tc local atomic environment in TcO_2. Similar results are reported also in the literature, for instance by Almahamid et al. [162] (1 Tc at 2.61 Å) and Hess et al. [65] (1 Tc at 2.59 ± 0.2 Å). Therefore, based on the analysis performed "Tc on partially oxidized magnetite" sample contains $TcO_2 \cdot 1.6H_2O_{(s)}$ solid phase without incorporation of Tc atoms into the magnetite crystalline lattice. Since Tc was incorporated into the magnetite lattice in the case of stoichiometric magnetite, the partial surface oxidation has changed the dominating mechnism of Tc immobilization. As was already discussed in the batch studies section (see paragraph 4.1.1.2), partial oxidation of the magnetite is changing the reduction properties of the material. Based on the EXAFS results, even after Tc(VII) reduction Tc(IV) speciation on the magnetite surface is different whether stoichiometric or partially oxidized material is used.

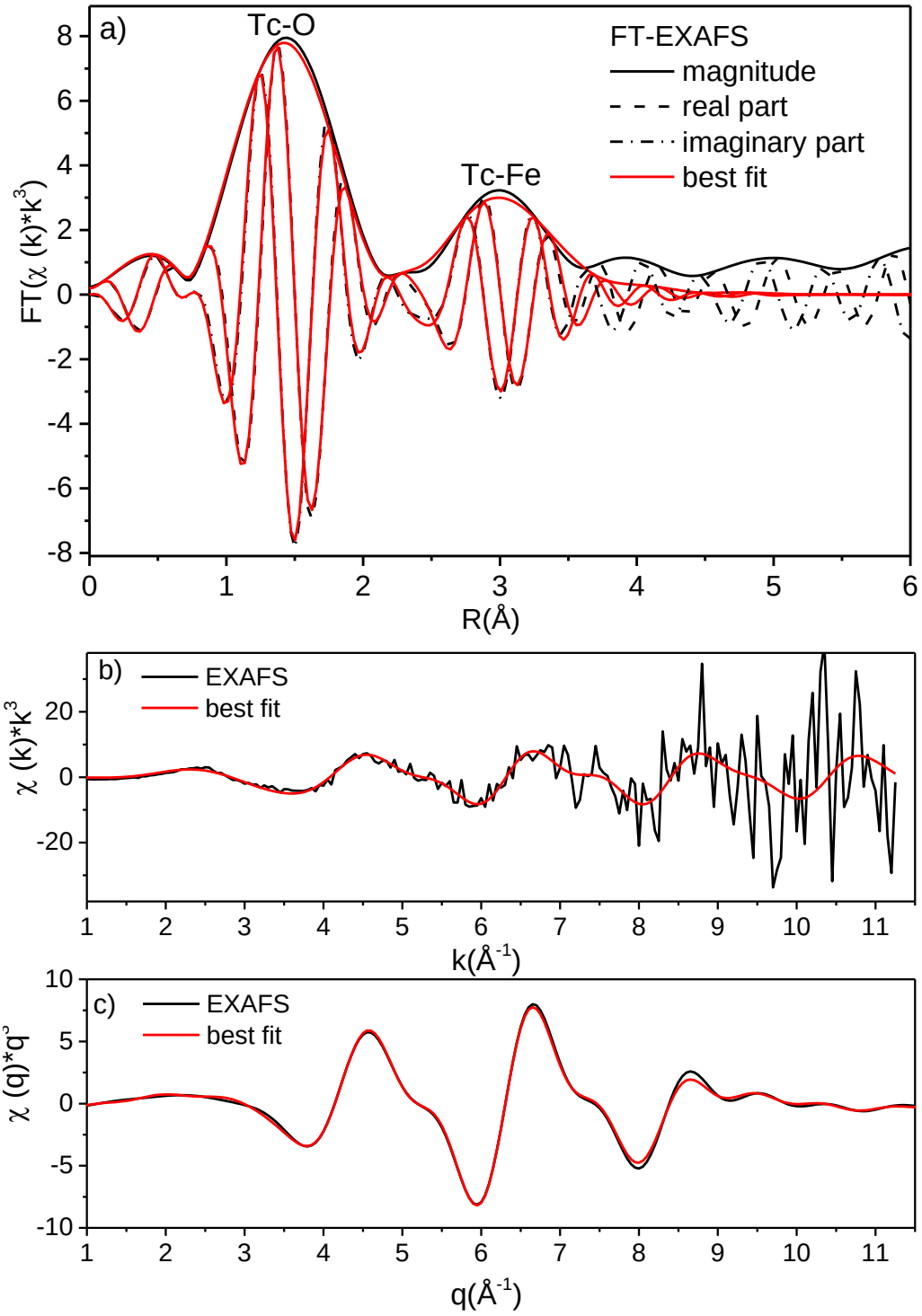

Figure 43. *Tc K-edge EXAFS spectra of "Tc_magn" sample and their best fits. (a) The Fourier transformation (FT) of the EXAFS spectrum, (b) the k^3-weighted EXAFS spectrum, and (c) back FT-EXAFS spectrum in q space.*

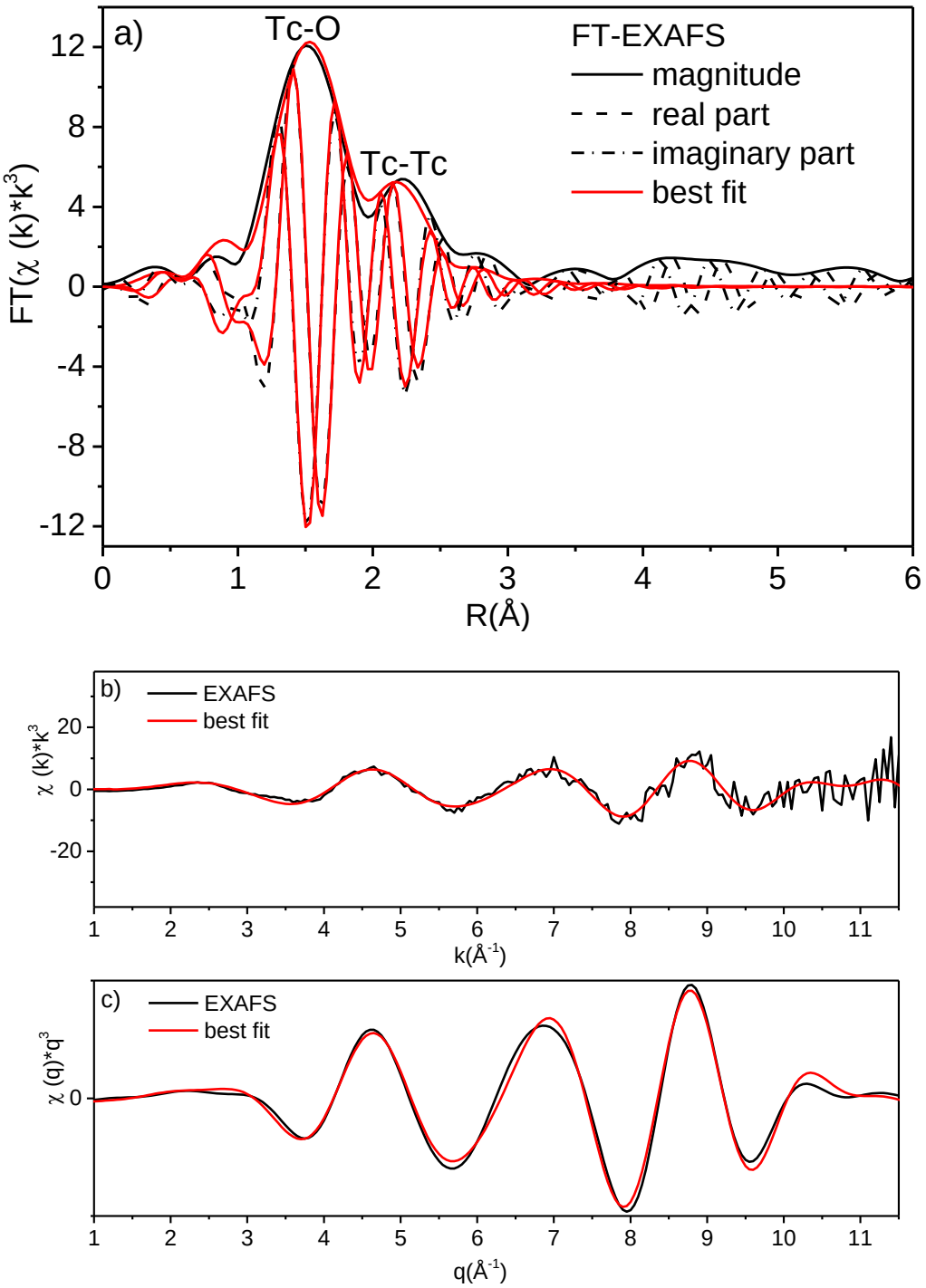

Figure 44. *Tc K-edge EXAFS spectra of "Tc_magn_ox" sample and their best fits. (a) The Fourier transformation (FT) of the EXAFS spectrum, (b) the k3-weighted EXAFS spectrum, and (c) back FT-EXAFS spectrum in q space.*

The main parameters derived from the EXAFS analyses are summarized in Table 15.

Table 15. *Scattering path (Path), coordination numbers (N), interatomic distances (R), mean-squared atomic displacement/Debye-Waller factor (σ^2) and energy shift of the ionization potential (ΔE_0) obtained from the best fit to the EXAFS spectrum of the EXAFS samples measured.*

Sample	Path	N	R, Å	σ^2, Å^2	ΔE_0, eV
Tc_magn	Tc-O	4.6 ± 0.3	1.97 ± 0.01	0.001 ± 0.0003	-8.5 ± 0.4
	Tc-Fe	7.2 ± 2.4	3.49 ± 0.01	0.01 ± 0.004	-8.5 ± 0.4
Tc_magn_ox	Tc-O	4.3 ± 1.9	1.99 ± 0.01	0.0004 ± 0.0006	5.7 ± 0.8
	Tc-Tc	0.8 ± 0.2	2.58 ± 0.01	0.0004 ± 0.0006	5.7 ± 0.8

4.3. Core migration studies

4.3.1. Hydraulic properties

The hydraulic properties of the Äspö core #2.2 were calculated using the equations (1) and (2). Since the pressure sensors around the core are located at the different heights (see Figure 19), the correction for the pressure difference between them should be taken into account in accordance with the hydraulic pressure equation (48):

$$p = \rho g h \tag{48}$$

where p is a pressure (Pa), ρ is a density (kg/m^3), g is a gravitational acceleration (m/s^2) and h is the difference in height of sensors (m).

Based on the differential pressure of the core measured during the experiments under three flow rates (10, 1.5 and 0.2 mL/h) the fracture permeability of $(4.4\pm0.4)\times10^{-14}$ m^2 and the hydraulic conductivity of $(4.3\pm0.4)\times10^{-7}$ m/s were calculated. The values obtained for the different granitic formation cover an enormous range between 10^{-13} m/s and 10^{-4} m/s and strongly depend on the fracture density [163]. The hydraulic conductivity of the granite in the Äspö HRL was measured *in-situ* by Walker et al. [164] in the range from 1.3×10^{-7} m/s to 3.0×10^{-9} m/s. The value obtained for the Äspö drill core #2.2 within the present work is also in this range.

4.3.1. HTO and $^{36}Cl^-$

Conservative tracer tests for the hydraulic characterization of the drill core were performed using HTO and the effect of potential anion exclusion was monitored in parallel using $^{36}Cl^-$. Typical breakthrough curves (BTC) for both radionuclides at different flow rates are shown in Figure 45 (the raw data is given in Table S 3 in supplementary materials). The long tailing of the BTC is most likely due to slow channelling in the fracture with different flow rates as identified by the flow field modelling on the basis of µCT data done within the Euratom CP-CROCK project [165]. A significant contribution of the experimental set-up to the observed tailing was excluded by additional tests bypassing the core. The injection functions for all flow rates are also presented in Figure 45.

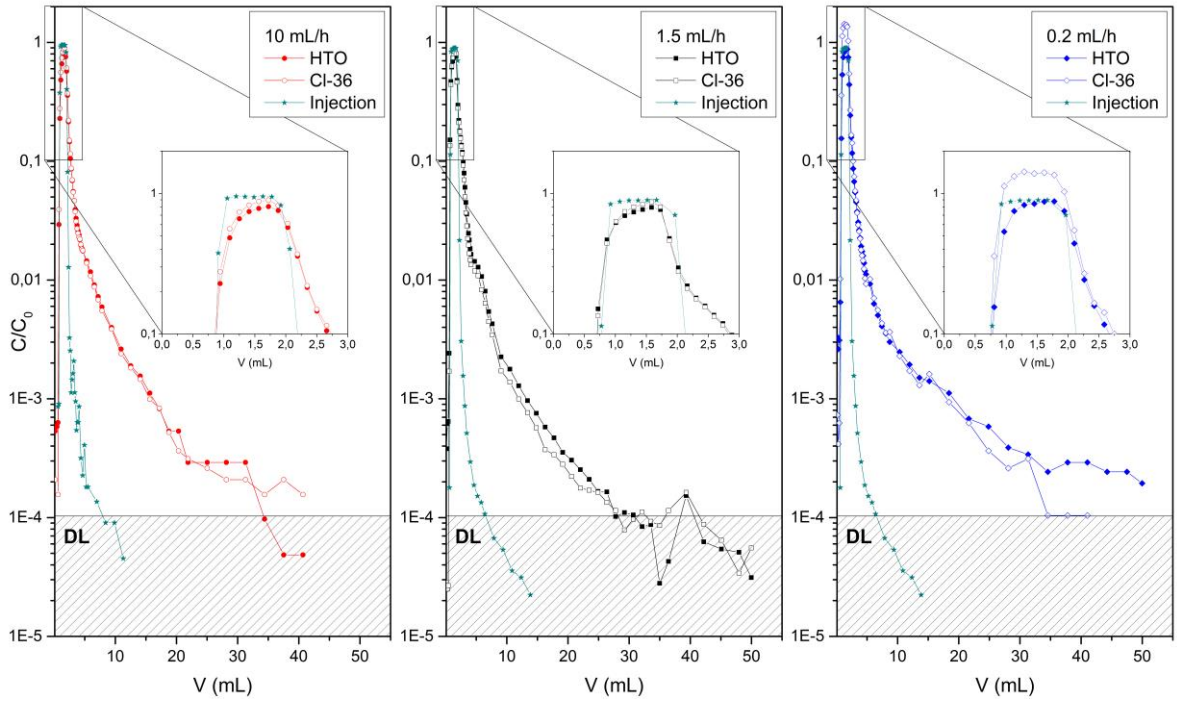

Figure 45. *HTO and ^{36}Cl breakthrough curves for a natural fracture in the Äspö core #2.2. DL fields indicate the approximate detection limit, which might be lower for some samples with higher volume. Green lines belong to the injection functions (injections with the disconnected core). The insets show the closer look of the peaks.*

The comparison of HTO and ^{36}Cl BTC for different flow velocities clearly shows an influence of fracture residence time on breakthrough tailing. As far as HTO and ^{36}Cl show similar behaviour, an anion exclusion effect was not observed in the fracture investigated under the hydraulic conditions established. In the work of Liu et al. [166] anion exclusion also was not observed on the crystalline rock. However, Park et al. [167] have reported the strong exclusion of Cl^- in their investigated granitic system.

4.3.1. Tc migration

4.3.1.1. Continuous flow

Results of Tc migration studies using 1 mL injections of ÄGWS containing ^{95m}Tc(VII) at trace concentrations below the Tc(IV) solubility limit (C_0 = ~10^{-11} M ^{95m}Tc(VII) was taken) are presented in Figure 46 (the data points for these plots are given in Table S 4 in supplementary materials). The same flow rates (0.2 mL/h, 1.5 mL/h and 10 mL/h) as for the conservative tracers study were applied.

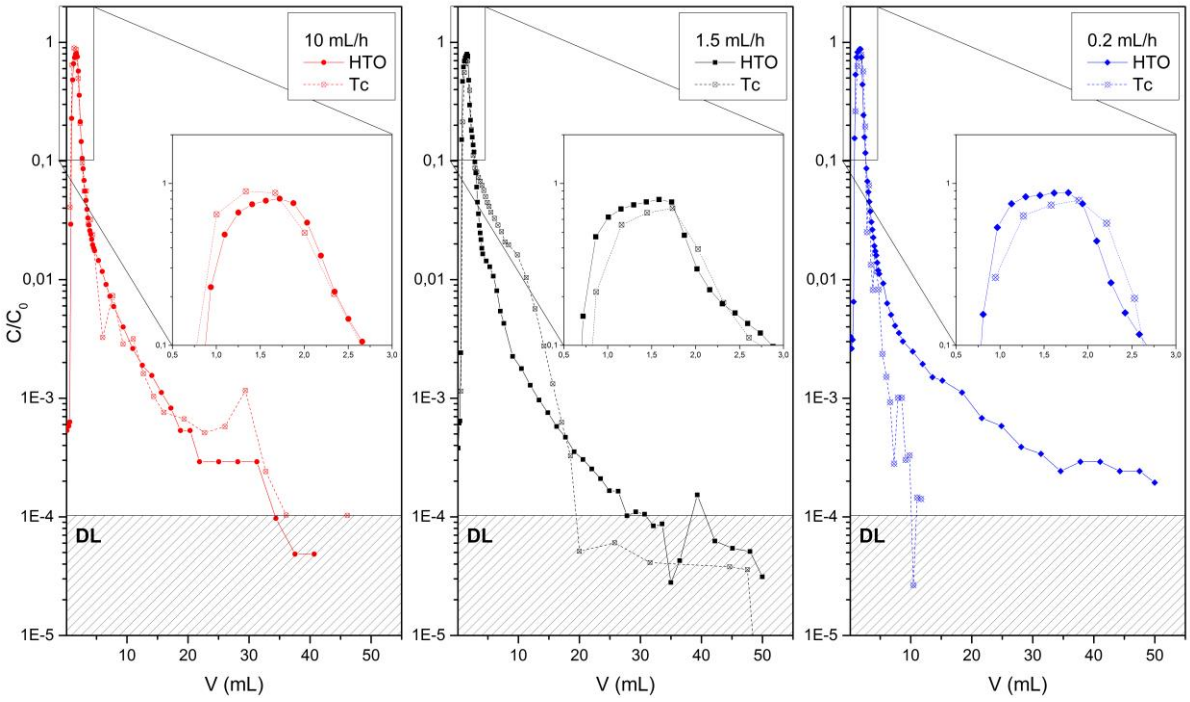

Figure 46. *^{95m}Tc(VII) and HTO breakthrough curves in the Äspö core #2.2. DL fields indicate the approximate detection limit, which might be lower for some samples with higher volume. The insets show the closer look of the peaks.*

Shoulders in the curve tailing are disappearing with decreasing flow rate probably due to higher contribution from diffusion, which is increasing the mass transfer to slow flow channels. Another effect, that may influence the decrease of curve tailing is the slow kinetics of Tc(VII) reduction followed by sorption of Tc(IV) species. At slow flow velocities more Tc(VII) is reduced during the tracer residence in the fracture, while in the fast flow experiments more Tc(VII) is passing the core as a conservative tracer and contributes to the longer tailing due to channelling and diffusion.

Under the highest flow rate applied (10 mL/h) Tc behaves as a conservative tracer (see Figure 46 (left)), whereas under the lowest rate (0.2 mL/h) the tailing of Tc BTC is much shorter than for HTO. Tracer recoveries are discussed below.

The redox potential of the groundwater simulant containing ~ 10^{-11} M ^{95m}Tc was measured as +370 mV (pH 8.0±0.1) before injection, which is similar to the results for the ÄGWS without Tc. Added $[Tc]_{tot}$ is too low compared to the Pt-electrode detection limit (~ 10^{-6} M for both constituents of the redox couple) to contribute to the redox electrode signal. The NO_3^- content after the separation on the Dowex column is estimated as < 10^{-11} M, which is also bellow the Pt-electrode sensitivity. After equilibration with the core the measured redox potential of ÄGWS in the effluent is +170 mV. Both of these values are located in the Tc(VII) stability field (see Figure 32). Since $[Tc]_{tot}$ is too low for $TcO_2 \cdot 1.6H_2O_{(s)}$ precipitation, the main retention mechanism under given conditions is surface reduction/complexation.

4.3.1.2. Stop-flow Tc injections

Longer Tc/fracture contact times (from 1 day up to 17 days) were achieved by stop-flow experiments. A typical stop-flow breakthrough curve is shown in Figure 47 (left), where the small peak after pumping restart corresponds to the mobile Tc fraction recovered from the core fracture. This peak also includes the Tc solution inside the small tubing parts on the both sides of the core (see Figure 47 (right) as a part of the general scheme shown in Figure 20), which was not in contact with the crystalline core. This amount can be easily calculated from the tubing length and inner diameter. This correction was taken into account for the total recovery estimation presented in paragraph 4.3.1.5.

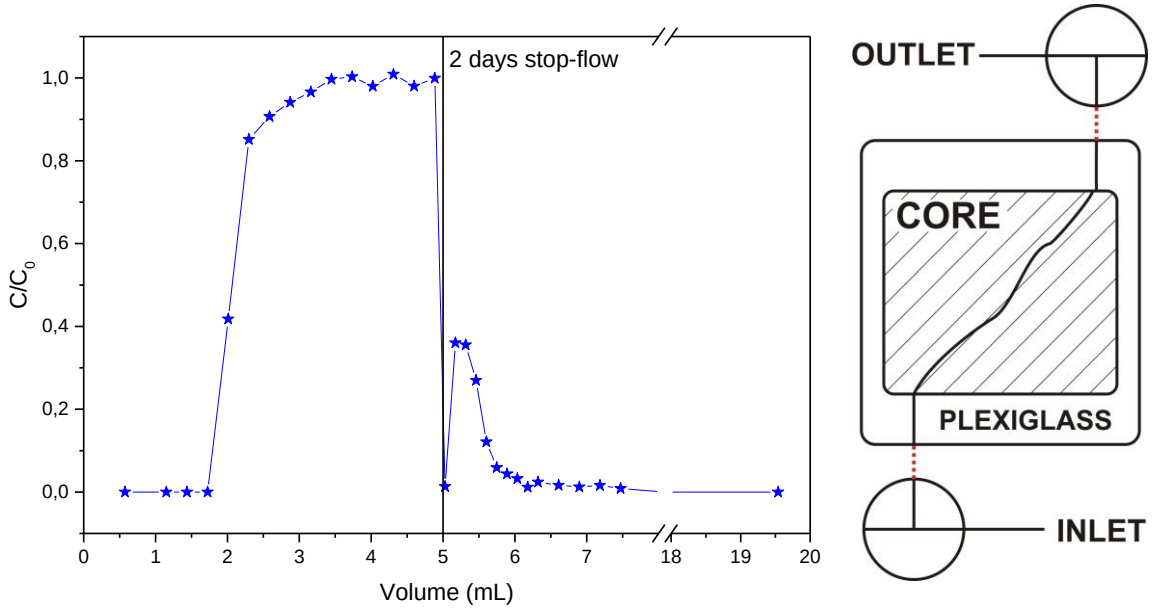

Figure 47. *(Left) Breakthrough curve for 2 days stop-flow injection of ^{95m}Tc(VII)-containing ÄGWS into Äspö core #2.2 (10 mL/h). (Right) Äspö core #2.2 with two valves. Red dashed lines marks the tubing filled with Tc-containing GW after washing of the device.*

A correlation of the Tc concentration and the Eh values of the eluate is shown in Figure 48. According to the experimental data, the eluate fractions containing Tc had also lower redox potential values compared to the ÄGWS eluent. It is explained by the equilibration of the GWS with the core and establishing more reducing conditions in the aqueous phase. After the groundwater contacted with the rock fracture is eluted, the Eh values increases back to ~ +270 mV. It is still lower than the redox potential of the ^{95m}Tc-containing ÄGWS (+370 mV) due to the short contact with the core. However, Figure 48 shows that after the longer contact time the Eh values of the groundwater is decreasing.

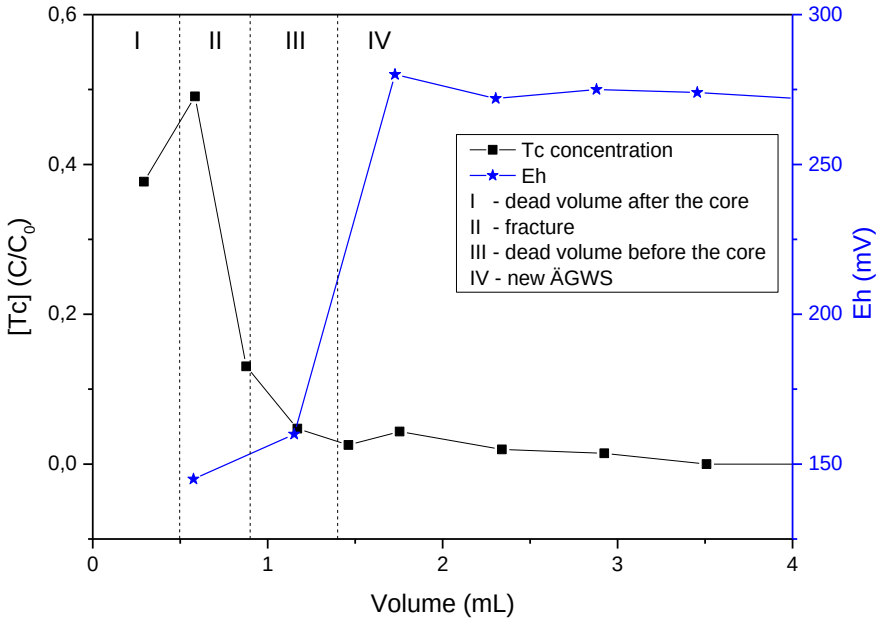

Figure 48. *Relative Tc concentration together with Eh values of the eluate after restart of the 1 day stop-flow experiment.*

The data presented in Figure 48 was obtained from the restart of the stop-flow experiment with one day contact time. The tubing of the device was washed with fresh ÄGWS except the core fracture volume and small tubing parts between the core and the valves (see Figure 47 (right), red dashed line). However, this amount of Tc cannot influence the redox potential measured with the Pt-electrode. On the other hand, it is contributing to the Tc concentration in the areas I and III (see Figure 48).

After the injections of ÄGWS containing log $[Tc]_{tot}$ = -11 similar experiments were performed with $[Tc]_{tot}$ = -9 for a better comparison to the results of batch sorption studies (see Table 16).

4.3.1.3. Tc interaction with natural Äspö groundwater

For better understanding of the processes taking place inside the fracture, Tc interaction with natural Äspö groundwater (ÄGWN) without the crystalline rock surface was investigated in parallel to the migration studies. Two ÄGWN samples were mixed with Tc(VII) stock solution to reach finally log $[Tc]_{tot}$ = -7 and -8. Since some black particles were observed in the ÄGWN, similar samples were prepared with filtrated ÄGWN. Filtered particles were analysed with SEM-EDX (see Figure 49) and the composition was determined as (Fe, S)-containing aluminosilicates. An additional SEM scan together with the respective EDX spectrum is presented in supplementary materials (Figure S 5).

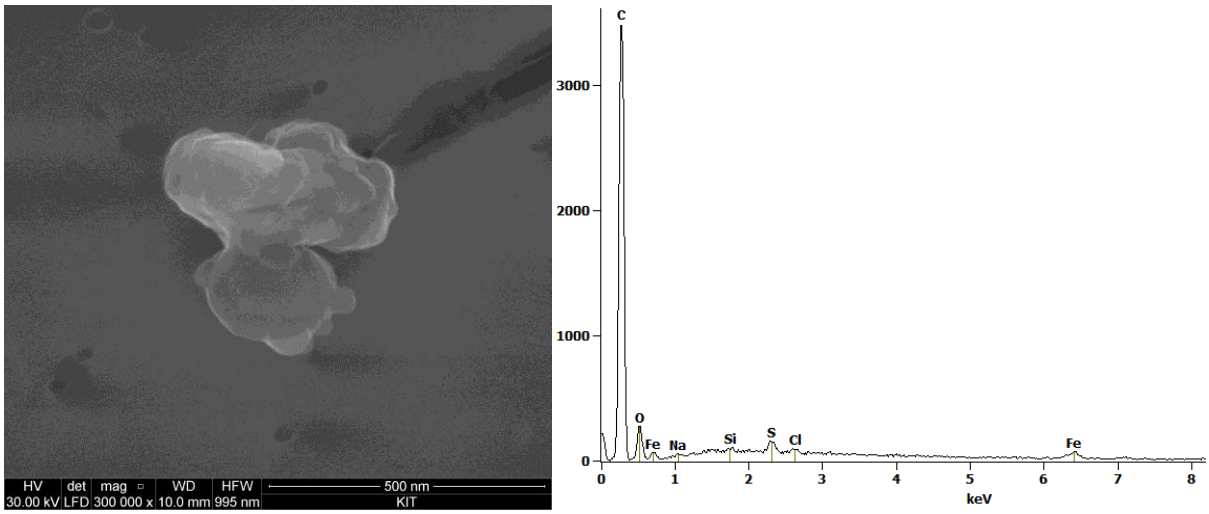

Figure 49. *SEM image (left) and EDX spectrum (right) of the particle filtered from the ÄGWN.*

Tc concentrations in the samples were measured during one month. Eh-pH conditions established (pH 8.1, ca. -100 – -200 mV for both samples) correspond to the Tc(IV) stability field (see Figure 32), but liquid-liquid extraction with (i) 1mM tetraphenylphosphonium chloride (Ph_4PCl) in chloroform and (ii) 1 mM 1-phenyl-3-methyl-4-benzoylpyrazolone-5 (PMBP) in xylol show only Tc(VII) in the solution. Also no significant change in the Tc concentration was observed even after one month of equilibration time. Thus, no $TcO_2 \cdot 1.6H_2O_{(s)}$ precipitation or another Tc(IV) immobilization occurs under the conditions applied. Comparison between ultracentrifuged and non-centrifuged samples showed no difference, hence Tc colloidal phases were not found. Consequently, Tc(VII) was not reduced in the liquid phase in the absence of rock surfaces.

4.3.1.4. Elution with natural ÄGW

Prior to the experiment the core was equilibrated with natural ÄGW (ÄGWN) by pumping 35 mL of groundwater with a flow rate of 1.5 mL/h.

Taking ÄGWN as an eluent in the core migration experiments increases the Tc retention. The main reason for this difference to previously described migration experiments with ÄGWS is the much lower Eh value (ca. -100 mV), which is below the limit of -90 mV, which has been identified in the Thermodynamic modelling chapter (see paragraph 4.1.2.5) as the Eh region where maximal Tc uptake in the presence of the solid phase occurs. Therefore, under ÄGWN Eh-pH conditions Tc(VII) should be reduced to Tc(IV) and immobilized on the mineral surface. As discussed before, the low Eh value is not sufficient to reduce Tc(VII) in such a short time. The mineral surface is apparently necessary to induce rapid reduction and sorption.

4.3.1.5. Parameters derived from Tc migration studies

Residence times and recoveries obtained from the Tc migration experiments are summarized in Table 16 together with Tc concentrations of the injected groundwater.

Table 16. *^{95m}Tc recovery results from the migration studies on Äspö core #2.2.*

Flow rate, mL/h	Injection volume, mL	Injection type	Eluent	$[Tc]_{tot}$, mol/L	Resi-dence time	Reco-very*, %	Recovery calculated from batch studies**, %
10	1.1	pulse	ÄGWS	2.1×10^{-11}	10 min	100	99.98
1.5	1.1	pulse	ÄGWS	1.4×10^{-11}	59 min	92	99.85
0.2	1.1	pulse	ÄGWS	9.3×10^{-12}	490 min	87	98.80
10	5.5	stop-flow	ÄGWS	3.7×10^{-12}	1 day	71	78
10	5.5	stop-flow	ÄGWS	3.5×10^{-12}	2 days	37	75
10	5.5	stop-flow	ÄGWS	2.8×10^{-12}	4 days	16	70
10	5.5	stop-flow	ÄGWS	2.8×10^{-12}	8 days	0	61
10	5.5	stop-flow	ÄGWS	10^{-9}	1 day	58	78
10	5.5	stop-flow	ÄGWS	10^{-9}	2 days	27	75
10	5.5	stop-flow	ÄGWS	10^{-9}	4 days	19	70
10	5.5	stop-flow	ÄGWS	10^{-9}	8 days	7	61
10	5.5	stop-flow	ÄGWS	10^{-9}	17 days	1	44
10	5.5	stop-flow	ÄGWN	9.2×10^{-13}	1 day	0	78
10	1.1	pulse	ÄGWN	7.1×10^{-13}	10 min	15	99.98
1.5	1.1	pulse	ÄGWN	6.2×10^{-13}	59 min	6	99.85
1.5	2000	continuous flow	ÄGWN	10^{-7}	59 min	95%	-

* relative analytical uncertainty of the recovery is ~ 5%.

** based on batch type kinetics for log $[Tc]_{tot}$ = -9.

A gradual decrease of the initial Tc concentration is caused by the radioactive decay of ^{95m}Tc isotope ($t_{1/2}$ = 61 day), which has been taken into account.

Sorption rates obtained from batch-type experiments (see Table 13) allow to predict the recovery in core migration studies (see Table 12 and Figure 50). The values calculated from experiments with log $[Tc]_{tot}$ = -9 are also given in Table 16 for comparison. For short term studies (up to 1 day) the recoveries for both batch and migration studies are almost similar, but with increasing contact time recoveries observed in the migration experiments are much lower than predicted. As a consequence reduction/sorption rates are faster than in batch experiments. The discrepancy between the results of these two techniques is well known and was observed by several investigators [168; 169]. Generally, it can be attributed to (i) different diffusion rates under static and dynamic conditions or/and to (ii) mineralogical features of the natural fractures compared to the bulk material. It is well known, that natural rock fractures contain secondary minerals, such as chlorite, pyrite, clay minerals, iron-oxyhydroxides, etc. [170], which might contain Fe(II) for Tc(VII) reduction.

A comparison of the Tc recoveries after injections of 10^{-11} and 10^{-9} M Tc is given in Figure 50, which also illustrates the difference between migration and batch-type study retention rates.

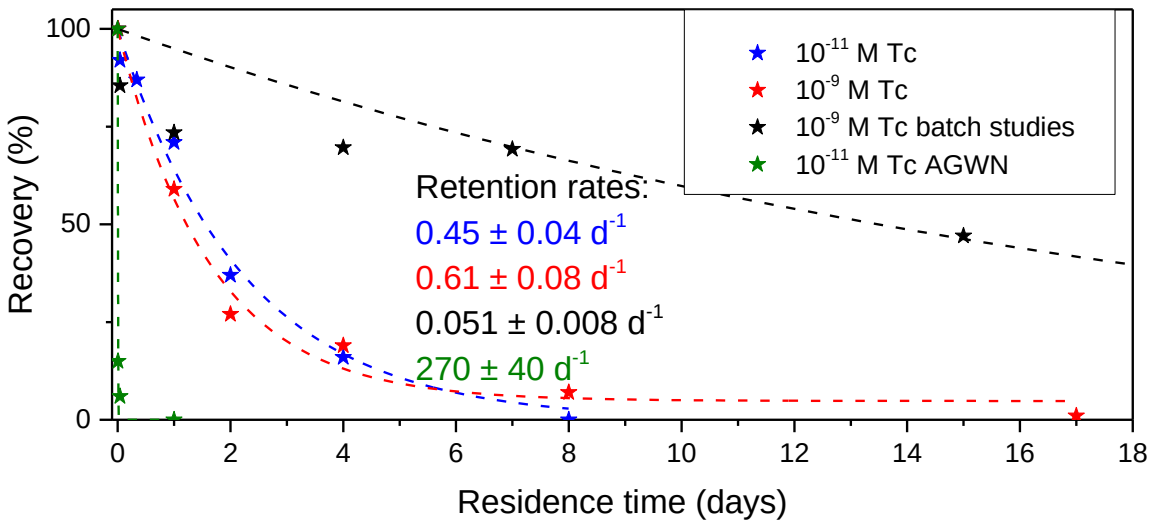

Figure 50. *Retention kinetics during the migration studies for 10^{-11} M and 10^{-9} M Tc compared with the 10^{-9} M Tc batch studies results and with 10^{-11} M Tc migration experiment with natural ÄGW. Dashed lines represent the exponential fitting curves.*

A general trend of faster retention kinetics for the higher initial Tc concentration was also found in batch sorption studies (see Table 13). As was shown in Figure 23, there are three different processes taking place simultaneously in the system. In the case of low Tc

concentrations (< 10^{-8} M) the bulk $TcO_2 \cdot 1.6H_2O_{(s)}$ precipitation does not occur, so only (i) Tc(VII) homogeneous reduction in the solution with further Tc(IV) sorption and (ii) heterogeneous Tc(VII) reduction on the Fe(II)-containing mineral surface contribute to the overall Tc retention. Taking into account the results of Tc interaction with ÄGWN without the solid phase, the homogeneous Tc(VII) reduction might be discarded. However, even if Tc reduction was not observed under ÄGWN conditions in the absence of granite, much faster Tc retention than in presence of ÄGWS was found in the bore core experiments (see Figure 50, green and blue markers for log $[Tc]_{tot}$ = -11).

Since both log $[Tc]_{tot}$ = -11 and log $[Tc]_{tot}$ = -9 are lower than the Tc(IV) solubility limit under the Eh/pH conditions applied, the deviation in the uptake rate is not as distinct as in batch sorption studies.

According to the work done by Zachara et al. [12], Tc(VII) reduction by aqueous Fe(II) solution at pH 8 is very fast (complete reduction within 1 hour). However, based on the Eh measurements and the extraction of ion-exchangeable Fe(II) in case of high Tc concentration available ferrous iron content in the solution is not enough for complete Tc reduction. Taking into account also the surface analysis data, where Tc(IV) hotspots were found only on Fe(II)-containing mica minerals, the surface reduction is the dominating process under the conditions applied.

Using the equation (32) the K_a values were derived from the results of core migration studies. However, since the data on long fracture residence times point to a complete retention with Tc recoveries is equal or very close to 0 (see Table 16), the calculations provide lower limit estimations for this parameter. From the migration experiments using ÄGWS as eluent for log $[Tc]_{tot}$ = -9: $K_a > 10^{-2}$ m; for log $[Tc]_{tot} \leq$ -11: $K_a > 5 \times 10^{-4}$ m, which was calculated from the penultimate kinetic point. Distribution coefficients for experiments with the natural groundwater were not calculated due to a big difference between the last two points (penultimate value is too high: 6%, see Figure 50), but it is comparable or higher than the one derived log $[Tc]_{tot} \leq$ -11 using ÄGWS as an eluent.

4.3.2. Post-mortem analysis of the Äspö core

As was described in the Materials and Methods section 3.2.6.3, for the accumulation of Tc species on the fracture surface in order to apply spectroscopic analyses the final Tc injection was performed with 1 L 5×10^{-7} M Tc(VII) solution in ÄGWN with a flow rate of 1.5 mL/h. The residence time of Tc species inside the fracture was 59 min with a total contact time of 28

days for the solution. Based on the comparison of Tc concentration in the stock solution and in the outlet bottle approx. 5% of $[Tc]_{tot}$ remained in the fracture. Liquid-liquid extraction of the eluate showed only Tc(VII) in the solution.

After disassembling the Äspö core #2.2 from the Plexiglas cylinder the fracture was opened and investigated with autoradiography to estimate the radionuclide distribution and to find Tc hotspots. The autoradiography scan with two reference drops of Tc solution is shown in Figure 51. The photograph of the setup is given in Figure 21.

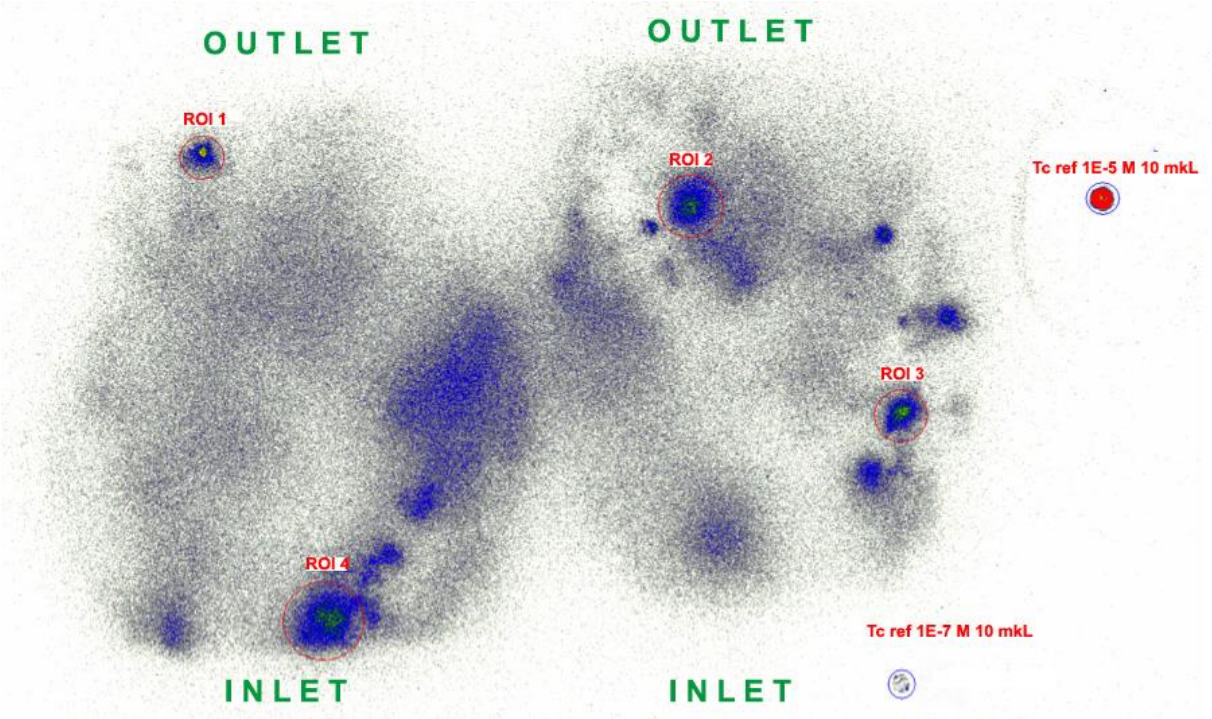

Figure 51. *Autoradiography scan of the Äspö core #2.2 fracture after migration studies.*

An estimation of the Tc amount on the fracture surface using the calibration by Tc solution drops is very imprecise due to the different apertures between the film and the core fracture and the surface roughness. Tc diffusion into the matrix and to the side channels is also significantly suppressing the autoradiography signal and decreasing the estimation accuracy. Nevertheless, this technique allows localizing Tc hotspots of the fracture surface for further investigation. A total Tc amount on the fracture surface was estimated as ~ 200 Bq with ~ 3 – 12 Bq in each marked hotspot. It is very consistent with the calculations based on the difference in Tc concentration in the inlet and outlet reservoirs (~ 300 Bq). The photograph of the fracture with activity distribution is shown in Figure 52.

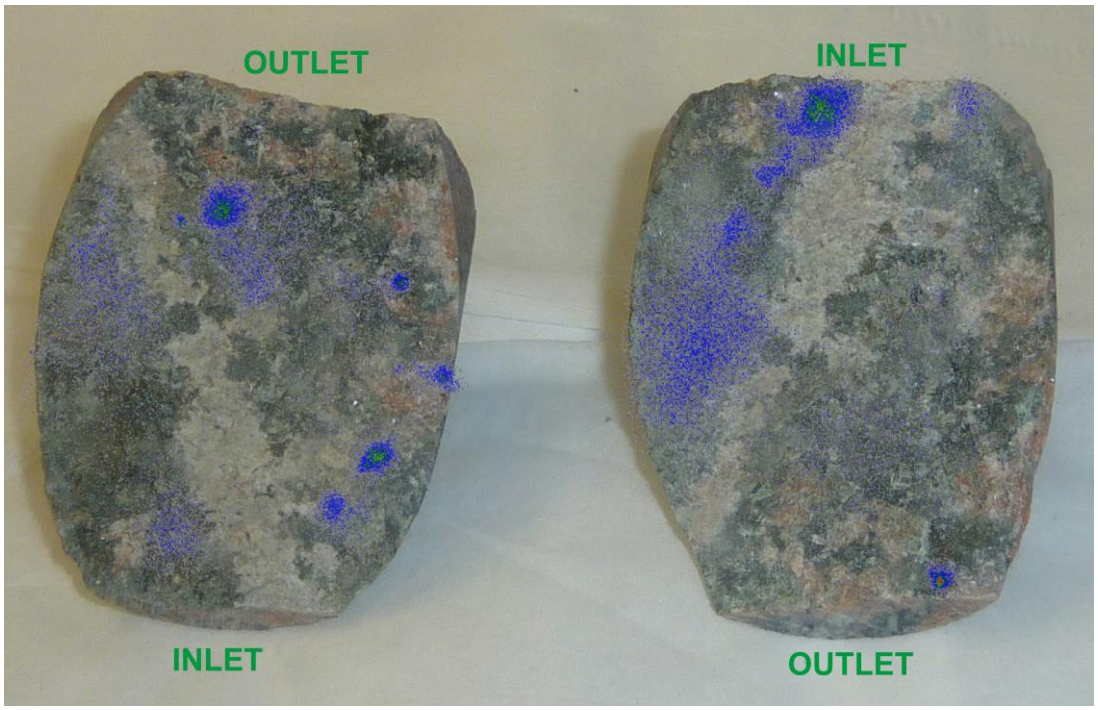

Figure 52. *Autoradiography of the fracture surface of the Äspö core #2.2 after the migration studies.*

Active hotspots were found on the mafic mica-type minerals, while a quartz vein does contain almost no Tc. One of the most active hotspot was found next to the injection point (ROI 4 in Figure 51). Two hotspots (ROI 1 and ROI 4 in Figure 51) were cut from the core using a chisel and a hammer and analysed with XPS, but Tc was not detected. Most probably, during the sample preparation, the surface was disturbed too much and Tc was removed from it. XPS survey analysis (see Figure S 3) shows ~ $3\%_{at}$ Fe in the ROI 1, but Tc concentration on the mineral surface is not enough to detect it using XPS.

According to the SEM-EDX analysis performed, the fracture surface contains significant amounts of Fe-bearing minerals mainly as aluminosilicates, but also as Fe oxide phases (see Figure 53). However, again Tc could not be detected on this spot using this technique as well.

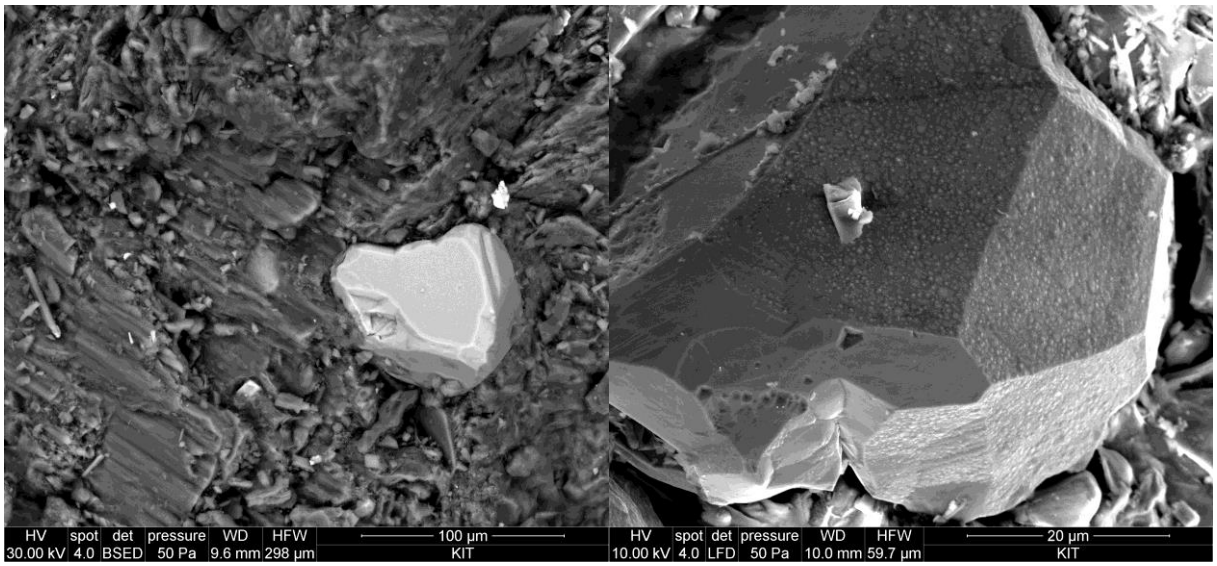

Figure 53. *SEM picture of the Fe oxide incorporation into the Äspö core fracture surface.*

The EDX analysis of the particle shown in Figure 53 indicates that this iron oxide phase possesses an O:Fe ratio ~ 1.32, which is close to the 1.33 ratio for the stoichiometric magnetite. The crystal shape also resembles magnetite instead of other Fe oxides. The presence of the magnetite inclusions are in a good agreement with bulk XRD analysis of Äspö diorite (see Table 6) showing > 1% of magnetite. These results show that accessory minerals as e.g. magnetite are at least a part of the natural ferrous iron pool being in direct contact with the water conducting feature and demonstrate the relevance of magnetite batch-type studies for the granitic rock media.

Half of the core (Figure 51, right part) was oxidized by air for one week and washed with ÄGWS as described in the Materials and Methods section. The washing fluid after the first washing step with a total contact time of ~ 5 minutes contained ~ 19 Bq ^{99}Tc. The second washing step after one day contact time yielded ~ 117 Bq ^{99}Tc.

Autoradiography of the fracture surface after the washing procedure was performed to investigate the impact of the surface associated Tc into the distribution of the radioactivity in the fracture. An additional autoradiography scan was conducted with a paper sheet between the core and the phosphor screen to increase the absorption of α-particles. The autoradiography scans obtained with (Figure 54, right) and without the paper sheet (Figure 54, right) show similar level of radioactivity of ROI 2&3. However, some other regions (for instance, the broad spot near the inlet edge) show lower intensity with the paper shielding, suggesting that these zones contain significant amount of natural α-emitters.

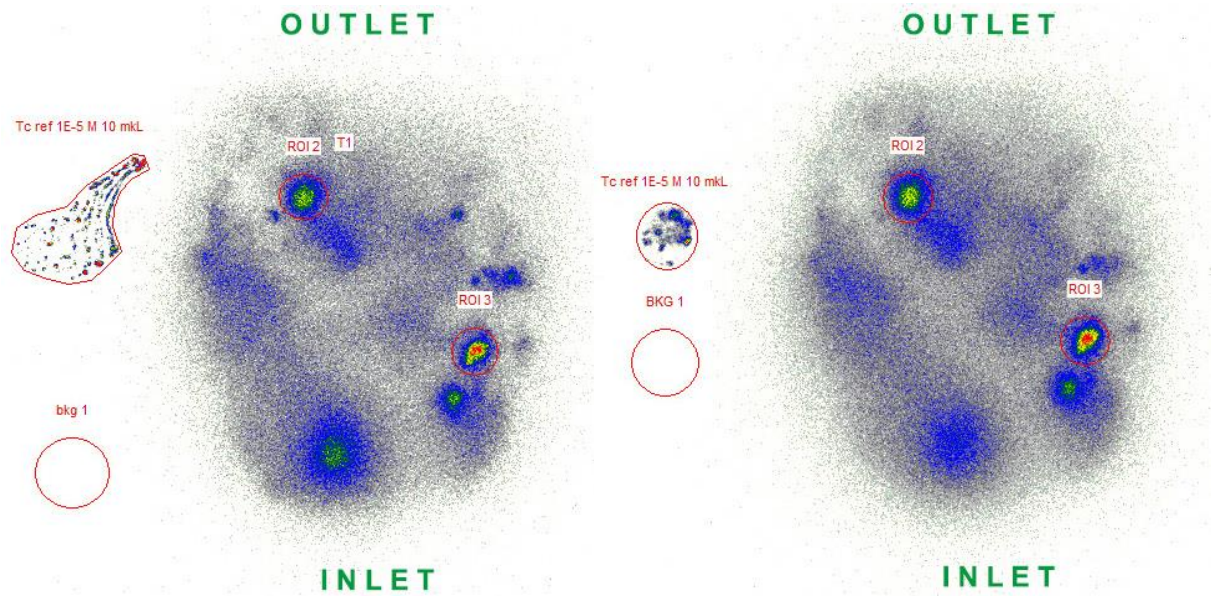

Figure 54. *Autoradiography scan of the Äspö core #2.2 fracture after the fracture washing without (left) and with (right) the paper sheet between the sample and the autoradiography screen.*

Summarising the results of the post-mortem analysis of the Äspö core, we can mention several main observations:

1. Hot spots on the fracture surface have been identified by autoradiography. However, SEM-EDX and XPS technique could not detect Tc on the fracture surface after the migration experiments;
2. Tc was found on the fracture surface of the core by the oxidation and washing procedure.
3. Fracture surface contains Fe(II)-bearing minerals, including magnetite, which mainly are responsible for Tc(VII) reduction.

Thus, Tc immobilization on the fracture surface of the crystalline rock was experimentally proven. Based on the results of the migration studies Tc uptake parameters (namely K_a value and the uptake rate) were estimated and the parameters are available for the safety assessment of HLW and SNF final disposal site.

5. Conclusions

In the frame of this work a comprehensive research of Tc retention behaviour in granitic rock media was performed under conditions relevant for the deep geological repositories of HLW and SNF. The main focus was laid on the effect of ferrous iron as a dominating parameter for Tc immobilization.

A batch type sorption/desorption study of Tc interaction with crushed granitic rock material from (i) the prospective site of SNF and HLW deep geological disposal in the Russian Federation (Nizhnekansky massif) and (ii) the generic URL in Sweden (Äspö HRL) was performed. Part of the crushed material from Äspö HRL used in the experiments has been obtained and handled under anoxic conditions before and during the experiments thus representing to a great extent natural *in-situ* rock material conditions (e.g. redox capacity) relevant to the far-field environment of a repository in crystalline rock. According to the experimental findings, Tc(VII) is reduced to Tc(IV) under natural anoxic conditions followed by either precipitation of $TcO_2 \cdot 1.6H_2O_{(s)}$ or/and surface complexation of soluble Tc(IV) species on the mineral surface of host rock. After contact of Tc(VII)-containing groundwater simulants with crystalline rock materials, Tc(IV) species were detected on mafic mica-type Fe-containing minerals. Apparently, the available ion-exchangeable Fe(II) (4 – 6 μg/g for un-oxidized ÄD, 1 – 3 μg/g for oxidized ÄD and 0.1 – 1 μg/g for NK granites) represents a redox buffer in the granite and is directly influencing the amount of Tc uptake on un-oxidized and oxidized material. Tc behaviour in presence of both oxidized ÄD and NK granite samples is quite similar, but it differs dramatically when in contact with un-oxidized ÄD samples. In general, artificially oxidized rock material could immobilize approx. 2 times less Tc compared to un-oxidized material. Distribution coefficients (K_d) and surface area normalized distribution coefficients (K_a) were determined for artificially oxidized and original un-oxidized ÄD together with oxidized NK rock material.

Comparison of samples with and without ultracentrifugation shows no detectable amount of Tc colloidal phases. Technetium desorption from the ÄD and NK rocks is insignificant under anoxic conditions, but after artificial oxidation of samples technetium mobility is increased due to re-oxidation of Tc(IV) to Tc(VII). The similar Tc desorption behaviour from the initially oxidized and un-oxidized ÄD samples indicates that Tc has the same speciation on the crystalline rocks for both types of the material even taking into account the difference in

the total uptake capacity. Samples from the batch sorption studies with high $[Tc]_{tot}$ show increased desorption values most probably due to faster re-oxidation of the $TcO_2 \cdot 1.6H_2O_{(s)}$ precipitate in comparison to surface complexed Tc(IV) species. According to the thermodynamics calculations, surface complexation of Tc(IV) is the predominant process for Tc immobilization at log [Tc] < -6, while at higher Tc concentration $TcO_2 \cdot 1.6H_2O_{(s)}$ precipitation plays the main role.

This work clearly highlights the importance of using well-preserved (un-oxidized) natural materials for the reliable estimation of the interaction of redox sensitive elements with these solid phases. The difference between artificially oxidized and un-oxidized material is highly significant. The data obtained gives important implications for the prediction of Tc behaviour under natural conditions for safety assessment of deep geological disposals of SNF and HLW in undisturbed and disturbed crystalline environments.

The comparison of the results of batch sorption studies with magnetite as a relevant Fe(II)-containing mineral with the studies with natural crystalline rock materials clearly shows that pertechnetate immobilization is much faster and more effective on magnetite than on natural granite samples due to the higher Fe(II) content. Partially oxidized magnetite exhibits the tendency of slower Tc uptake following the decreasing $Fe(II)/Fe_{tot}$ ratio at the mineral surface. The K_d and K_a values were derived from the experimental data, and were found to be several orders of magnetite higher than for the crystalline rocks (for instance, pH 8, log $[Tc]_{tot}$ = -5: K_a (un-oxidized ÄD) = 6.8×10^{-6} m, K_a (magnetite) = 7.5×10^{-2} m). The same batch studies performed on maghemite reveal no Tc uptake. That proves the hypothesis that ferrous iron in mineral phases represents the driving force for the Tc immobilization process.

Surface (XPS) and bulk (XAS) spectroscopic analyses indicate the presence of Tc(IV) species on the magnetite and crystalline rocks samples, which is consistent with the proposed mechanism of Tc(VII) immobilization.

Core migration experiments show much faster retention kinetics than batch sorption studies suggest (0.61 ± 0.08 d^{-1} and 0.051 ± 0.008 d^{-1} for 10^{-9} M Tc, respectively). The altered fracture surface contains Fe(II)-bearing secondary phases (including magnetite detected by SEM-EDX) reducing Tc(VII). With the natural groundwater as an eluent Tc immobilization is faster than with the groundwater simulant due to the lower redox potential, which is again showing the importance of maintaining the relevant *in-situ* conditions for getting reliable results. Anion exclusion was not observed for the core material in use.

The experimental data provide valuable input data for reactive transport models being developed with the aim of assessing and upscaling technetium migration in the frame of safety assessment studies for various scenarios relevant to deep geological repositories in crystalline rock.

6. Acknowledgements

The research leading to these results has received funding from the Federal Ministry of Economics and Technology (BMWi) collaborative project VESPA (Behavior of long-lived fission and activation products in the near field of a repository and possible retention mechanisms) under contract № 02 E 10800 and the European Union's European Atomic Energy Community's (Euratom) 7th Framework Programme FP7/2007-2011 under grant agreement № 269658 (CROCK project).

I would like to thank the supervisor of my PhD work Prof. Dr. Horst Geckeis for giving me an opportunity to work at the Institute for Nuclear Waste Disposal (INE), Karlsruhe Institute of Technology (KIT) as a great facility to perform up-to-date scientific research and also the professional and amicable community.

I especially would like to thank my scientific advisor Prof. Dr. Thorsten Schäfer for the time that he spent with me discussing the ideas of the new experiments and the obtained results. I am very grateful to him for the knowledge and experience that I have got during these discussions and for the always positive and friendly attitude.

I greatly appreciate the help from Dr. Florian Huber starting from the sample preparation and ending with the correction of the PhD thesis and papers. I would like to thank Stephanie Heck for the materials supply in the laboratory.

I would like thank Dr. Dieter Schild for the XPS and SEM-EDX measurements (together with Eva Soballa), processing of the results and the fruitful discussions. I am very thankful to the ANKA INE-beamline group, namely Dr. Tonya Vitova and Ivan Pidchenko for the XAS measurements and the data evaluation. I would also like to thank Markus Fuss for the γ-spectroscopy measurements and Tanja Kisely for the BET surface area analyses. I am also very thankful to Dr. Rémi Marsac for his help in thermodynamic calculations.

I am grateful to the INE Radiation Protection group, especially to Gerhard Christill for the care of our health and security during the work and also for the help in sample transfers.

I would like to thank my former scientific advisor Prof. Dr. Stepan Kalmykov (MSU, Russia) for the knowledge and experience in radiochemistry that were essential for the work performed for this PhD thesis and also for the supply of the Russian crystalline rock material.

I am very thankful to all my colleagues from the INE for the great help and a friendly atmosphere during the work and after it and also to the colleagues from the MSU and other institutes and facilities around the world for the productive collaboration and interesting communication.

7. References

1. IAEA, 2009. Classification of Radioactive Waste. General Safety Guide No. GSG-1, Vienna.
2. Bodansky, D., 2007. Nuclear Energy: Principles, Practices, and Prospects. Springer New York.
3. WNA, 2015. Storage and Disposal Options. World Nuclear Association website.
4. Gaurina-Medjimurec, N., 2014. Handbook of Research on Advancements in Environmental Engineering. IGI Global.
5. Streffer, C., 2011. Radioactive waste : technical and normative aspects of its disposal. Ethics of science and technology assessment,. Springer, Berlin, xxiv, 464 pages pp.
6. Anderson, Y.B., Lyubtseva, Y.F., Savonenkov, V.G., Shabalev, S.I., Alekseev, N.L., 2005. Creation of an Underground Storage Facility for Spent Nuclear Fuel near the City of Zheleznogorsk (Eastern Siberia), An International Spent Nuclear Fuel Storage Facility - Exploring a Russian Site as a Prototype: Proceedings of an International Workshop. The National Academies Press, pp. 166-176.
7. Laaksoharju, M. et al., 2008. Hydrogeochemical evaluation and modelling performed within the Swedish site investigation programme. Applied Geochemistry, 23(7): 1761-1795.
8. NEA, 2001. The role of underground laboratories in nuclear waste disposal programmes, OECD/NEA, Paris, France.
9. SKB, 2006. Äspö Hard Rock Laboratory. Brochure.
10. Kratz, J.V., Lieser, K.H., 2013. Nuclear and Radiochemistry: Fundamentals and Applications. Wiley.
11. Um, W., Serne, R.J., 2005. Sorption and transport behavior of radionuclides in the proposed low-level radioactive waste disposal facility at the Hanford site, Washington. Radiochimica Acta, 93(1): 57-63.
12. Zachara, J.M. et al., 2007. Reduction of pertechnetate [Tc(VII)] by aqueous Fe(II) and the nature of solid phase redox products. Geochimica et Cosmochimica Acta, 71(9): 2137-2157.
13. Meyer, R.E., Arnold, W.D., Case, F.I., Okelley, G.D., 1991. Solubilities of Tc(IV) Oxides. Radiochimica Acta, 55(1): 11-18.
14. Jaisi, D.P. et al., 2009. Reduction and long-term immobilization of technetium by Fe(II) associated with clay mineral nontronite. Chemical Geology, 264(1-4): 127-138.
15. Peretyazhko, T. et al., 2008. Heterogeneous reduction of Tc(VII) by Fe(II) at the solid-water interface. Geochimica et Cosmochimica Acta, 72(6): 1521-1539.
16. Peretyazhko, T. et al., 2008. Reduction of Tc(VII) by Fe(II) Sorbed on Al (hydr)oxides. Environmental Science & Technology, 42(15): 5499-5506.
17. Heald, S.M. et al., 2007. XAFS study of the chemical and structural states of technetium in Fe(III) oxide Co-precipitates. X-Ray Absorption Fine Structure-XAFS13, 882: 173-175.
18. Fredrickson, J.K. et al., 2009. Oxidative dissolution potential of biogenic and abiogenic TcO2 in subsurface sediments. Geochimica et Cosmochimica Acta, 73(8): 2299-2313.
19. Petrov, V.G. et al., 2012. Characterisation of rock samples from areas of the proposed. Russian HLW and SNF repository (Nizhnekansky massive) and first sorption studies. 1st Workshop Proceedings of the Collaborative Project „Crystalline Rock Retention Processes“ (7th EC FP CP CROCK): 37-42.

20. Schäfer, T., Stage, E., Büchner, S., Huber, F., Drake, H., 2012. Characterization of new crystalline material for investigations within CP CROCK. 1st Workshop Proceedings of the Collaborative Project „Crystalline Rock Retention Processes“ (7th EC FP CP CROCK): 63-72.
21. Marschall, P., Horseman, S., Gimmi, T., 2005. Characterisation of gas transport properties of the Opalinus Clay, a potential host rock formation for radioactive waste disposal. Oil & Gas Science and Technology, 60(1): 121-139.
22. Grambow, B., 2008. Mobile fission and activation products in nuclear waste disposal. Journal of Contaminant Hydrology, 102(3-4): 180-186.
23. Bath, A., 2011. Infiltration of dilute groundwaters and resulting groundwater compositions at repository depth. 2011:22, SSM.
24. 2009. CP-CROCK Annex I - “Description of Work”.
25. Silveira, L., Usunoff, E.J., 2009. Groundwater, Vol. II. Eolss Publishers Co Ltd.
26. Xu, S., Wörman, A., 1999. Implications of sorption kinetics to radionuclide migration in fractured rock. Water Resources Research, 35(11): 3429-3440.
27. Appelo, C.A.J., Postma, D., 2005. Geochemistry, Groundwater And Pollution. A.A. Balkema Publishers.
28. McNaught, A.D., Wilkinson, A., International Union of Pure and Applied Chemistry., 1997. Compendium of chemical terminology : IUPAC recommendations. Blackwell Science, Oxford England ; Malden, MA, USA, 450 pp.
29. Sparks, D.L., 2005. Sorption | Metals. In: Hillel, D. (Ed.), Encyclopedia of Soils in the Environment. Elsevier Ltd., pp. 532-537.
30. Crini, G., Badot, P.M., 2010. Sorption Processes and Pollution: Conventional and Non-conventional Sorbents for Pollutant Removal from Wastewaters. Presses universitaires de Franche-Comté.
31. Somasundaran, P., 2006. Encyclopedia of Surface and Colloid Science. Taylor & Francis.
32. Kaplan, D.I., Roberts, K., Coates, J., Siegfried, M., Serkiz, S., 2008. Saltstone and concrete interactions with radionuclides: sorption (Kd), desorption, and reduction capacity measurements. SRNS-STI-2008-00045, SRNL.
33. Powell, B.A., Fjeld, R.A., Coates, J.T., Kaplan, D.I., Serkiz, S.M., 2002. Plutonium oxidation state geochemistry in the SRS subsurface environment. WSRC-TR-2003-00035, SRC.
34. Neretnieks, I., 1980. Diffusion in the Rock Matrix - an Important Factor in Radionuclide Retardation. Journal of Geophysical Research, 85(Nb8): 4379-4397.
35. OECD/NEA, 2001. Radionuclide Retention in Geologic Media. Workshop Proceedings., Oskarshamn, Sweden.
36. Rabung, T., Garcia, D., Montoya, V., 2014. Final Workshop Proceedings of the Collaborative Project "Crystalline Rock Retention Processes" (7th EC FP CP CROCK). KIT Scientific Publishing.
37. Perrier, C., Segre, E., 1937. Some Chemical Properties of Element 43. The Journal of Chemical Physics, 5(9): 712-716.
38. NuDat_Database, http://nucleardata.nuclear.lu.se/database/nudat/.
39. Dalrymple, G.B., 2001. The age of the Earth in the twentieth century: a problem (mostly) solved. Geological Society, London, Special Publications, 190(1): 205-221.
40. Ihsanullah, 1993. Losses of Technetium during Various Steps in the Development of a Procedure for Environmental-Samples. Journal of Radioanalytical and Nuclear Chemistry-Letters, 176(4): 303-313.
41. CEFAS, 2012. Radioactivity in food and the environment, 2011. RIFE - 17.

42. Holm, E., Rioseco, J., Garcia-León, M., 1984. Determination of 99Tc in environmental samples. Nuclear Instruments and Methods in Physics Research, 223(2–3): 204-207.
43. Chen, Q.J., Dahlgaard, H., Hansen, H.J.M., Aarkrog, A., 1990. Determination of Tc-99 in Environmental-Samples by Anion-Exchange and Liquid-Liquid-Extraction at Controlled Valency. Analytica Chimica Acta, 228(1): 163-167.
44. Uchida, S., Tagami, K., 1997. Separation and concentration of technetium using a Tc-selective extraction chromatographic resin. Journal of Radioanalytical and Nuclear Chemistry, 221(1-2): 35-39.
45. Wacker, L., Fifield, L.K., Tims, S.G., 2004. Developments in AMS of Tc-99. Nuclear Instruments & Methods in Physics Research Section B-Beam Interactions with Materials and Atoms, 223: 185-189.
46. Dixon, P. et al., 1997. Analysis of Naturally Produced Technetium and Plutonium in Geologic Materials. Analytical Chemistry, 69(9): 1692-1699.
47. Kim, C.-K. et al., 1989. Application of Inductively Coupled Plasma Mass Spectrometry to the Determination of 99Tc in Soil Samples. Radioisotopes, 38(3): 151-152.
48. Song, M., Probst, T.U., 2000. Rapid determination of technetium-99 by electrothermal vaporization-inductively coupled plasma-mass spectrometry with sodium chlorate and nitric acid as modifiers. Analytica Chimica Acta, 413(1-2): 207-215.
49. Hou, X., Roos, P., 2008. Critical comparison of radiometric and mass spectrometric methods for the determination of radionuclides in environmental, biological and nuclear waste samples. Analytica Chimica Acta, 608(2): 105-139.
50. Bondietti, E.A., Francis, C.W., 1979. Geologic Migration Potentials of Technetium-99 and Neptunium-237. Science, 203(4387): 1337-1340.
51. Icenhower, J.P., Qafoku, N., Martin, W.J., Zachara, J.M., 2008. The Geochemistry of Technetium: A Summary of the Behavior of an Artificial Element in the Natural Environment. PNNL-18139.
52. Cobble, J.W., Smith, W.T., Boyd, G.E., 1953. Thermodynamic Properties of Technetium and Rhenium Compounds. II. Heats of Formation of Technetium Heptoxide and Pertechnic Acid, Potential of the Technetium-(IV)-Technetium(VII) Couple, and a Potential Diagram for Technetium1,2. Journal of the American Chemical Society, 75(23): 5777-5782.
53. Cartledge, G.H., Smith, W.T., 1955. Revision of the Electrode-Potential Diagram for Technetium. Journal of Physical Chemistry, 59(10): 1111-1112.
54. Meyer, R.E., Arnold, W.D., 1991. The Electrode Potential of the Tc(IV)-Tc(VII) Couple. Radiochimica Acta, 55(1): 19-22.
55. Rard, J.A., Rand, M.H., Anderegg, G., Wanner, H., 1999. Chemical Thermodynamics of Technetium. Chemical Thermodynamics, 3. Elsevier.
56. Koch-Steindl, H., Prohl, G., 2001. Considerations on the behaviour of long-lived radionuclides in the soil. Radiation and Environmental Biophysics, 40(2): 93-104.
57. Lieser, K.H., Bauscher, C., 1987. Technetium in the Hydrosphere and in the Geosphere .1. Chemistry of Technetium and Iron in Natural-Waters and Influence of the Redox Potential on the Sorption of Technetium. Radiochimica Acta, 42(4): 205-213.
58. Tagami, K., Uchida, S., 1997. Concentration of global fallout Tc-99 in rice paddy soils collected in Japan. Environmental Pollution, 95(2): 151-154.
59. Vandecasteele, C.M., Dehut, J.P., Vanlaer, S., Deprins, D., Myttenaere, C., 1989. Long-Term Availability of Tc Deposited on Soil after Accidental Releases. Health Physics, 57(2): 247-254.

60. Echevarria, G., Vong, P.C., Leclerc-Cessac, E., Morel, J.L., 1997. Bioavailability of Technetium-99 as Affected by Plant Species and Growth, Application Form, and Soil Incubation. J. Environ. Qual., 26(4): 947-956.
61. Cui, D., Eriksen, T.E., 1996. Reduction of Pertechnetate in Solution by Heterogeneous Electron Transfer from Fe(II)-Containing Geological Material. Environmental Science & Technology, 30(7): 2263-2269.
62. Fredrickson, J.K. et al., 2004. Reduction of TcO4− by sediment-associated biogenic Fe(II). Geochimica et Cosmochimica Acta, 68(15): 3171-3187.
63. Liu, D.J., Yao, J., Wang, B., Bruggeman, C., Maes, N., 2007. Solubility study of Tc(IV) in a granitic water. Radiochimica Acta, 95(9): 523-528.
64. Eriksen, T.E., Ndalamba, P., Bruno, J., Caceci, M., 1992. The Solubility of TcO2 . nH2O in Neutral to Alkaline-Solutions under Constant pCO2. Radiochimica Acta, 58-9: 67-70.
65. Hess, N.J., Xia, Y.X., Rai, D., Conradson, S.D., 2004. Thermodynamic model for the solubility of TcO2 center dot xH(2)O(am) in the aqueous Tc(IV)-Na+-Cl--H+-OH--H2O system. Journal of Solution Chemistry, 33(2): 199-226.
66. Duro, L. et al., 2006. Determination and assessment of the concentration limits to be used in SR-Can. TR-06-32, SKB.
67. Hu, Q.H., Zavarin, M., Rose, T.P., 2008. Effect of reducing groundwater on the retardation of redox-sensitive radionuclides. Geochemical Transactions, 9.
68. Zachara, J.M. et al., 2007. Geochemical processes controlling migration of tank wastes in Hanford's vadose zone. Vadose Zone Journal, 6(4): 985-1003.
69. Sekine, T. et al., 2004. Technetium(IV) oxide colloids produced by radiolytic reactions in aqueous pertechnetate solution. Colloids and Surfaces A: Physicochemical and Engineering Aspects, 249(1–3): 105-109.
70. Sekine, T. et al., 2002. Radiolytic formation of Tc(IV) oxide colloids. Radiochimica Acta, 90(9-11): 611-616.
71. Rard, J.A., 1985. Chemistry and thermodynamics of ruthenium and some of its inorganic compounds and aqueous species. Chemical Reviews, 85(1): 1-39.
72. Lukens, W.W., Bucher, J.J., Edelstein, N.M., Shuh, D.K., 2002. Products of Pertechnetate Radiolysis in Highly Alkaline Solution: Structure of TcO2·xH2O. Environmental Science & Technology, 36(5): 1124-1129.
73. Maes, A. et al., 2004. Evidence for the Interaction of Technetium Colloids with Humic Substances by X-ray Absorption Spectroscopy. Environmental Science & Technology, 38(7): 2044-2051.
74. Wharton, M.J. et al., 2000. An X-ray absorption spectroscopy study of the coprecipitation of Tc and Re with mackinawite (FeS). Applied Geochemistry, 15(3): 347-354.
75. Bruggeman, C., Maes, A., Vancluysen, J., 2007. The identification of FeS2 as a sorption sink for Tc(IV). Physics and Chemistry of the Earth, 32(8-14): 573-580.
76. Lukens, W.W., Bucher, J.J., Shuh, D.K., Edelstein, N.M., 2005. Evolution of technetium speciation in reducing grout. Environmental Science & Technology, 39(20): 8064-8070.
77. German, K.E. et al., 2015. Technetium sulfide – formation kinetics, structure and particle speciation. Radiochimica Acta, 103(3): 199.
78. Wildung, R.E., Garland, T.R., McFadden, K.M., Cowan, C.E., 1986. Technetium Sorption in Surface Soils. In: Desmet, G., Myttenaere, C. (Eds.), Technetium in the Environment. Springer Netherlands, pp. 115-129.
79. Kaplan, D.I., Serne, R.J., 1998. Pertechnetate exclusion from sediments. Radiochimica Acta, 81(2): 117-124.

80. Jakubick, A.T., Church, W., 1986. Oklo natural reactors: geological and geochemical conditions - A review. INFO-0179.
81. Torstenfelt, B., Allard, B., Andersson, K., Olofsson, U., 1981. Technetium in the geologic environment. Report Prav 4.28, Department of Nuclear Chemistry, Chalmers Univercity of Technology, Göteborg, Sweden.
82. Geraedts, K. et al., 2002. Evidence for the existence of Tc(IV) - humic substance species by X-ray absorption near-edge spectroscopy. Radiochimica Acta, 90(12): 879-884.
83. Wolfrum, C., Bunzl, K., 1986. Sorption and Desorption of Technetium by Humic Substances under Oxic and Anoxic Conditions. Journal of Radioanalytical and Nuclear Chemistry-Articles, 99(2): 315-323.
84. Sekine, T., Watanabe, A., Yoshihara, K., Kim, J.I., 1993. Complexation of Technetium with Humic Acid, Radiochimica Acta, pp. 87.
85. Geraedts, K., 2007. The interaction between technetium and Gorleben humic substances PhD Thesis, Katholieke Universiteit Leuven.
86. Kim, E., Benedetti, M.F., Boulegue, J., 2004. Removal of dissolved rhenium by sorption onto organic polymers: study of rhenium as an analogue of radioactive technetium. Water Research, 38(2): 448-454.
87. Baston, G.M.N. et al., 2002. Technetium behaviour in Boom Clay - a laboratory and field study. Radiochimica Acta, 90(9-11): 735-740.
88. McCubbin, D., Leonard, K.S., McDonald, P., Bonfield, R., Boust, D., 2006. Distribution of Technetium-99 in sub-tidal sediments of the Irish Sea. Continental Shelf Research, 26(4): 458-473.
89. Jansson, M., Eriksen, T.E., 2004. In situ anion diffusion experiments using radiotracers. Journal of Contaminant Hydrology, 68(3–4): 183-192.
90. Ramebäck, H. et al., 2000. Transport and leaching of technetium and uranium from spent UO2 fuel in compacted bentonite clay. Journal of Nuclear Materials, 277(2–3): 288-294.
91. Druteikienė, R. et al., 2014. Behaviour of 99Tc in aqueous solutions in the presence of iron oxides and microorganisms. Applied Radiation and Isotopes, 89(0): 85-94.
92. Haines, R.I., Owen, D.G., Vandergraaf, T.T., 1987. Technetium-iron oxide reactions under anaerobic conditions: a Fourier Transform Infrared, FTIR study. Nuclear Journal of Canada, 1(2): 32-37.
93. Milonjic, S.K., Kopecni, M.M., Ilic, Z.E., 1983. The Point of Zero Charge and Adsorption Properties of Natural Magnetite. Journal of Radioanalytical Chemistry, 78(1): 15-24.
94. Cui, D., Eriksen, T.E., 1996. Reduction of Pertechnetate by Ferrous Iron in Solution: Influence of Sorbed and Precipitated Fe(II). Environmental Science & Technology, 30(7): 2259-2262.
95. McBeth, J.M. et al., 2011. Redox interactions of technetium with iron-bearing minerals. Mineralogical Magazine, 75(4): 2419-2430.
96. Marshall, T.A. et al., 2014. Incorporation and Retention of 99-Tc(IV) in Magnetite under High pH Conditions. Environmental Science & Technology, 48(20): 11853-11862.
97. Kobayashi, T., Scheinost, A.C., Fellhauer, D., Gaona, X., Altmaier, M., 2013. Redox behavior of Tc(VII)/Tc(IV) under various reducing conditions in 0.1 M NaCl solutions. Radiochimica Acta, 101(5): 323-332.
98. Yalcintas, E. et al., 2015. Redox chemistry of Tc(VII)/Tc(IV) in dilute to concentrated NaCl and MgCl2 solutions. Radiochimica Acta, 103(1): 57-72.

99. Fried, S., Friedman, A.M., Cohen, D., Hines, J.J., Strickert, R.G., 1978. Migration of long-lived radioactive processing wastes in selected rocks: annual report to the Office of Waste Handling, Project AN0115A, FY 1977, United States.
100. Allard, B., Kigatsi, H., Torstenfelt, B., 1979. Technetium - Reduction and Sorption in Granitic Bedrock. Radiochemical and Radioanalytical Letters, 37(4-5): 223-229.
101. Liu, D.J., Fan, X.H., Yao, J., Wang, B., 2006. Diffusion of Tc-99 in granite under aerobic and anoxic conditions. Journal of Radioanalytical and Nuclear Chemistry, 268(3): 481-484.
102. Kienzler, B., Vejmelka, P., Römer, J., Schild, D., Jansson, M., 2009. Actinide migration in fractures of granite host rock: laboratory and in situ investigations. Nuclear Technology, 165(2): 223-240.
103. Videnska, K., Havlova, V., 2012. Retention of Anionic Species on Granite: Influence of Granite Composition, Waste Management 2012, Phoenix, Arizona, USA.
104. Kienzler, B. et al., 2003. Swedish-German actinide migration experiment at ASPO hard rock laboratory. Journal of Contaminant Hydrology, 61(1-4): 219-233.
105. Schwertmann, U., Cornell, R.M., 2000. Iron Oxides in the Laboratory. Wiley.
106. Patterson, A.L., 1939. The Scherrer Formula for X-Ray Particle Size Determination. Physical Review, 56(10): 978-982.
107. Smilgies, D.-M., 2009. Scherrer grain-size analysis adapted to grazing-incidence scattering with area detectors. Journal of Applied Crystallography, 42(Pt 6): 1030-1034.
108. Gorski, C.A. et al., 2012. Fe Atom Exchange between Aqueous Fe2+ and Magnetite. Environmental Science & Technology, 46(22): 12399-12407.
109. Byegård, J., Johansson, H., Skålberg, M., Tullborg, E.-L., 1998. The interaction of sorbing and non-sorbing tracers with different Äspö rock types. Sorption and diffusion experiments in the laboratory scale. SKB TR-98-18.
110. Kornfält, K.-A., Persson, P.-O., Wikman, H., 1997. Granitoids from the Äspö area, southeastern Sweden - geochemical and geochronological data. GFF, 119(2): 109-114.
111. Huber, F. et al., 2012. Natural micro-scale heterogeneity induced solute and nanoparticle retardation in fractured crystalline rock. Journal of Contaminant Hydrology, 133(0): 40-52.
112. Huber, F. et al., 2010. Laboratory study on colloid migration and colloid-radionuclide interaction under Grimsel groundwater conditions simulating glacial melt-water intrusion in the Äspö system. “Colloid project” activity report, unpublished, KIT INE.
113. Nockolds, S.R., 1954. Average Chemical Compositions of Some Igneous Rocks. Geological Society of America Bulletin, 65(10): 1007-&.
114. Heron, G., Crouzet, C., Bourg, A.C.M., Christensen, T.H., 1994. Speciation of Fe(II) and Fe(III) in contaminated aquifer sediments using chemical extraction techniques. Environ. Sci. Technol., 28: 1698-1705.
115. Stookey, L.L., 1970. Ferrozine - a New Spectrophotometric Reagent for Iron. Analytical Chemistry, 42(7): 779-781.
116. Viollier, E., Inglett, P.W., Hunter, K., Roychoudhury, A.N., Van Cappellen, P., 2000. The ferrozine method revisited: Fe(II)/Fe(III) determination in natural waters. Applied Geochemistry, 15(6): 785-790.
117. Heck, S., Schäfer, T., 2012. Short Note: CP CROCK groundwater sample characterization
118. Boyd, G.E., Larson, Q.V., Motta, E.E., 1960. Isolation of Milligram Quantities of Long-Lived Technetium from Neutron Irradiated Molybdenum. Journal of the American Chemical Society, 82(4): 809-815.

119. Tagami, K., Uchida, S., 1999. Comparison of the TEVA center dot Spec resin and liquid-liquid extraction methods for the separation of technetium in soil samples. Journal of Radioanalytical and Nuclear Chemistry, 239(3): 643-648.
120. Kohler, R., Duck, R., Ausperger, B., Alex, R., 2003. A numeric model for the kinetics of water vapor sorption on cellulosic reinforcement fibers. Composite Interfaces, 10(2-3): 255-276.
121. Albinsson, Y., Christiansensatmark, B., Engkvist, I., Johansson, W., 1991. Transport of Actinides and Tc through a Bentonite Backfill Containing Small Quantities of Iron or Copper. Radiochimica Acta, 52-3: 283-286.
122. USEPA, 1999. The Kd model, methods of measurement, and application of chemical reaction codes. EPA 402-R-99-004A, United States Environmental Protection Agency, Office of Air and Radiation.
123. Kopunec, R., Abudeab, F.N., Skraskova, S., 1997. Extraction of pertechnetate with tetraphenylphosphonium in the presence of various acids, salts and hydroxides. PhD Thesis.
124. Rajec, P., Mikulaj, V., Kadrabova, J., 1979. Solvent-Extraction of Reduced Technetium from Mineral Acid-Solutions. Journal of Radioanalytical Chemistry, 51(1): 85-95.
125. Park, C.K., Kienzler, B., Vejmelka, P., Jeong, J.T., 2012. Modeling and analysis of the migration of HTO and (NP)-N-237 in a fractured granite core at the Aspo hard rock laboratory. Radiochimica Acta, 100(3): 197-205.
126. Grosvenor, A.P., Kobe, B.A., Biesinger, M.C., McIntyre, N.S., 2004. Investigation of multiplet splitting of Fe 2p XPS spectra and bonding in iron compounds. Surface and Interface Analysis, 36(12): 1564-1574.
127. Aronniemi, M., Sainio, J., Lahtinen, J., 2005. Chemical state quantification of iron and chromium oxides using XPS: the effect of the background subtraction method. Surface Science, 578(1-3): 108-123.
128. Rothe, J. et al., 2012. The INE-Beamline for actinide science at ANKA. Review of Scientific Instruments, 83(4).
129. Ravel, B., Newville, M., 2005. ATHENA, ARTEMIS, HEPHAESTUS: data analysis for X-ray absorption spectroscopy using IFEFFIT. Journal of Synchrotron Radiation, 12: 537-541.
130. Rehr, J.J., Albers, R.C., 2000. Theoretical approaches to x-ray absorption fine structure. Reviews of Modern Physics, 72(3): 621-654.
131. Rehr, J.J., Kas, J.J., Vila, F.D., Prange, M.P., Jorissen, K., 2010. Parameter-free calculations of X-ray spectra with FEFF9. Phys Chem Chem Phys, 12(21): 5503-13.
132. Parkhurst, D.L., Appelo, C.A.J., 1999. User's Guide to PHREEQC (Version 2) - A Computer Program for Speciation, Batch-Reaction, One-Dimensional Transport, and Inverse Geochemical Calculations. Water-Resources Investigations Report 99-4259.
133. Guillaumont, R. et al., 2003. Update on the Chemical Thermodynamics of Uranium, Neptunium, Plutonium, Americium and Technetium. Chemical Thermodynamics, 5. Elsevier.
134. Lemire, R.J. et al., 2013. Chemical Thermodynamics of Iron, Part 1. Chemical Thermodynamics, 13a. OECD.
135. Westsik Jr, J.H., Cantrell, K.J., Serne, R.J., Qafoku, N.P., 2014. Technetium Immobilization Forms. Literature Survey. PNNL-23329.
136. Wildung, R.E. et al., 2004. Technetium reduction in sediments of a shallow aquifer exhibiting dissimilatory iron reduction potential. Fems Microbiology Ecology, 49(1): 151-162.

137. Yalcintas, E., 2015. Redox, solubility and sorption chemistry of technetium in dilute to concentrated saline systems. PhD Thesis, KIT-INE, Karlsruhe.
138. Kirsch, R. et al., 2011. Oxidation State and Local Structure of Plutonium Reacted with Magnetite, Mackinawite, and Chukanovite. Environmental Science & Technology, 45(17): 7267-7274.
139. Grenthe, I., Stumm, W., Laaksuharju, M., Nilsson, A.C., Wikberg, P., 1992. Redox Potentials and Redox Reactions in Deep Groundwater Systems. Chemical Geology, 98(1-2): 131-150.
140. Cumpson, P.J., Seah, M.P., 1997. Elastic Scattering Corrections in AES and XPS. II. Estimating Attenuation Lengths and Conditions Required for their Valid Use in Overlayer/Substrate Experiments. Surface and Interface Analysis, 25(6): 430-446.
141. Boonstra, A.H., Mutsaers, C.A.H.A., 1975. Adsorption of hydrogen peroxide on the surface of titanium dioxide. The Journal of Physical Chemistry, 79(18): 1940-1943.
142. Latta, D.E. et al., 2012. Influence of Magnetite Stoichiometry on U(VI) Reduction. Environmental Science & Technology, 46(2): 778-786.
143. Huber, F. et al., 2012. U(VI) removal kinetics in presence of synthetic magnetite nanoparticles. Geochimica et Cosmochimica Acta, 96(0): 154-173.
144. Gorski, C.A., Nurmi, J.T., Tratnyek, P.G., Hofstetter, T.B., Scherer, M.M., 2010. Redox Behavior of Magnetite: Implications for Contaminant Reduction. Environmental Science & Technology, 44(1): 55-60.
145. Altmaier, M., Gaona, X., Fellhauer, D., Buckau, G., 2011. Intercomparison of redox determination methods on designed and near-natural aqueous systems. KIT Scientific Reports 7572, KIT Scientific Publishing.
146. Freundlich, H., 1906. Über die Adsorption in Lösungen. Wilhelm Engelmann.
147. Marsac, R. et al., 2015. Modeling plutonium sorption to kaolinite: Accounting for redox equilibria and the stability of surface species. Chemical Geology, 400(0): 1-10.
148. Marsac, R. et al., 2015. Neptunium redox speciation at the illite surface. Geochimica Et Cosmochimica Acta, 152: 39-51.
149. Burlakov, V.M., Sutton, A.P., Briggs, G.A.D., Tsukahara, Y., 2000. Simulation of Porous Si and SiOx Layer Growth. In: MSM (Editor), Technical Proceedings of the 2000 International Conference on Modeling and Simulation of Microsystems, University of Oxford, UK, pp. 95-97.
150. Jeppu, G.P., Clement, T.P., 2012. A modified Langmuir-Freundlich isotherm model for simulating pH-dependent adsorption effects. Journal of Contaminant Hydrology, 129–130(0): 46-53.
151. Ito, K., Kanno, T., 1988. Sorption Behavior of Carrier-Free Technetium-95m on Minerals, Rocks and Backfill Materials under Both Oxidizing and Reducing Conditions. Journal of Nuclear Science and Technology, 25(6): 534-539.
152. McKinley, I.G., Scholtis, A., 1993. A comparison of radionuclide sorption databases used in recent performance assessments. Journal of Contaminant Hydrology, 13(1–4): 347-363.
153. Morris, K. et al., 2008. An X-ray absorption study of the fate of technetium in reduced and reoxidised sediments and mineral phases. Applied Geochemistry, 23(4): 603-617.
154. Burke, I.T. et al., 2006. Reoxidation Behavior of Technetium, Iron, and Sulfur in Estuarine Sediments. Environmental Science & Technology, 40(11): 3529-3535.
155. Begg, J.D.C., Burke, I.T., Charnock, J.M., Morris, K., 2008. Technetium reduction and reoxidation behaviour in Dounreay soils. Radiochimica Acta, 96(9-11): 631-636.
156. Wester, D.W. et al., 1987. Synthesis and Characterization of Technetium Complexes with Phosphorus-Containing Ligands - the Homoleptic Trimethylphosphite,

Dimethylmethylphosphonite and Methyldiethylphosphinite Technetium(I) Cations. Inorganica Chimica Acta, 131(2): 163-169.
157. Burke, I.T. et al., 2010. The fate of technetium in reduced estuarine sediments: Combining direct and indirect analyses. Applied Geochemistry, 25(2): 233-241.
158. Altmaier, M., Kienzler, B., Duro, L., Grivé, M., Montoya, V., 2011. 3rd Annual Workshop Proceedings of the Collaborative Project "Redox Phenomena Controlling Systems" (7th EC FP CP RECOSY). KIT-SR 7603, KIT INE.
159. Buechele, A.C., McKeown, D.A., Lukens, W.W., Shuh, D.K., Pegg, I.L., 2012. Tc and Re behavior in borosilicate waste glass vapor hydration tests II. Journal of Nuclear Materials, 429(1-3): 159-165.
160. McKeown, D.A., Buechele, A.C., Lukens, W.W., Shuh, D.K., Pegg, I.L., 2007. Tc and Re behavior in borosilicate waste glass vapor hydration tests. Environmental Science & Technology, 41(2): 431-436.
161. Newville, M., 2014. Fundamentals of XAFS. Reviews in Mineralogy and Geochemistry, 78(1): 33-74.
162. Almahamid, I. et al., 1995. Electronic and Structural Investigations of Technetium Compounds by X-Ray-Absorption Spectroscopy. Inorganic Chemistry, 34(1): 193-198.
163. Mejías, M., Renard, P., Glenz, D., 2009. Hydraulic testing of low-permeability formations: A case study in the granite of Cadalso de los Vidrios, Spain. Engineering Geology, 107(3–4): 88-97.
164. Walker, D., Rhen, I., Gurban, I., 1997. Summary of hydrogeologic conditions at Aberg, Beberg and Ceberg. TR 97-23, SKB, Stockholm, Sweden.
165. KIT-INE, 2012. Characterization of experimental material. CROCK Deliverable 1.2.
166. Liu, C.L. et al., 2001. Diffusion of Tc-99 in granite: A small scale laboratory simulation experiment. Radiochimica Acta, 89(10): 639-642.
167. Park, C.K., Cho, W.J., Hahn, P.S., 2006. Transport properties of sorbing contaminants in a fractured granite under oxidizing conditions. Korean Journal of Chemical Engineering, 23(5): 741-746.
168. Vejmelka, P. et al., 2000. Sorption and migration of radionuclides in granite (HRL Äspö, Sweden). FZKA 6488, INE KIT.
169. Triay, I.R., Mitchell, A.J., Ott, M.A., 1992. Radionuclide migration laboratory studies for validation of batch sorption data, Sorption Workshop Proceedings, Los Alamos National Laboratory.
170. Puigdomeneck, I., 2001. Hydrochemical stability of groundwaters surrounding a spent nuclear fuel repository in a 100,000 year perspective. TR-01-28, SKB, Stockholm, Sweden.

8. Appendix

8.1. Supplementary materials

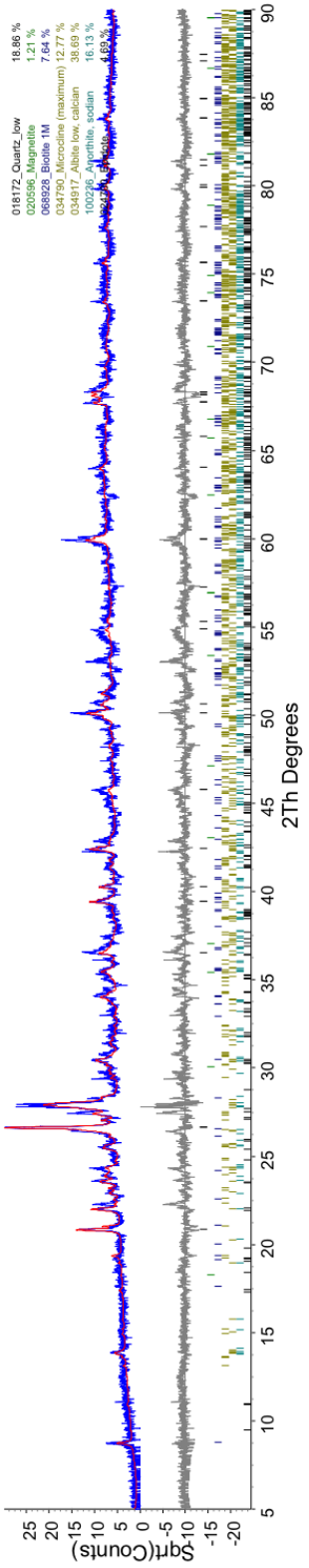

Figure S 1. *Fitting of the XRD spectrum of Äspö diorite.*

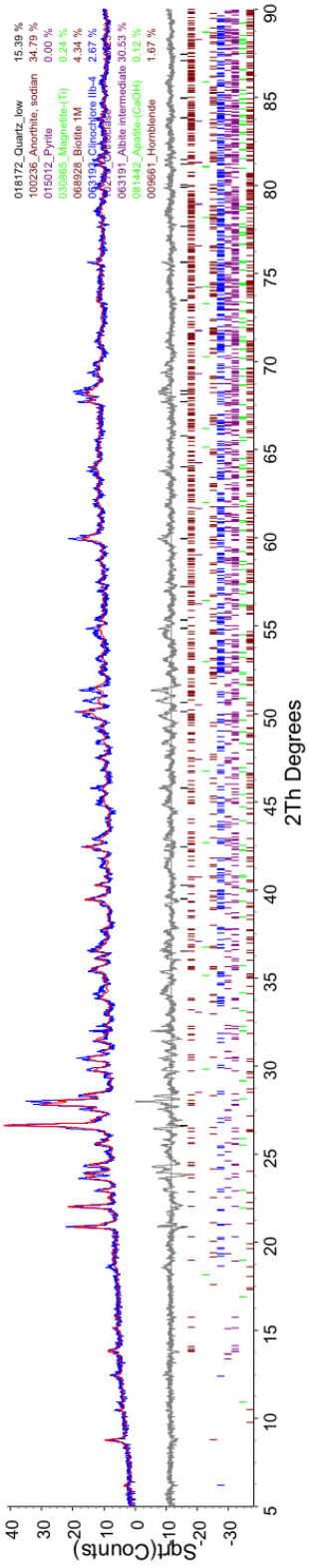

Figure S 2. *Fitting of the XRD spectrum of Nizhnekansky massif granitic rock.*

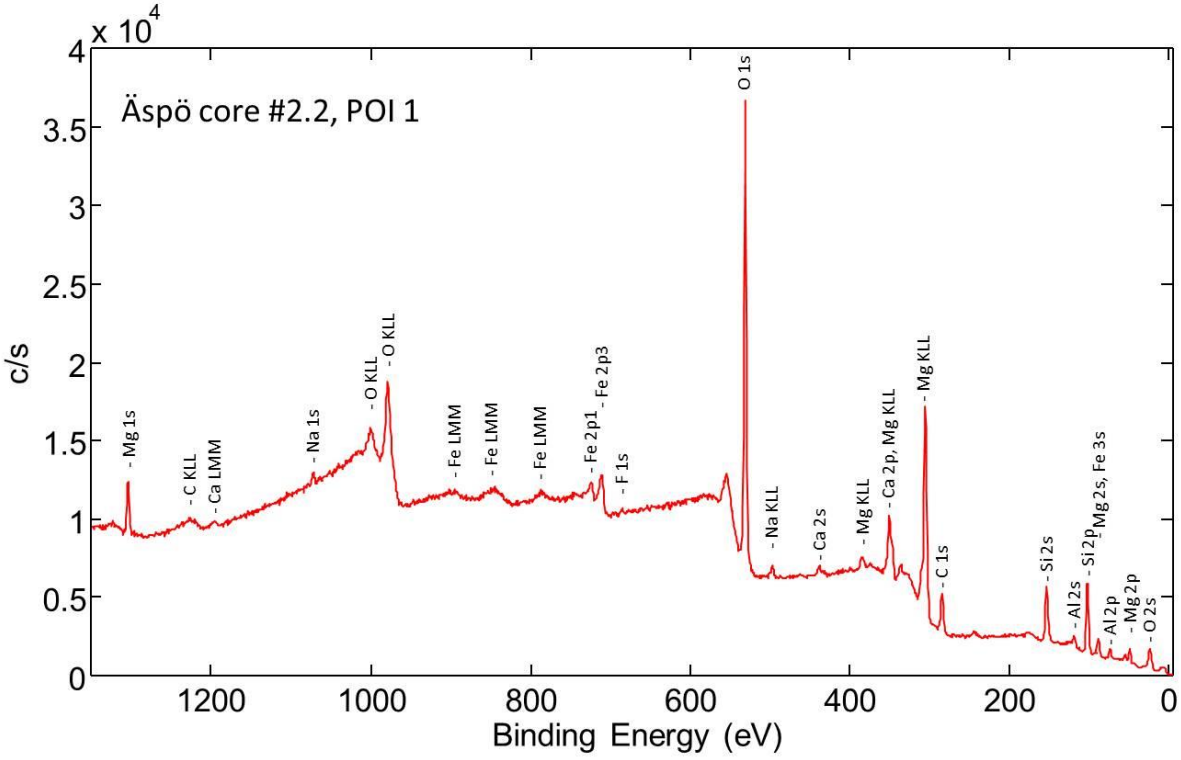

Figure S 3. *XPS survey spectrum of the Äspö core #2.2 (POI 1) after Tc migration studies.*

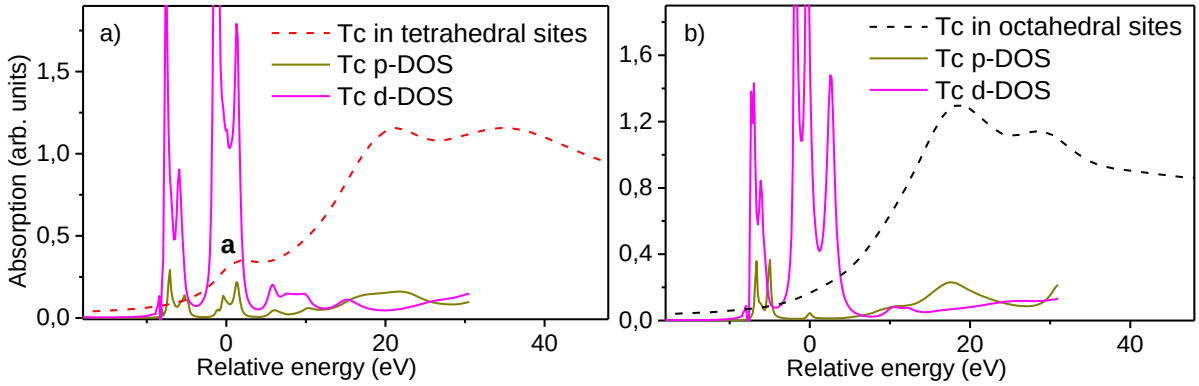

Figure S 4. *Calculated Tc K-edge XANES spectra and Tc p and d angular momentum projected density of states (p-DOS , d-DOS) for Tc occupying tetrahedral (a) or octahedral (b) Fe sites in Fe_3O_4. The Fermi energy denotes the transition from occupied to unoccupied states at 0 eV.*

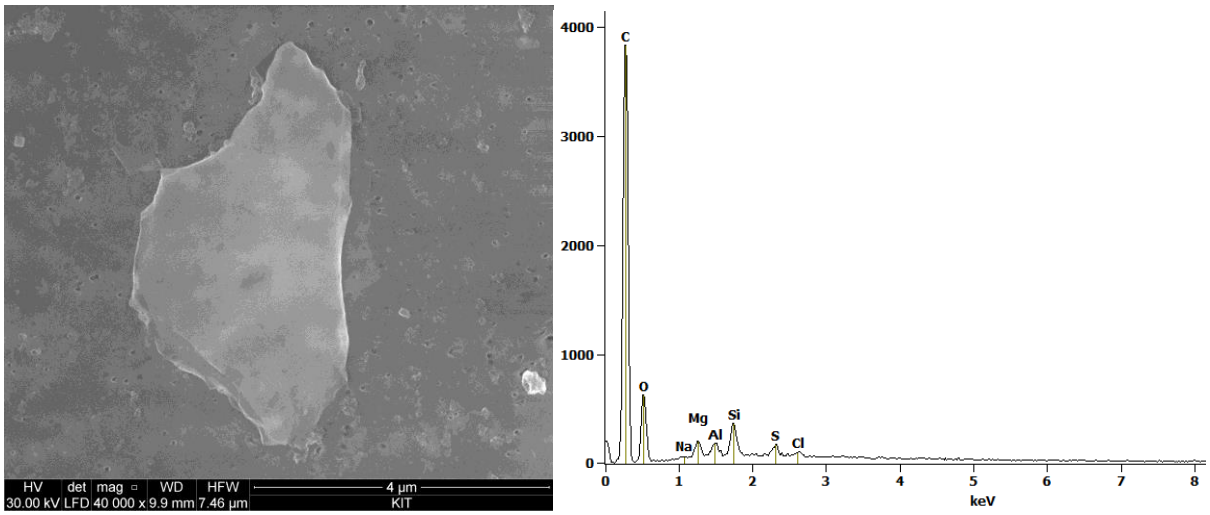

Figure S 5. *SEM image (left) and EDX spectrum (right) of the particle filtered from the natural ÄGW (additional).*

Table S 1. *List of samples of Tc interaction with magnetite suspension.*

pH	Con-tact time, days	Tc uptake, % log [Tc] = -5				log [Tc] = -8				log [Tc] = -9			
		Magn	±, %	UC	±, %	Magn	±, %	UC	±, %	Magn	±, %	UC	±, %
7	1	94.28	0.02	94.09	0.02	93.49	0.81	88.36	0.95	74.00	8.64	70.01	8.77
	3	99.74	0.00	99.91	0.00	98.99	0.65	100.20	0.60	100.00	7.21	98.01	7.79
	7	99.98	0.00	99.99	0.00	100.00	0.56	100.43	0.59	96.86	7.83	100.00	7.38
	14	99.83	0.00	100.00	0.00	100.34	0.60			106.57	7.47		
	17	99.82	0.00	99.99	0.00	99.62	0.62	99.80	0.62	102.57	7.62		
	36			99.68	0.01			100.92	0.57			106.57	7.47
	63	99.89	0.00	99.97	0.00	99.84	0.61	100.11	0.60	88.29	8.14	96.29	7.86
	90	99.40	0.01	99.97	0.00	99.12	0.64	100.20	0.60	95.14	7.90	98.57	7.77
	184			100.00	0.00			99.80	0.62			111.71	7.27
8	1	99.87	0.04	99.98	0.04	81.51	1.10	54.03	1.56	68.86	8.80	73.43	8.64
	3	99.73	0.01	99.97	0.00	99.30	0.63	96.37	0.73	95.14	7.55	85.99	8.23
	7	99.97	0.00	99.96	0.00	100.00	0.56	99.26	0.64	105.43	7.52	91.14	8.04
	14	99.78	0.00	99.99	0.00	100.25	0.60	98.04	0.68	106.57	7.47		
	17	99.78	0.00			99.71	0.62			100.86	7.69		
	36	99.17	0.01			100.70	0.58			98.57	7.77		
	63	99.81	0.00	99.90	0.00	100.34	0.60	99.62	0.62	104.86	7.54	98.00	7.79
	90	99.71	0.01	99.81	0.00	99.66	0.23	100.97	0.57	96.86	7.83	102.57	7.62
	184			99.94	0.00			100.34	0.60			110.00	7.34

Magn – separated by magnet; UC – separated by ultracentrifugation.

Table S 2. *List of samples from the batch sorption studies and long-term sorption experiments on un-oxidized and oxidized ÄD and NK materials.*

Material	Contact time. days	Tc uptake. % log [Tc] = -5		log [Tc] = -6		log [Tc] = -7		log [Tc] = -8		log [Tc] = -9		log [Tc] = -10		log [Tc] = -11	
		%	±. %	%	±. %	%	±. %	%	±. %	%	±. %	%	±. %	%	±. %
un-oxidized ÄD	0.04	7.10	0.06					3.57	2.16	14.51	8.08				
	1	8.38	0.06					13.42	2.00	25.14	7.59				
	1	12.80	0.06					10.82	2.02	27.94	7.59				
	4	19.94	0.06					19.04	1.95	33.15	7.40				
	4	6.47	0.06					23.95	1.89	27.54	7.54				
	7	35.15	0.05					41.64	1.67	35.55	7.33				
	7	11.54	0.06					29.96	1.82	25.95	7.59				
	15	15.37	0.08					76.46	1.15	52.74	6.85				
	15	33.37	0.07					62.74	1.38	53.14	6.83				
	21	25.12	0.08					83.88	1.00	53.14	6.83				
	21	19.14	0.08					73.74	1.20	86.73	5.76				
	30	22.43	0.08					93.48	0.77	71.13	6.28				
	57	13.90	0.09					79.66	1.09	70.35	6.31				
	57	39.59	0.07					95.86	0.70	97.14	5.41				
	91	20.26	0.08					97.56	0.65	96.34	5.43				
	91	22.63	0.08					97.90	0.64	94.34	4.98				
	141	44.76	0.12	48.19	0.19	48.70	0.24	53.83	0.23	90.85	0.51	81.65	1.73	95.06	4.15
	141	46.67	0.12	25.49	0.16	41.41	0.21	85.39	0.40	90.34	0.49	76.36	0.99	95.65	4.66
	178	20.70	0.08					99.44	0.58	100.00	5.12				
	178							98.88	0.60	99.54	5.12				
oxi-dized ÄD	0.04	5.69	0.09					7.61	2.06	-3.45	8.35				
	0.04							4.02	2.10	8.15	8.06				
	1	9.40	0.09					7.65	2.06	18.96	7.78				
	1	9.31	0.09					8.59	2.05	-5.84	8.39				
	4	7.08	0.09					12.12	2.02	9.76	8.01				
	4	9.45	0.09					11.74	2.02	10.56	7.99				
	7	8.83	0.09					23.04	1.90	5.35	8.11				
	7	9.69	0.09					15.23	1.98	14.95	7.87				
	15	6.75	0.09					14.51	1.99	25.36	7.61				
	15	8.59	0.09					16.21	1.97	24.95	7.61				
	21	13.09	0.09					2.57	2.11	33.35	7.40				
	21	10.08	0.09					13.49	2.00	13.36	7.92				
	30	10.38	0.09					11.23	2.03	22.96	7.68				
	57	9.90	0.09					76.91	1.14	39.35	7.23				
	57	9.82	0.09					43.11	1.66	42.55	7.14				
	91	10.51	0.09					53.55	1.52	23.37	7.66				
	91	12.21	0.09					36.51	1.74	57.77	6.71				
	141	3.07	0.71	13.79	2.61	17.12	0.21	18.52	0.78	77.49	6.44	80.46	8.38	67.14	7.04
	178							54.83	1.82	90.15	5.67				
	178	11.69	0.09					39.70	1.82	77.75	6.07				

Material	Contact time. days	Tc uptake. %											
		log [Tc] = -5		log [Tc] = -6		log [Tc] = -7		log [Tc] = -8		log [Tc] = -9		log [Tc] = -10		log [Tc] = -11	
		%	±. %	%	±. %	%	±. %	%	±. %	%	±. %	%	±. %	%	±. %
oxidized NK	0.04	19.26	0.08					23.26	1.89	23.42	7.53				
	0.04	12.62	0.09					15.46	1.98	30.96	7.33				
	1	15.40	0.08					17.93	1.95	17.47	7.69				
	1	16.75	0.08					14.86	1.98	22.22	7.55				
	3	15.41	0.08					21.04	1.92	33.73	7.24				
	3	16.30	0.08					16.06	1.97	35.32	7.22				
	14	15.77	0.08					18.23	1.95	42.07	7.03				
	14	20.53	0.08					15.12	1.98	44.85	6.94				
	21	16.17	0.08					17.25	1.96	45.24	6.93				
	21	16.30	0.08					15.04	1.98	47.23	6.87				
	31	16.46	0.08					24.75	1.87	44.45	5.57				
	31	17.26	0.08					20.87	1.92	46.03	6.91				
	91	19.01	0.08					35.26	1.76	42.06	7.24				
	91	17.13	0.08					19.34	1.94	100.00	5.13				
	150	7.16	0.01	10.09	0.06	23.16	0.46	40.67	2.16						
	195	21.20	0.08					29.56	1.83	29.76	7.57				
	195	16.73	0.08					27.81	1.85	30.95	7.54				

Table S 3. *Breakthrough curves data obtained for HTO and ^{36}Cl on the Äspö core #2.2.*

10 mL/h			1.5 mL/h			0.2 mL/h		
V, mL	C/C_0		V, mL	C/C_0		V, mL	C/C_0	
	HTO	^{36}Cl		HTO	^{36}Cl		HTO	^{36}Cl
0.16	5.34E-04	2.08E-04	0.14	3.79E-04	2.85E-05	0.16	0.0033	7.29E-04
0.31	5.83E-04	0	0.29	6.16E-04	2.49E-05	0.32	0.00262	4.17E-04
0.47	5.83E-04	0	0.43	6.44E-04	2.67E-05	0.48	0.00311	6.25E-04
0.63	6.31E-04	1.56E-04	0.58	0.00241	0.00171	0.65	0.00651	0.01021
0.78	0.02928	0.03918	0.72	0.15115	0.13498	0.81	0.15539	0.35801
0.94	0.22862	0.27757	0.86	0.46782	0.44217	0.97	0.53455	1.1279
1.09	0.48298	0.5602	1.01	0.61936	0.63188	1.13	0.7489	1.3242
1.25	0.66076	0.73811	1.15	0.69446	0.74317	1.29	0.82708	1.426
1.41	0.74268	0.82438	1.30	0.73706	0.8022	1.45	0.84388	1.38474
1.56	0.78235	0.87752	1.44	0.76837	0.83692	1.62	0.8734	1.40453
1.72	0.80552	0.89659	1.58	0.79595	0.87278	1.78	0.87739	1.35233
1.88	0.75574	0.81896	1.73	0.76682	0.80198	1.94	0.74919	1.03089
2.03	0.57272	0.61016	1.87	0.47852	0.46228	2.10	0.44102	0.54618
2.19	0.35799	0.37025	2.02	0.29624	0.27941	2.26	0.24338	0.26965
2.35	0.21439	0.22063	2.16	0.22041	0.21099	2.42	0.15879	0.16608
2.50	0.14568	0.14973	2.31	0.18047	0.17725	2.59	0.11684	0.14243
2.66	0.10538	0.11513	2.45	0.15843	0.15537	2.75	0.08663	0.10034
2.82	0.08585	0.087	2.59	0.1364	0.13348	2.91	0.0673	0.07429
2.97	0.06847	0.0696	2.74	0.11899	0.11555	3.07	0.05478	0.05626

10 mL/h			1.5 mL/h			0.2 mL/h		
V, mL	C/C_0		V, mL	C/C_0		V, mL	C/C_0	
	HTO	^{36}Cl		HTO	^{36}Cl		HTO	^{36}Cl
3.13	0.05555	0.05491	2.88	0.09821	0.09233	3.23	0.04536	0.04678
3.28	0.04662	0.04647	3.03	0.07927	0.06953	3.39	0.03759	0.03678
3.44	0.03904	0.03761	3.17	0.06018	0.05015	3.55	0.03059	0.02907
3.60	0.03302	0.03115	3.31	0.04496	0.03671	3.72	0.02632	0.02563
3.75	0.02884	0.02709	3.46	0.03584	0.02849	3.88	0.02263	0.0223
3.91	0.02583	0.02469	3.60	0.0286	0.02227	4.04	0.01923	0.01792
4.07	0.02409	0.02292	3.75	0.0247	0.01967	4.20	0.01738	0.01605
4.22	0.02185	0.02205	3.89	0.0217	0.01668	4.36	0.01602	0.01459
4.38	0.01962	0.0199	4.03	0.01837	0.01479	4.52	0.01389	0.0124
4.54	0.01845	0.01818	4.18	0.01643	0.01342	4.69	0.01195	0.01032
4.69	0.01753	0.01766	4.75	0.01435	0.01191	4.85	0.01117	0.00927
5.32	0.01447	0.01391	5.33	0.01282	0.01085	5.49	0.00927	0.01016
5.94	0.0117	0.01084	5.91	0.01068	0.00829	6.14	0.00631	0.00703
6.57	0.00908	0.00875	6.48	0.00805	0.00637	6.79	0.00505	0.00557
7.20	0.00724	0.00682	7.06	0.00542	0.00446	7.43	0.00408	0.00432
7.82	0.00592	0.00552	7.64	0.00428	0.00345	8.08	0.00354	0.00359
9.38	0.00398	0.00386	9.08	0.00225	0.00172	8.72	0.00301	0.00365
10.95	0.00262	0.0024	10.52	0.00178	0.00138	10.34	0.00248	0.00229
12.51	0.00189	0.00182	11.96	0.00129	9.95E-04	11.96	0.00194	0.00172
14.08	0.00155	0.00146	13.40	9.65E-04	7.64E-04	13.57	0.00151	0.0013
15.64	0.00112	9.90E-04	14.84	7.55E-04	5.69E-04	15.19	0.00141	0.00162
17.21	8.26E-04	8.34E-04	16.28	5.77E-04	3.72E-04	18.42	0.00112	9.38E-04
18.77	5.34E-04	5.21E-04	17.72	4.69E-04	3.38E-04	21.65	6.80E-04	6.25E-04
20.33	5.34E-04	3.65E-04	19.16	3.53E-04	2.81E-04	24.88	5.83E-04	3.65E-04
21.90	2.91E-04	3.13E-04	20.60	3.04E-04	2.22E-04	28.11	3.88E-04	2.60E-04
25.03	2.91E-04	2.60E-04	22.04	2.53E-04	1.77E-04	31.34	3.40E-04	3.13E-04
28.15	2.91E-04	2.08E-04	23.48	2.10E-04	1.70E-04	34.58	2.43E-04	1.04E-04
31.28	2.91E-04	2.08E-04	24.92	1.66E-04	1.63E-04	37.81	2.91E-04	1.04E-04
34.41	9.71E-05	1.56E-04	26.36	1.64E-04	1.34E-04	41.04	2.91E-04	1.04E-04
37.54	4.86E-05	2.08E-04	27.80	1.02E-04	1.14E-04	44.27	2.43E-04	0
40.67	4.86E-05	1.56E-04	29.24	1.10E-04	7.87E-05	47.50	2.43E-04	0
			30.69	1.05E-04	9.66E-05	49.99	1.94E-04	0
			32.13	8.38E-05	1.11E-04			
			33.57	8.71E-05	9.30E-05			
			35.01	2.79E-05	8.59E-05			
			36.45	4.28E-05	1.14E-04			
			39.33	1.53E-04	1.63E-04			
			42.21	6.25E-05	8.76E-05			
			45.09	5.43E-05	6.44E-05			
			47.97	5.10E-05	3.40E-05			
			49.99	3.12E-05	5.55E-05			

***Table S 4**. Breakthrough curves data obtained for ^{95m}Tc on the Äspö core #2.2.*

10 mL/h		1.5 mL/h		0.2 mL/h	
V, mL	C/C_0	V, mL	C/C_0	V, mL	C/C_0
0.33	0	0.29	0	0.32	0
0.67	0.04081	0.58	0.00115	0.63	0
1.00	0.64443	0.87	0.21333	0.95	0.26268
1.34	0.89364	1.16	0.55566	1.26	0.63097
1.67	0.87439	1.45	0.65829	1.58	0.7349
2.00	0.49612	1.74	0.70237	1.90	0.7862
2.34	0.20746	2.03	0.39385	2.21	0.56784
2.67	0.09591	2.32	0.18336	2.53	0.1952
3.01	0.05583	2.61	0.11147	2.85	0.02512
3.34	0.05583	2.90	0.08702	3.16	0.06221
3.68	0.02941	3.19	0.08073	3.48	0.01334
4.01	0.03202	3.48	0.07253	3.79	0.00818
4.34	0.02392	3.77	0.06737	4.11	0.01655
6.01	0.00326	4.06	0.06216	4.43	0.01166
7.69	0.00732	4.35	0.05637	4.74	0.00825
9.36	0.00286	4.64	0.05006	5.38	0.00236
11.03	0.00317	4.93	0.0447	6.01	0.00151
12.70	0.00161	5.22	0.0413	6.64	9.25E-04
14.37	0.00104	5.51	0.0369	7.27	2.81E-04
16.04	7.60E-04	6.09	0.03279	7.91	0.00101
19.38	6.69E-04	6.67	0.02875	8.54	0.00101
22.72	5.12E-04	7.24	0.02529	9.17	3.02E-04
26.06	5.77E-04	7.82	0.02076	9.80	3.29E-04
29.41	0.00116	8.40	0.01965	10.44	2.66E-05
32.75	2.41E-04	9.85	0.01613	11.07	1.45E-04
36.09	1.03E-04	11.30	0.01041	11.70	1.41E-04
39.43	0	12.75	0.00566	12.33	0
42.77	0	14.20	0.00276	12.97	0
46.11	1.03E-04	15.65	0.00132	13.60	0
47.28	0	17.10	6.26E-04	14.23	0
		18.55	3.26E-04	14.86	0
		20.00	5.12E-05	15.50	0
		25.79	6.04E-05	16.13	0
		31.59	4.11E-05	16.76	0
		44.63	3.79E-05	17.39	0
		47.53	3.59E-05	18.03	0
		49.99	1.11E-06	18.66	0
				20.24	0
				21.82	0
				23.40	0
				26.56	0
				29.73	0
				32.89	0

10 mL/h		1.5 mL/h		0.2 mL/h	
V, mL	C/C_0	V, mL	C/C_0	V, mL	C/C_0
				36.05	0
				39.21	0
				42.38	0
				45.00	0

8.2. List of abbreviations

ÄD	Äspö diorite
AMCSD	American Mineralogist Crystal Structure Database
BET	Surface area analysis based on Brunauer-Emmett-Teller theory
BTC	Breakthrough curve
CT	Computed tomography
D.L.	Detection limit
DOI	Declaration of Intent
DOS	Density of states
EDX	Energy-dispersive X-ray spectroscopy
EW	Exempt waste
EXAFS	Extended X-ray absorption fine structure
FT	Fourier transformation (or transformed)
FWHM	Full width at half maximum
GW	Groundwater
GWS	Groundwater simulant
HA	Humic substance
HLW	High level waste
HPGe	High-purity germanium
HPLC	High-performance liquid chromatography
HRL	Hard rock laboratory
IAEA	International Atomic Energy Agency
ICP-MS	Inductively coupled plasma mass spectrometry
IGEM RAS	Institute of Geology of Ore Deposits, Petrography, Mineralogy and Geochemistry of the Russian Academy of Sciences
ILW	Intermediate level waste
IUPAC	International Union of Pure and Applied Chemistry
JGU	Johannes Gutenberg University
KIT-INE	Karlsruhe Institute of Technology, Institute for Nuclear Waste Disposal
LLD	Lower limit of detection
LLW	Low-level waste
LOI	Loss on ignition
LSC	Liquid scintillation counting
n.a.	Not applicable
n.d.	Not detected
n.m.	Not measured
NK	Nizhnekansky (massif. granite)
PMBP	1-Phenyl-3-methyl-4-benzoylpyrazolone-5
RMS	Root square mean

RN	Radionuclide
SEM	Scanning electron microscope
SNF	Spent nuclear fuel
TIMS	Thermal ionization mass spectrometry
TRU	Transuranic waste
UC	Ultracentrifuge (ultracentrifugation)
URL	Underground research laboratory
VLLW	Very low-level waste
VSLW	Very short-lived waste
XAFS	X-ray absorption fine structure
XANES	X-ray absorption near edge structure
XAS	X-ray absorption spectroscopy
XPS	X-ray photoelectron spectroscopy
XRD	X-ray diffraction
XRF	X-Ray fluorescence analysis
zpc	Zero point of charge

8.3. List of parameters

Parameter	Unit	Meaning
μ	Pa×s	dynamic viscosity of the liquid
A	Bq/mL	specific activity of the radionuclide in the solution
a	nm	crystalline lattice parameter
C	mol/m^3 or mol/L (M)	concentration of solute
c	g/m^3	mass concentration of solute
c_{surf}	g/m^2	mass of solute on the mineral phase per specific surface area of the solid
D	m^2/s	diffusion coefficient
D_a	m^2/s	apparent diffusion coefficient
d_{inf}	nm	information depth
Eh	mV	redox potential
E_k	eV	kinetic energy
g	m/s^2	acceleration due to gravity
h	m	height
h. k. l	dimensionless	Miller indices of the crystalline lattice
J	$mol/m^2/s$	solute mass flux per unit area per unit time
k	m^2	hydraulic permeability
K	m/s	hydraulic conductivity
K_a	m	surface area normalized distribution coefficient
K_d		distribution coefficient
K_f	mg/g	Freundlich adsorption value
K_{sch}	dimensionless	Scherrer constant (a dimensionless shape factor)
m	mass	mass
m_a	g/mol	mean atomic weight
N_A	dimensionless	Avogadro number. $N_A = 6.022\times10^{23}$
n_e	dimensionless	effective porosity
p	Pa	pressure
q	mol/m^3	surface concentration
r	$time^{-1}$	uptake rate
S	%	sorption percentage
S_{BET}	m^2/g	specific surface area
t	time	time
$t_{1/2}$	time	half-life
v	m/s	fluid velocity
V	volume	volume
Z	dimensionless	mean nuclear charge of the material
β	radians	FWHM value of the XRD diffraction line
θ	radians	Bragg angle
λ	nm	wavelength
ρ	kg/m^3	density
τ	nm	mean size of the ordered (crystalline) domains
χ	nm	attenuation length of the electron flux

8.4. List of figures

Supplementary materials:

8.5. List of tables

8.6. List of publications

Totskiy, Y.; Geckeis, H.; Schäfer, T. Sorption of Tc(VII) on Äspö Diorite (ÄD). In: (Rabung, T., Molinero, J., García, D., and Montoya, V. Eds.) 1st Workshop Proceedings of the Collaborative Project "Crystalline Rock Retention Processes" (7th EC FP CP CROCK) KIT Scientific Report 7629, 2012, pp. 97-106.

Totskiy, Y.; Geckeis, H.; Schäfer, T. Sorption of Tc(VII) on crystalline rock material from Äspö (Sweden). Joint ITU-INE Research Fellow's Day, JRC-KIT, Karlsruhe, 22 June, 2012, pp. 118-119.

Totskiy, Y.; Stage, E., Geckeis, H.; Schäfer, T., Kalmykov, S. Sorption of Tc(VII), Cs(I), Eu(III), U(VI) and Am(III) on crystalline rock material from Äspö (Sweden) and Nizhnekansky massif (Russia). Proceedings of the 7th Russian Conference on Radiochemistry "Radiochemistry-2012", Dimitrovgrad, Russia, 15-19 October, 2012, p. 350.

Totskiy, Y., Huber, F., Schäfer, T., Geckeis, H. Tc(VII) immobilization on granitoid rocks from Äspö (Sweden). Book of Abstracts, 14th International Conference on the Chemistry and Migration Behaviour of Actinides and Fission Products in the Geosphere, Brighton, UK, 8-13 September, 2013, 238-239.

Totskiy, Y.; Huber, F., Schild, D., Schäfer, T., Kalmykov, S., Geckeis, H. Tc(VII) immobilization on granitic rocks from Äspö (Sweden) and Nizhnekansky massif (Russia). Book of abstracts, TRePro III – Workshop on Modelling of Coupled Reactive and Transport Processes, Karlsruhe, Germany, 5-7 March, 2014, p. 138-139.

Totskiy, Y., Huber, F., Schild, D., Schäfer, T., Kalmykov, S., Geckeis, H. Tc(VII) immobilization on granitic rocks from Äspö HRL (Sweden) and Nizhnekansky massif (Russia). Book of Abstracts "Goldschmidt 2014", Sacramento, USA, 7-13 June, 2014, p. 2506.

Totskiy, Y., Yalcintas, E., Huber, F., Gaona, X., Schäfer, T., Altmaier, M., Kalmykov, S., Geckeis, H. A contribution from fundamental and applied technetium chemistry to the nuclear waste disposal safety case. Book of abstracts "Key Topics in Deep Geological Disposal", Cologne, Germany, 25-26 September, 2014, p. 56.

Totskiy, Y., Huber, F., Marsac, R., Schild, D., Pidchenko, I., Vitova, T., Kalmykov, S., Geckeis, H., Schäfer, T. Tc interaction with crystalline rock from Äspö (Sweden) and Nizhnekansky massif (Russia). Geochimica et Cosmochimica Acta, 2015, *submitted*.